CONSORZIO RFX
Ricerca Formazione Innovazione

Consiglio Nazionale delle Ricerche

Magnetic chaos healing and helical self-organization in plasma pinches

Susanna Cappello

in collaboration with **D. Bonfiglio, D.F. Escande, M. Veranda, G. Di Giannatale, A. Kryzhanovskyy and the RFX team**

CONSORZIO RFX
Associazione Euratom-ENEA sulla Fusione - PADOVA - ITALY
partnership of CNR, ENEA, INFN and Padova University

RFX lab in Padova Italy – Overview

1. **RFX site - CNR area**
2. **RFX team**
3. **RFX device: Reversed Field Pinch (and Tokamak)**

RFX = Ricerca Formazione Innovazione
Reverse Field eXperiment

Consorzio RFX is hosted in the Padova "CNR research area"

CNR: National Research Council

Consorzio RFX is hosted in the Padova “CNR research area”

“Palazzo della Ragione”

From the web

Padova University historical site

From the web

“Palazzo della Ragione” medieval town hall https://en.wikipedia.org/wiki/Palazzo_della_Ragione,_Padua

Padova University historical site https://en.wikipedia.org/wiki/University_of_Padua

Padova: Area della Ricerca del CNR

Consorzio RFX:

1) NBTF Neutral Beam Test Facilty for ITER

Padova: Area della Ricerca del CNR

Consorzio RFX:

2) RFX:
RFP Device

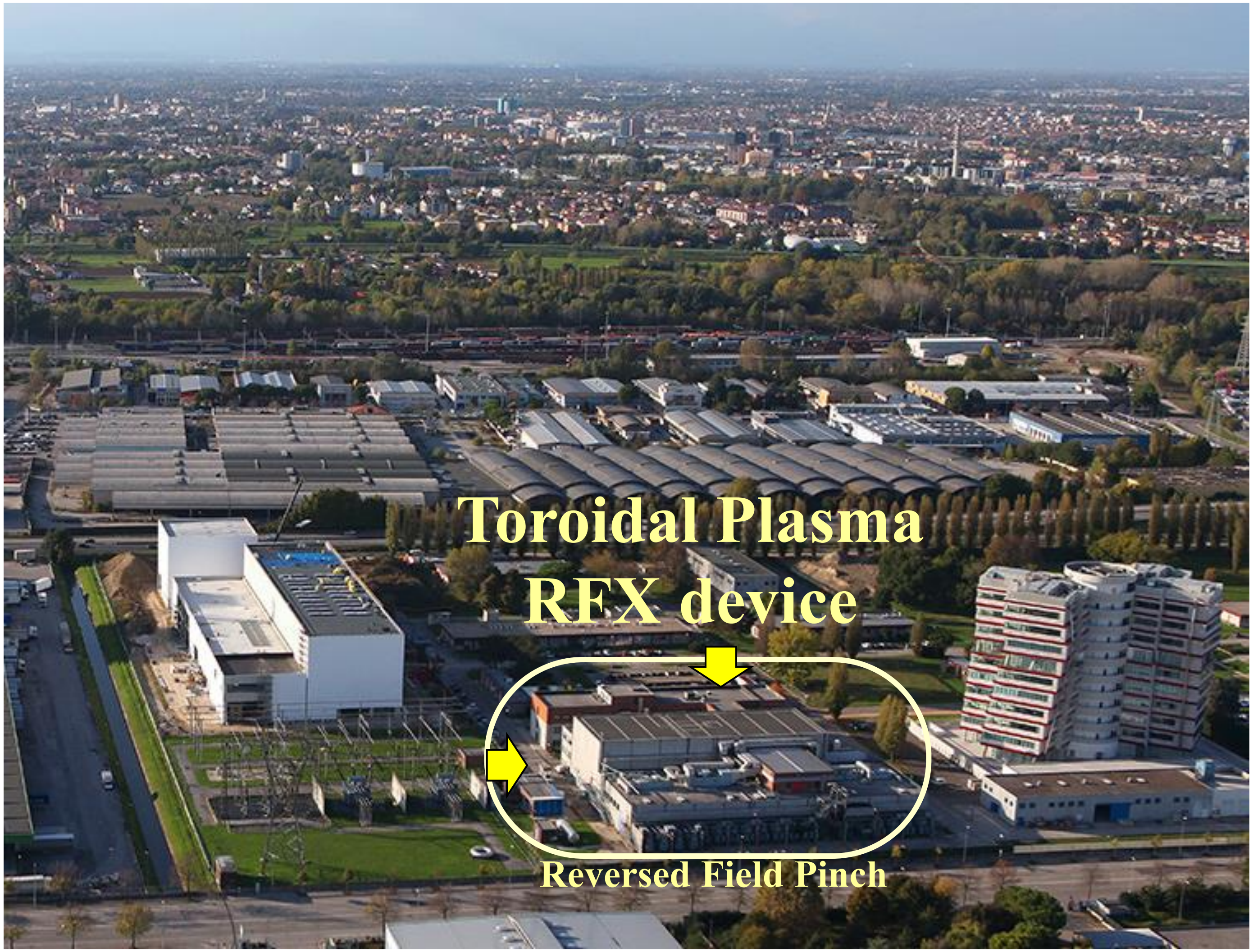

Reversed Field Pinch, RFP, partners:

USA - Sweden - Japan – China

RFX group


About 1 5 0 people
+ 25-30 students (international Padova – Ghent Universisites PhD
in FUSION SCIENCE AND ENGINEERING)

(1992 – 1999)

RFX

(2004 – 2015)

RFX-mod

(2021 …)

RFX-mod2

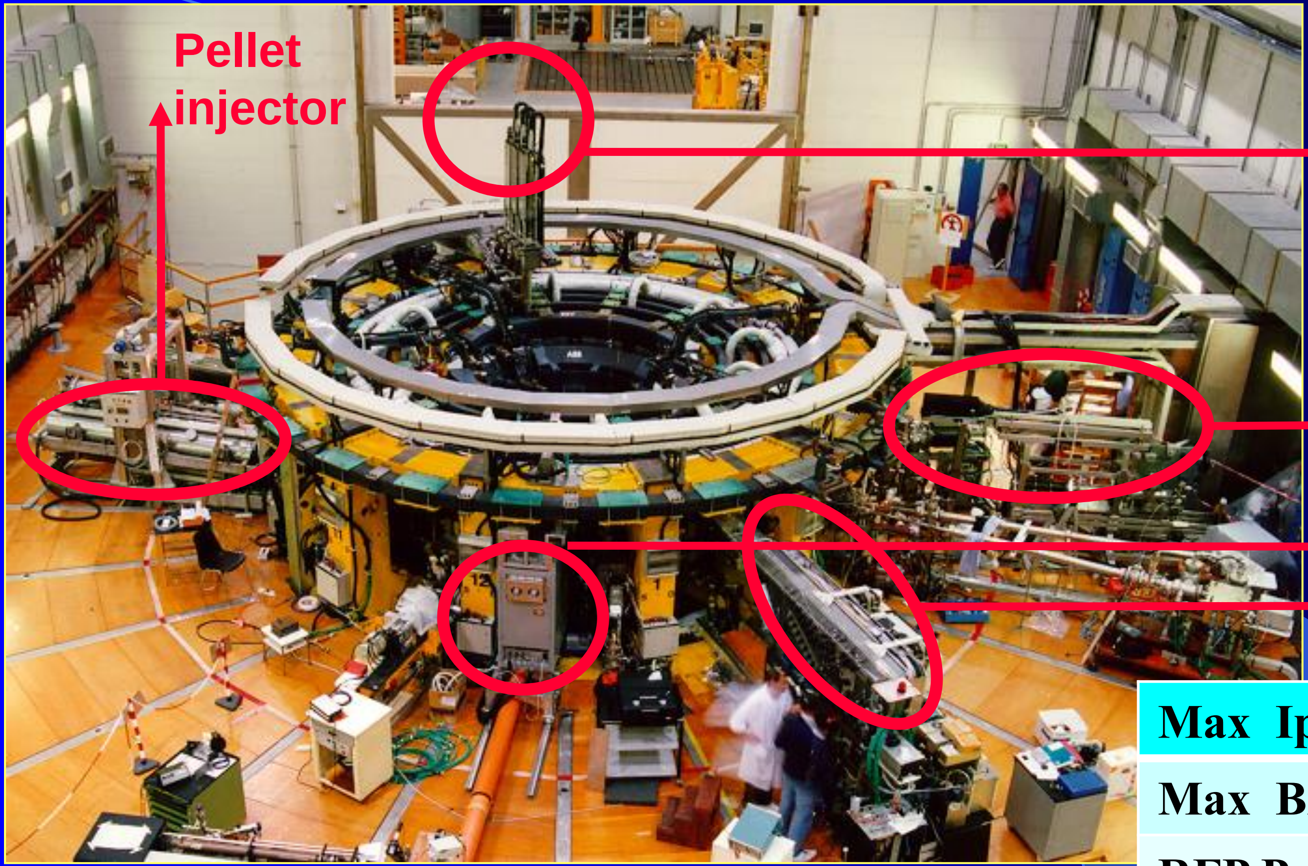

Max Ip	2 MA
Max Bz	0.7 T
RFP Pulse duration Tokamak Pulse	0.6 s 1 s

The place of the RFP in MCF

Increase plasma current

Steady state	Confinement	Light Tech expected
Coils Complexity	Disruption risk	Confinement
Stellarator	Tokamak	RFP

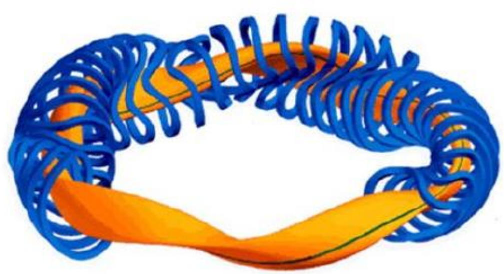

[*]

FIG. 1.14. Schematic of stellarator magnetic field coils and plasma configuration (courtesy of Ref. [1.62]).

R = 5.5 m W7-X
(R = 3.9 m LHD)

[*] Book: Fusion Physics IAEA 2012

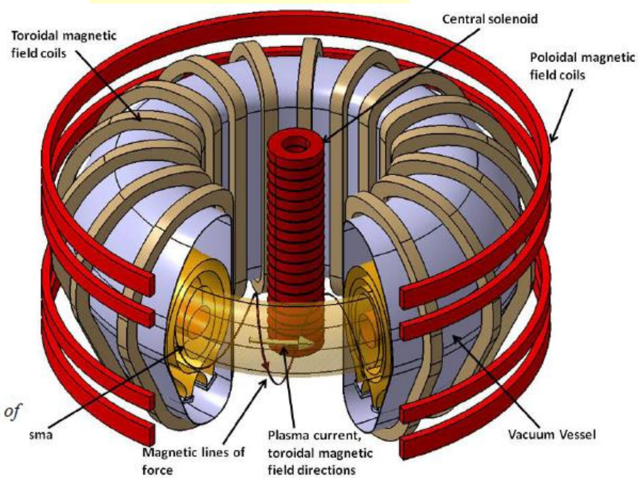

FIG. 1.12. Schematic of a tokamak.

R = 3 m JET

(R = 6.21 m ITER)

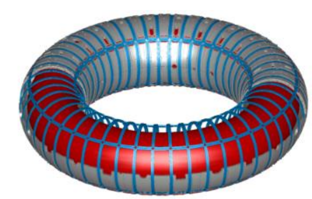

R = 2.0 m RFX

(1.5 m MST USA
1.4 m KTX Hefei China)

Several common physics issues: transport barrier formation, density limit … magnetic relaxation …

OUTLINE

Introduction to the RFP: *a* *<u>Toroidal Pinch</u>* *with* *Field Reversal,*

Helical self-organization:

a) Experimental facts (mainly from RFX)

- Quasi helical states (QSH) in high current discharges (Ip > 0.8MA):
  - Electron transport barriers, eITB, and Impurity screening effect;

b) 3D non linear MHD modeling and magnetic chaos healing

- Transition to helical regimes,
- Key role of edge Magnetic Perturbations (MP) and realistic Boundary conditions :

Non-Resonant and Resonant MPs … "synergistically interact" with helical self-organization process

- Magnetic chaos healing, Lagrangian Coherent Structures detection.

… New regimes to be experimentally explored in **RFX-mod2 from 2021**

Summary

RFP device and configuration set up

RFX device coils

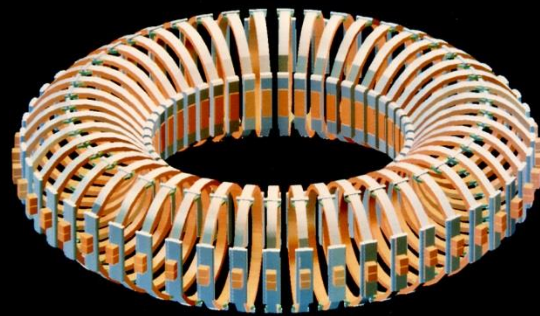

toroidal magnetic field

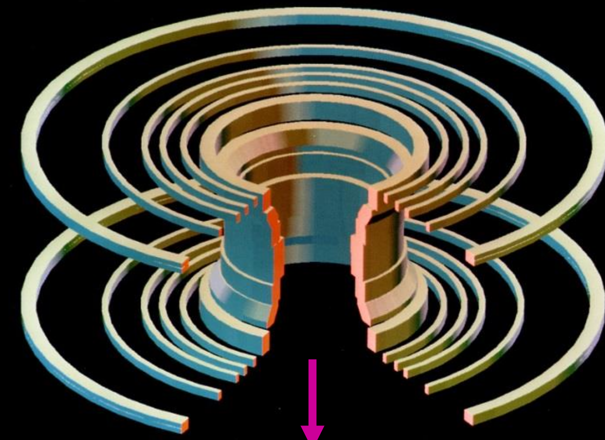

poloidal magnetic field

induction of plasma current

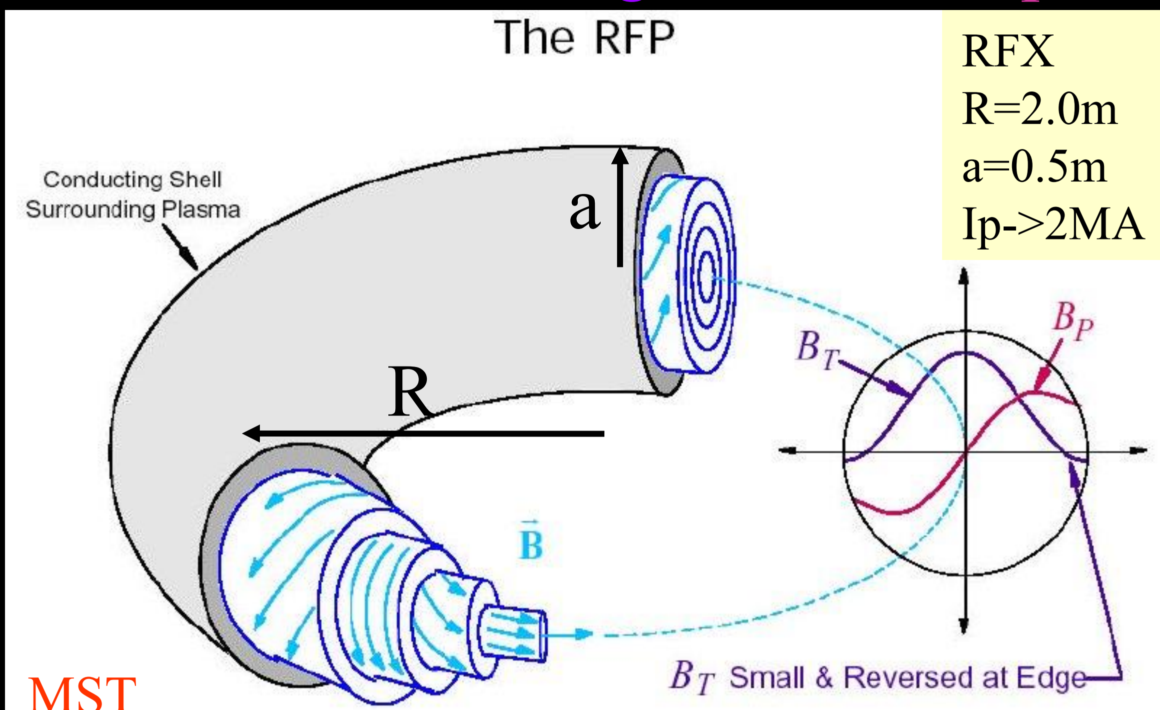

RFX
R=2.0m
a=0.5m
Ip->2MA

mean magnetic field radial profiles

RFP Distinctive features:

The RFP is a simple ohmic device.
No auxiliary: – heating – current drive – momentum sources (typically used in Tokamaks)

No relaxation to «primitive» axissymmetric or helical Taylor's states

Rather then relaxing to the «primitive» Taylor's relaxed state…
the RFP tends to approach a contiguous helical ohmic equilibrium resulting from the **nonlinear saturation of a resistive-kink/tearing mode,**
(… to which a pinch configuration is normally prone, Tokamaks too,)

In fact, **the RFP plasma kinks according to B pitch in the plasma core**.

RFP Distinctive features: "kink self-organization" in MHD

Since early '90ties,

3D nonlinear MHD simulations envisaged the transition to ordered helical regimes :

- as ruled by *dissipative parameters (with ideal magnetic boundary),*
  (then clearly observed in experiments starting in the late '90ties),

More recently (2013 onward),

Refined Boundary Conditions schematically mimicking real magnetic front-end:

- *seed edge Magnetic Perturbations* (with suitable pitch choice),

predicted new «stimulated» helical states, … then successfully obtained in experiments,

- *thin resistive shell + vacuum layer* provide much closer quantitative description of

experimental behavior.

RFP self-organization

a) Experimental facts and b) Modeling results

RFP self-organization

RFX

RFP ↔ saturated KINKED plasma

for Ip above ~ 1 MA

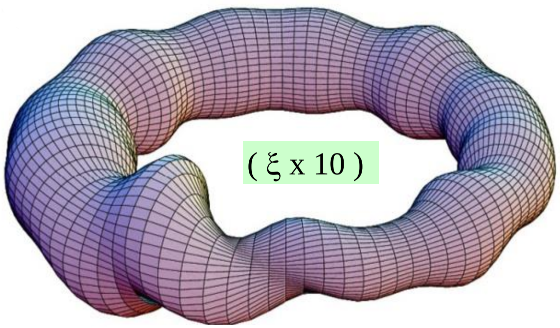

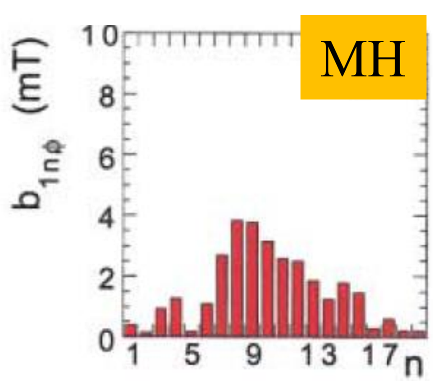

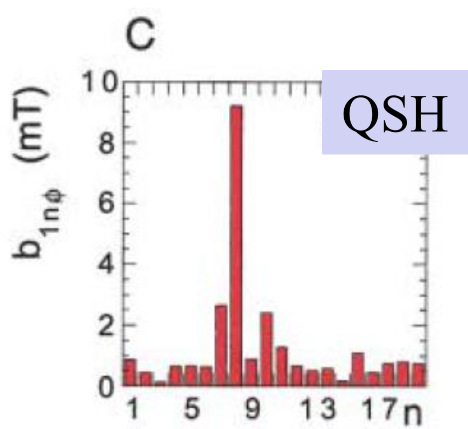

MHD spectrum: resistive kink-tearing modes

Advanced operation required in RFX-mod

CLEAN MODE CONTROL
and/or
NON CONVENTIONAL SCENARIOS (PPCD-OPCD)

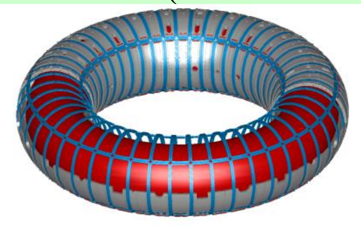

Feedback coils system
Typical operation:
Ip ~ 1.7 MA
Te up to 1.2 keV

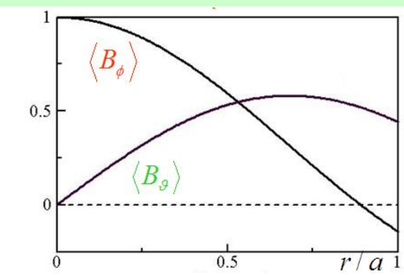

RFP self-organization

RFX

RFP ↔ saturated KINKED plasma

for Ip above ~ 1 MA

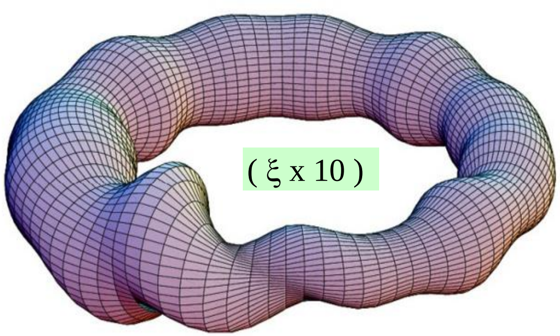

Advanced operation required in RFX-mod

CLEAN MODE CONTROL
and/or
NON CONVENTIONAL
SCENARIOS (PPCD-OPCD)

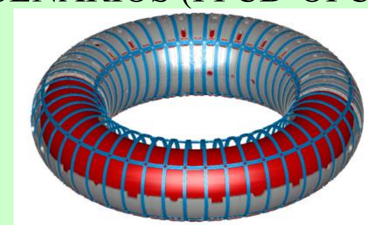

MH

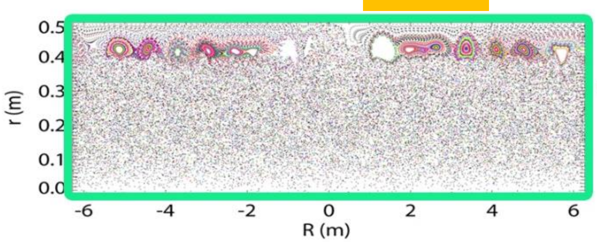

SH

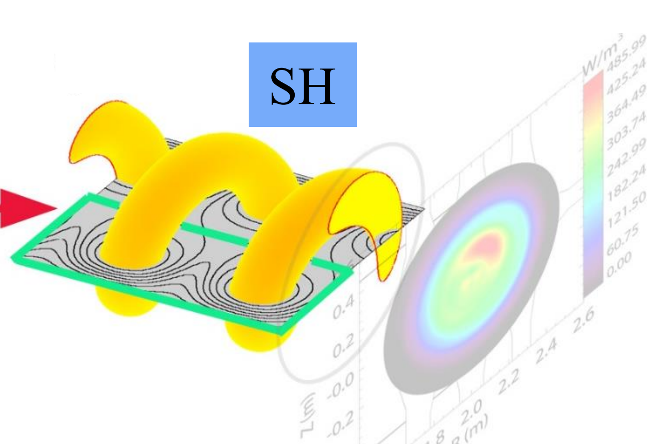

Feedback coils system
Typical operation:
Ip ~ 1.7 MA
Te up to 1.2 keV

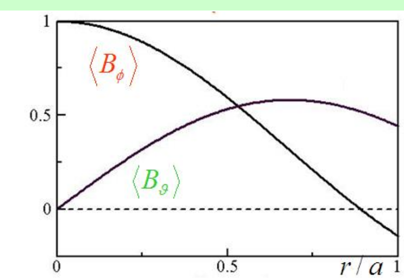

MHD spectrum impact on magnetic topology

RFP helical self-organization: several experiments RFX – TPE – MST –T2R

RFX

FIG. 3 (color). Schematic view of a $n = 7$ helical structure inside the RFX vessel.

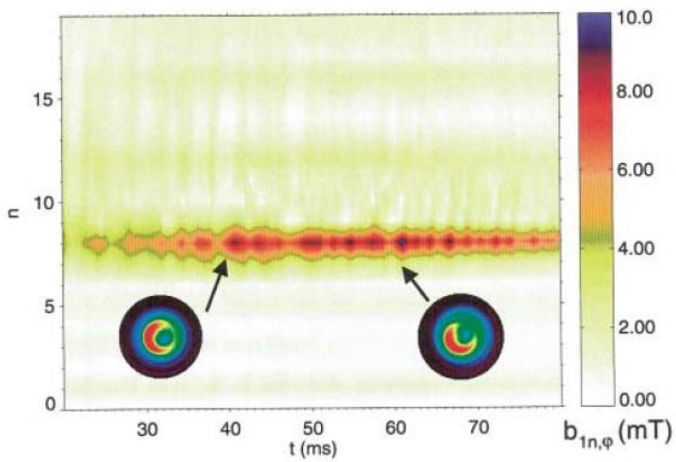

FIG. 5 (color). $m = 1$ modes n-spectrum vs time and SXR emissivity patterns at selected times ($t = 40$ ms and $t = 60$ ms) in a plasma (No. 11336) where the QSH state is permanent. The dominant mode in this case is $n = 8$.

Escande, Martin, Ortolani et al. PRL 2000

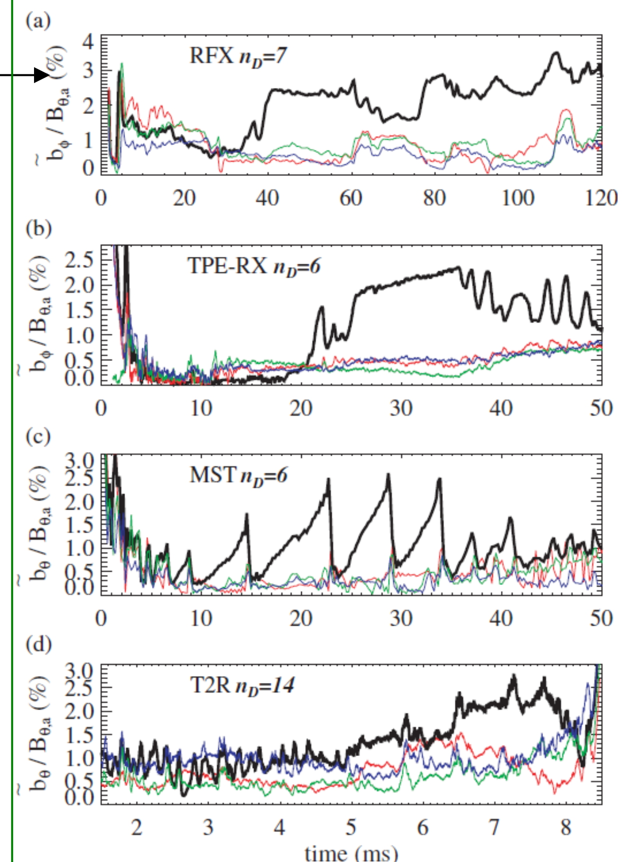

Martin, Marrelli, Spizzo et al. NF 2003

TPE-RX Japan
MST USA
T2R Sweden

More recently also:
RELAX (Japan), KTX (Hefei- China)

RFP helical self-organization: a robust process

HELICAL persistency increases with current - up to > 85% of flat top

Ip=1,5 MA deuterium RFP discharge (#36451)

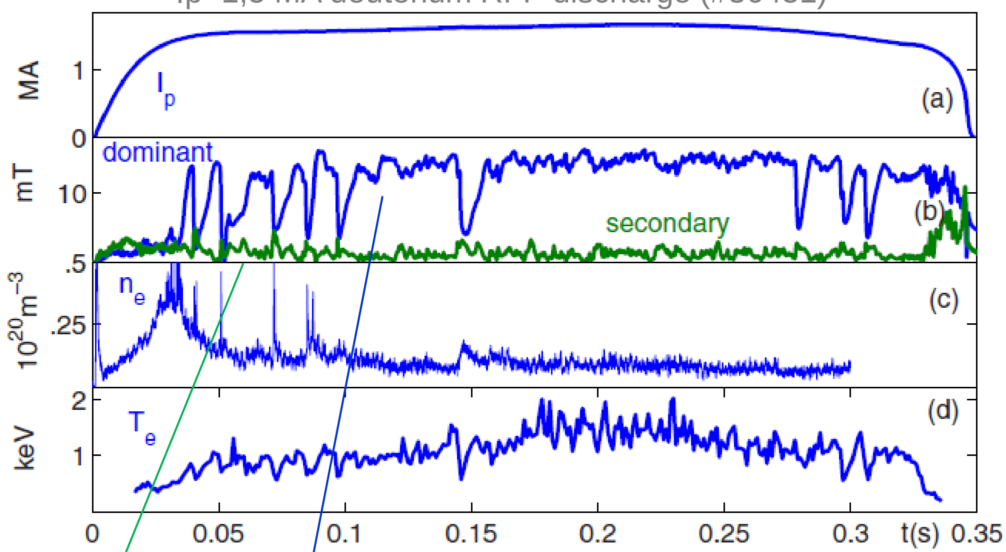

Dominant mode (internal)

ave secondary modes

Puiatti, Dal Bello, Marrelli et al. NF 2015

Flattop fraction with helical state (%)

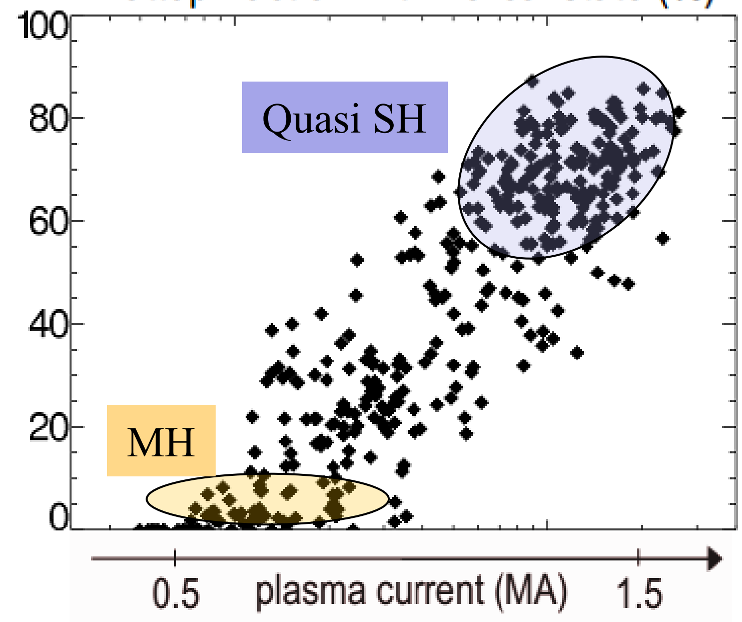

(hydrogen RFP discharges)

Piovesan, Zuin et al NuclFus 2009

Similar behavior in MST experiment:
- Chapman et al IAEA EX/P6-01 (2012)
- Sarff et al Nucl Fus 2013

RFP helical self-organization: barriers formation

RFX -mod

Formation of e-Transport Barriers

24598, 117ms
I_P=1.3MA
n/n_G=0.20

22201, 35ms
I_P=0.7MA
n/n_G=0.22

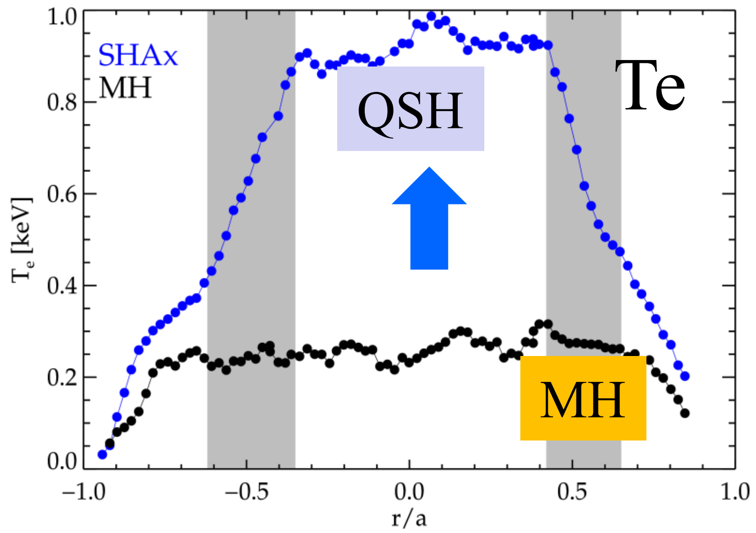

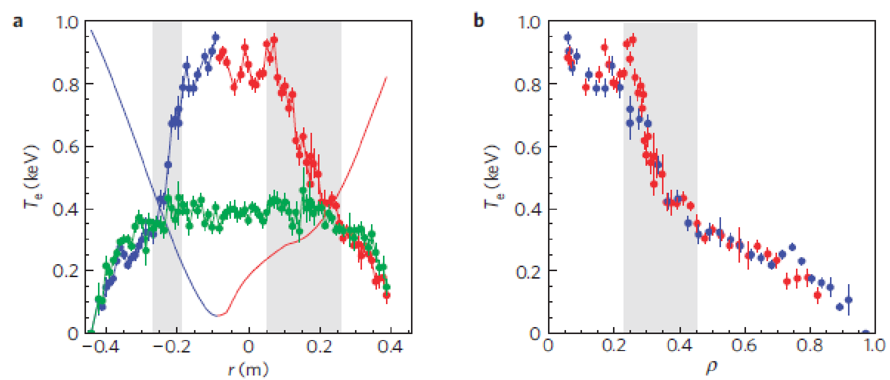

Lorenzini, Martines, Piovesan et al NatPhys 2009
Piovesan, Zuin, Alfier et al NF 2009

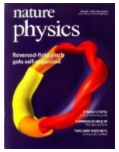

… the barrier foot is close to the vanishing magnetic shear location

Helical q: q(ρ) gives the number of toroidal turns field lines perform for one poloidal turn around the helical axis

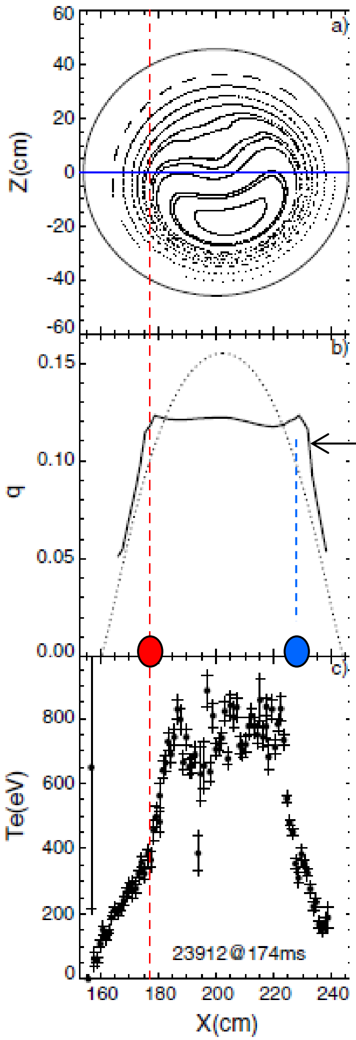

Helical flux surfaces

Helical q

Te

Position of the eITB vs the maximum_q location for RFX-mod experimental SHAx states.

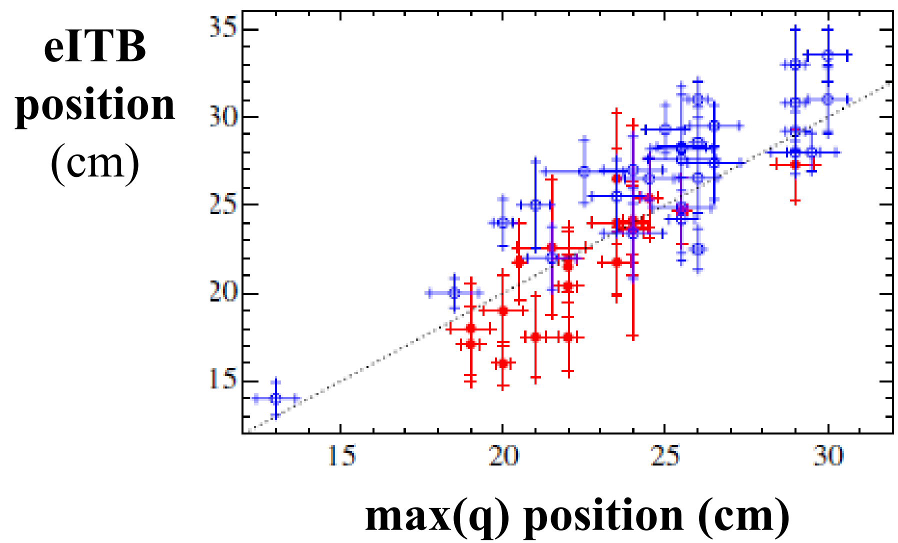

Error bars in the abscissas are due to uncertainties in equilibrium reconstruction.

Gobbin, Bonfiglio, Escande et al PRL 2011

RFP helical self-organization: barriers formation

RFX -mod

41st EPS Conference on Plasma Physics

… and Impurity screening effect

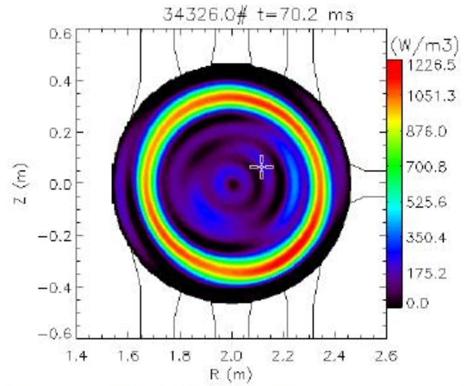

Fig.2 Experimental tomographic inversion of SXR emissivity at the maximum of the W LBO emission

Tungsten
Laser Blow Off
in QSH

a.u.

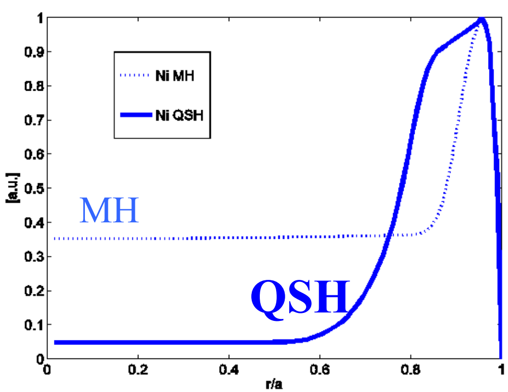

Simulation of Ni normalized total density at the steady state, after Ni target Laser Blow Off

Puiatti, Valisa, Agostini et al NF 2011
Carraro, Auriemma, Barbui et al EPS 2014
Menmuir, Carraro, Alfier et al PPCF 2010

TESPEL experiments (RFX-mod2) planned in collaboration with NIFS

Isotopic effect: Deuterium discharges

QSH improvement in persistence and Te

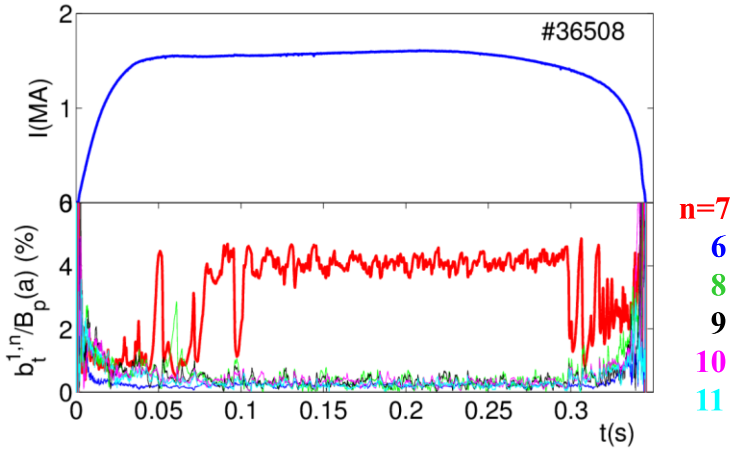

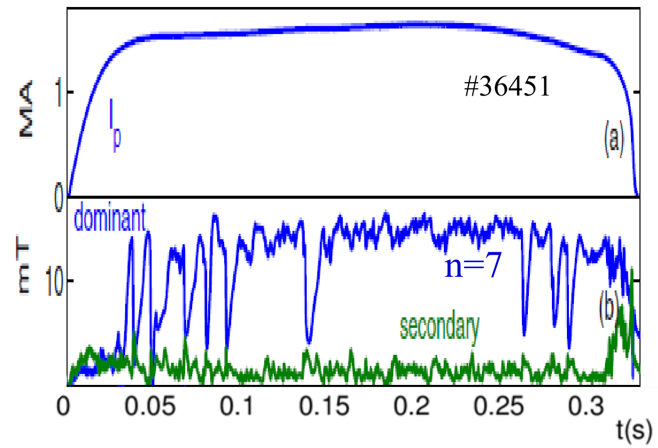

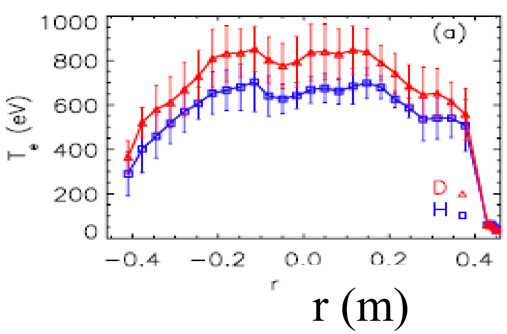

Lorenzini, Agostini, Auriemma et al NF 2015

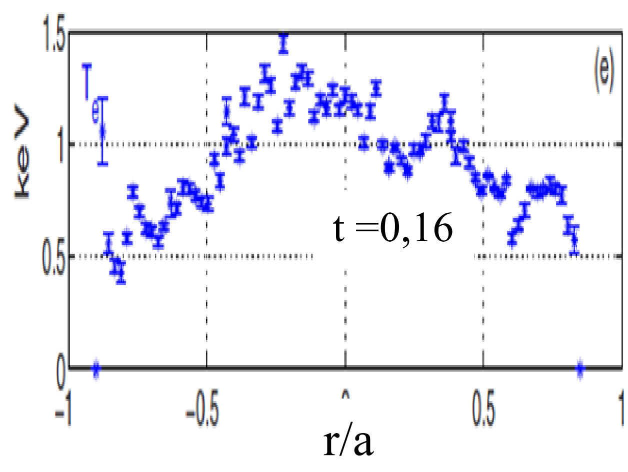

Puiatti, Dal Bello, Marrelli, et al. NF 2015

RFP self-organization

a) Experimental and **b) Modeling**

Transition to helical states:

- Simple description from a toy model:
  current carrying wire in a flux conserver,
- 3D nonlinear viscoresistive Magnetohydrodynamic modeling:
  - ✓ Transition to helical regimes, and
  - ✓ Magnetic chaos healing

RFP *Toy model*: **intuitive RFP**

… a current carrying wire in a flux conserver:

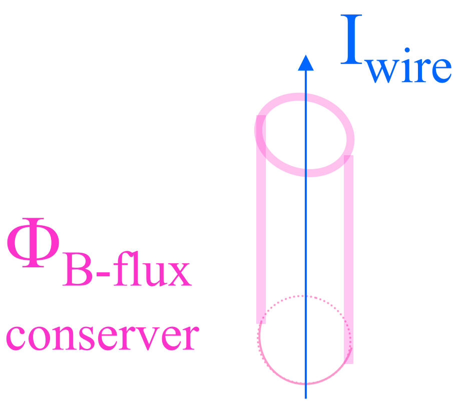

Kink
unstable

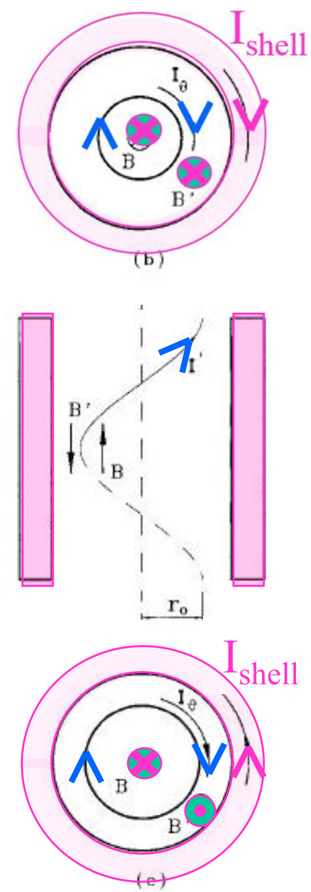

solenoidal effect
by the wire itself

… saturates when
edge field reversal
is reached

Early elements:
Verhage-Furzer-Robinson NF 1978
Kadomtsev 1992 (Sawer PoF1959)

Elaborated in:
Benisti Escande EFTC 1998
Escande et al. PPCF 2000

$r_0 \rightarrow 1$ (disruption) for too small $\frac{I_{wire}}{\Phi}$
(Tokamak case)

RFP Toy model: useful to describe the “slinky -phase locking- effect ”

After kinking …

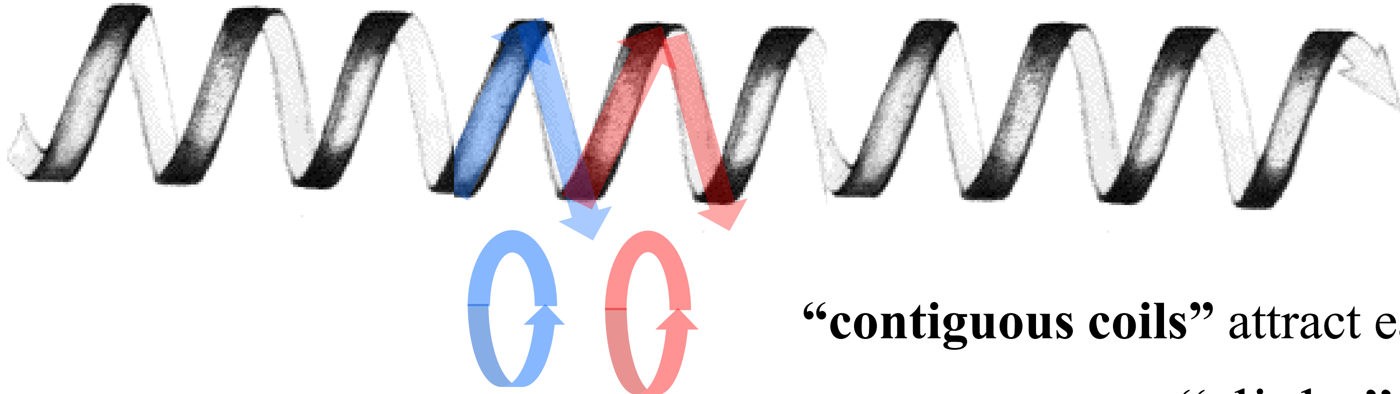

“contiguous coils” attract each other …

…“slinky” instability

… localized collapse

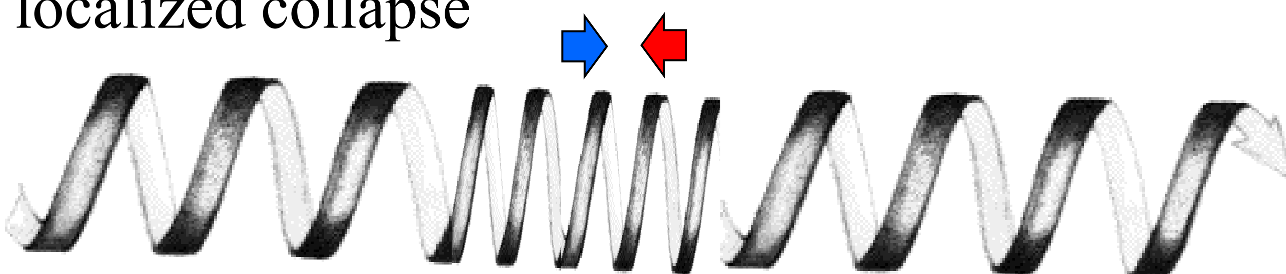

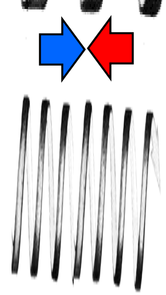

plasma buldging-collapse at a toroidal location, similarly in experiments and nonlinear modeling…

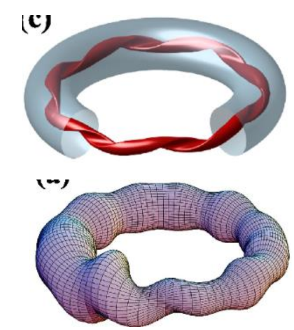

Cappello et al., Theory of Fusion Plasmas - Varenna 2008

3D nonlinear MHD

SpeCyl code - simple visco-resistive approx.

Cappello & Biskamp Nucl. Fus. 1996

$$\frac{\partial \boldsymbol{B}}{\partial t} = \nabla \wedge (\boldsymbol{v} \wedge \boldsymbol{B}) - \nabla \wedge (\boxed{\eta}\, \boldsymbol{J})$$

$$\frac{\mathrm{d}\boldsymbol{v}}{\mathrm{d}t} = \boldsymbol{J} \wedge \boldsymbol{B} + \boxed{\nu}\, \nabla^2 \boldsymbol{v}$$

$$\rho \equiv 1, \quad p \equiv 0$$

$\eta = \tau_A/\tau_R$

$\nu = \tau_A/\tau_v$

two dimensionless parameters with assigned radial profiles

Lundquist: **S = 1 / η**

Viscous Lundquist **M = 1 / ν**

Magnetic Prandtl **P** = ν/η = M/S

Hartmann number **H** = (**νη**) $^{-1/2}$

Cappello & Escande PRL 2000

r	Finite difference
θ, φ	Spectral formulation
t	Predictor-corrector + semi-implicit

Geometry: axially periodic cylinder

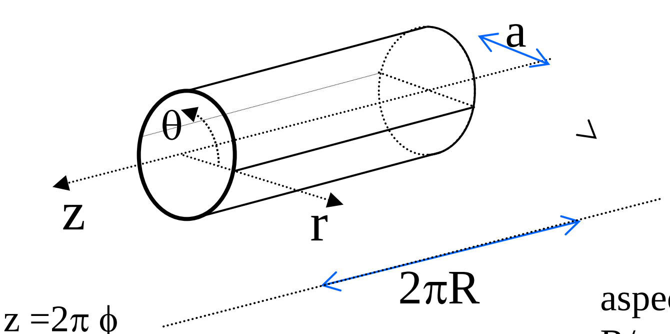

aspect ratio
R/a= 4 (RFX)

3D nonlinear MHD

SpeCyl code - simple visco-resistive approx.

Cappello & Biskamp Nucl. Fus. 1996

$$\frac{\partial \boldsymbol{B}}{\partial t} = \nabla \wedge (\boldsymbol{v} \wedge \boldsymbol{B}) - \nabla \wedge (\boxed{\eta}\, \boldsymbol{J})$$

$$\frac{\mathrm{d}\boldsymbol{v}}{\mathrm{d}t} = \boldsymbol{J} \wedge \boldsymbol{B} + \boxed{\nu}\, \nabla^2 \boldsymbol{v}$$

$$\rho \equiv 1, \quad p \equiv 0$$

$\eta = \tau_A/\tau_R$ two dimensionless parameters with assigned radial profiles

$\nu = \tau_A/\tau_v$

Lundquist: $\mathbf{S = 1 / \eta}$

Viscous Lundquist $\mathbf{M = 1 / \nu}$

r	Finite difference
θ, ϕ	Spectral formulation
t	Predictor-corrector + semi-implicit

"typical" boundary conditions:

- $B'_z = 0$ (**constant magnetic flux Φ**)
- Constant Ez (or **constant total toroidal current Iz**)

m,n
- Ideal boundary
- With MP on B r m,n (~ 2%, 4 %...)
- Thin shell + vacuum layer +ideal wall

- velocity field: no slip.

Geometry: axially periodic cylinder

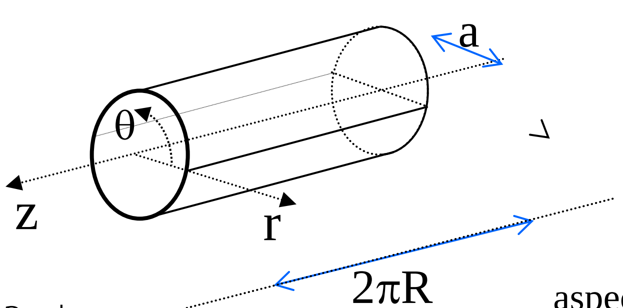

z =2π ϕ

aspect ratio
R/a= 4 (RFX)

initial conditions define Φ, Iz

SpeCyl 3D simulations: after relaxation to reversed state,
a continuous transition between different regimes is found (ideal BC):

Saturated kink
Single Helicity - SH

nearly-periodic relaxations
Multiple Helicity - MH

High dissipation

Low dissipation

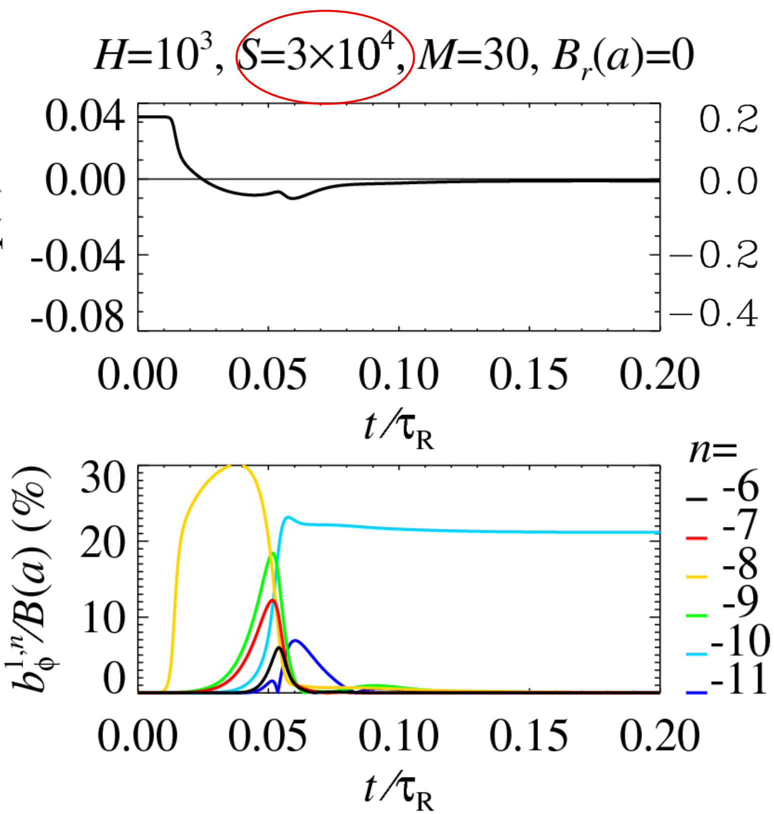

F(t)

Mode energy

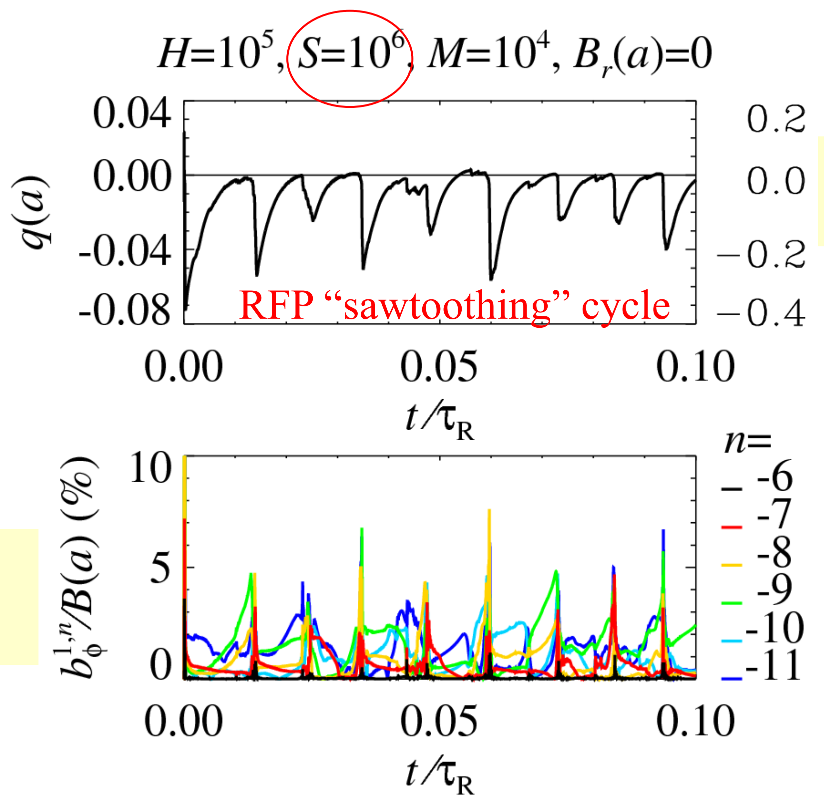

F

Example of QSH regime similar to experimental ones with MP (1,7)

(Ideal wall + MP)

Typical RFP sawtoothing

Mode amplitude

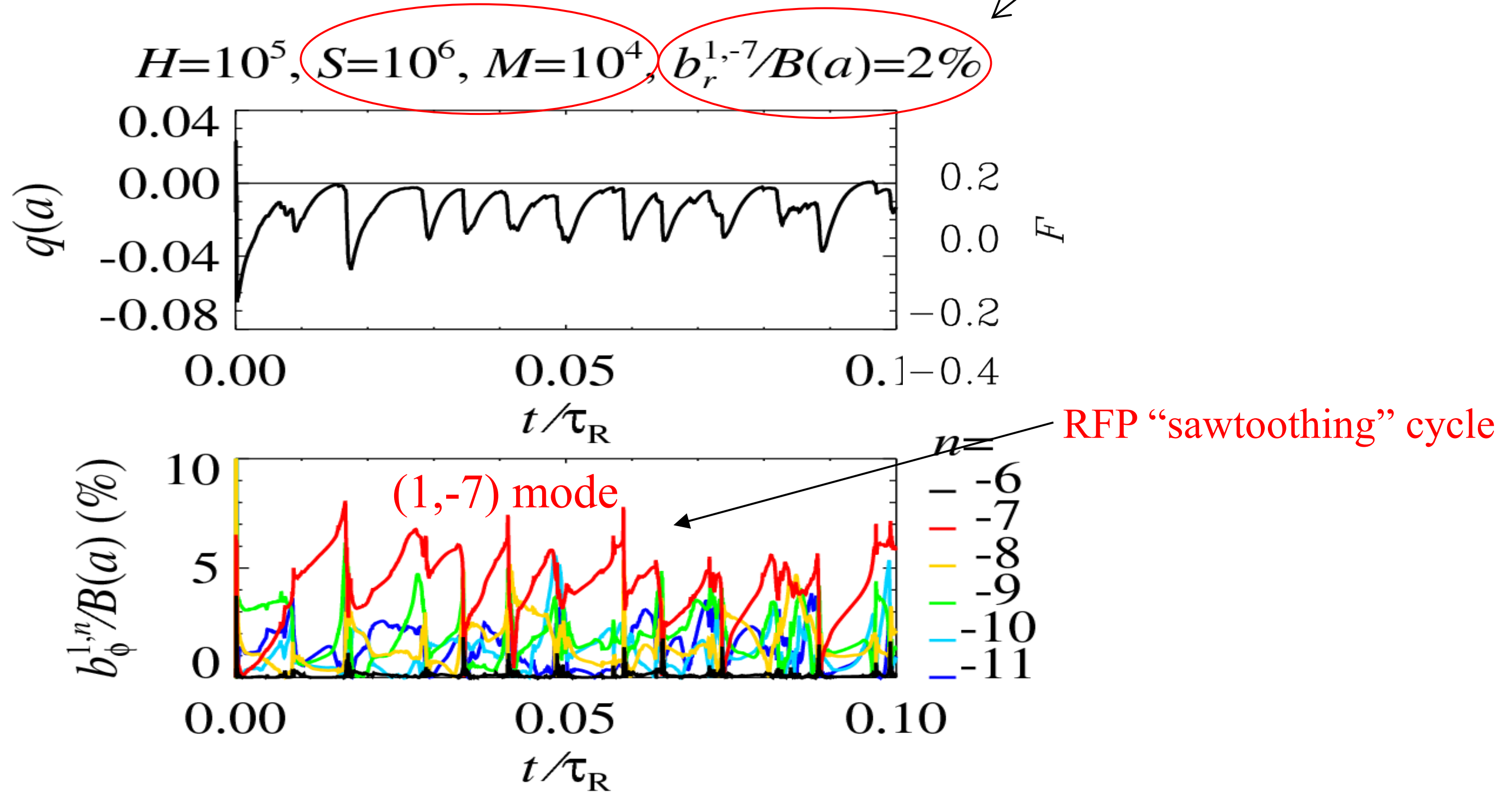

Bonfiglio NF 2011
Veranda PPCF 2013
Bonfiglio PRL 2013

The amplitude of secondary modes decreases with Lundquist, S,
The threshold MP% to excite a dominant mode decreases with S too.

Example of QSH regime similar to experimental ones - no MP

thin resistive shell +vacuum layer+ ideal wall

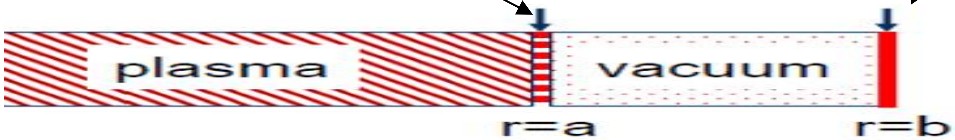

$S=10^6$, $M=10^4$, $b/a=1.2$, $\tau_W/\tau_R=10^{-2}$

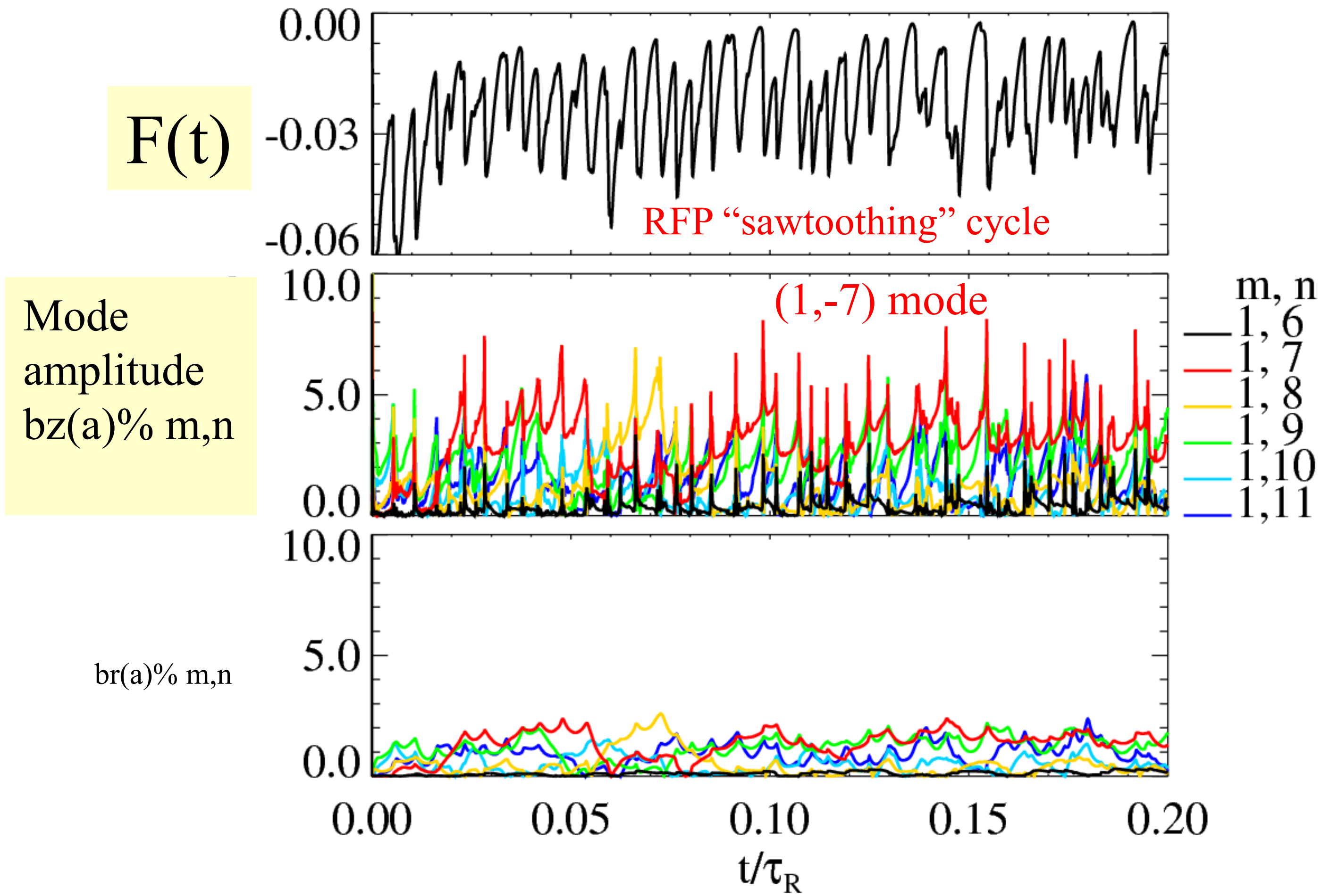

Bonfiglio EPS 2019

Chaos healing effect due to helical structure

Inspection of magnetic topology during a typical QSH sawtoothing cycle in simulations

We shall see an intermediate situation in between MH and SH

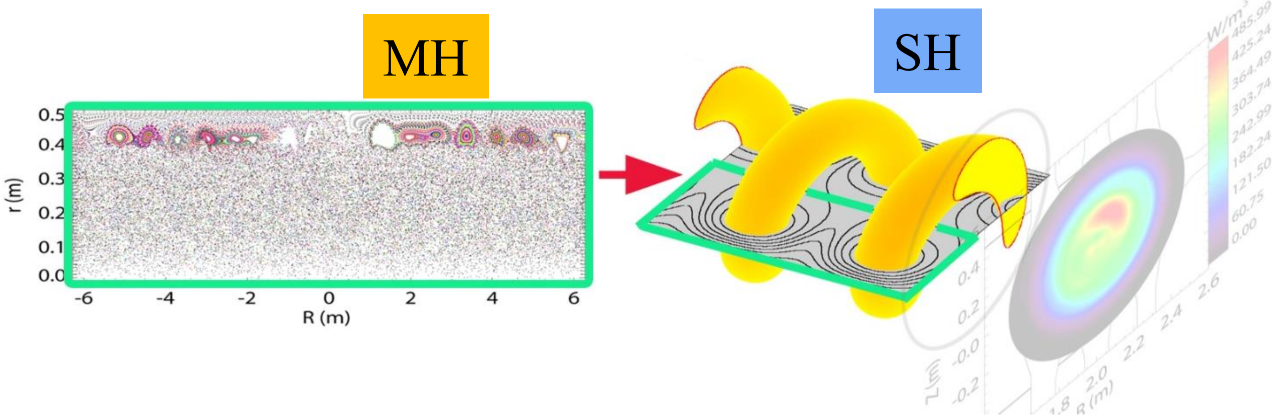

Chaos healing effect due to helical structure

[Dominant mode separatrix expulsion Escande et al PRL (2000)]

The width of conserved helical core evolves

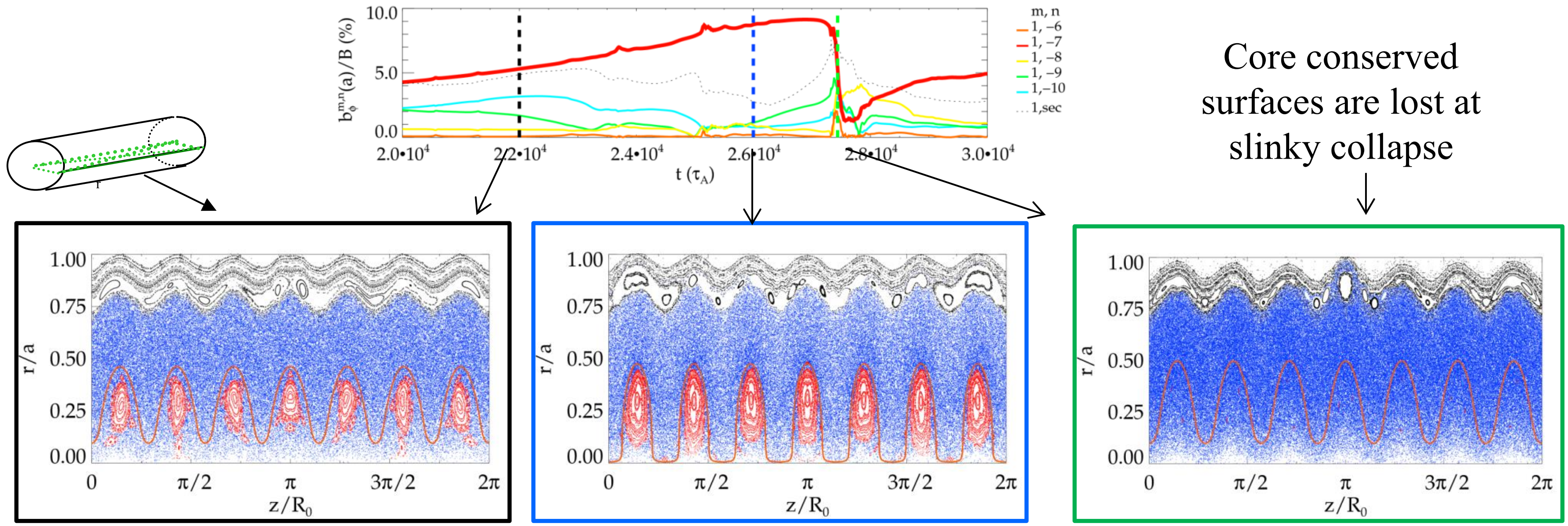

Core conserved surfaces are lost at slinky collapse

Max_q surface **(orange curve)** encompasses conserved magnetic surfaces

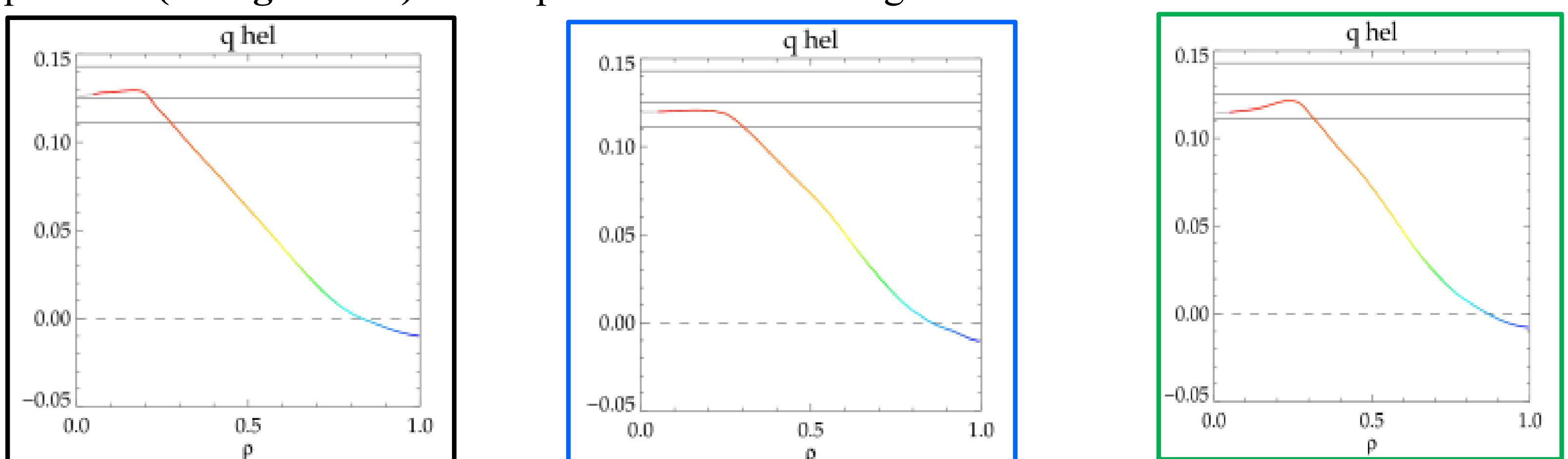

Poincare plots: secondary modes divided by 5 to match experimental amplitudes (as scaled to S= 10^7)

… in passing, a brief digression to mention the reconnection events features:

- current sheets formation,
- mode phase locking,
- excitation of Alfven waves

RFP "sawtoothing" cycle

F(t)

Mode amplitude bz(a)% m,n

Total MAGNETIC energy

Total KINETIC energy

Magnetic Energy and Helicity dissipation rates

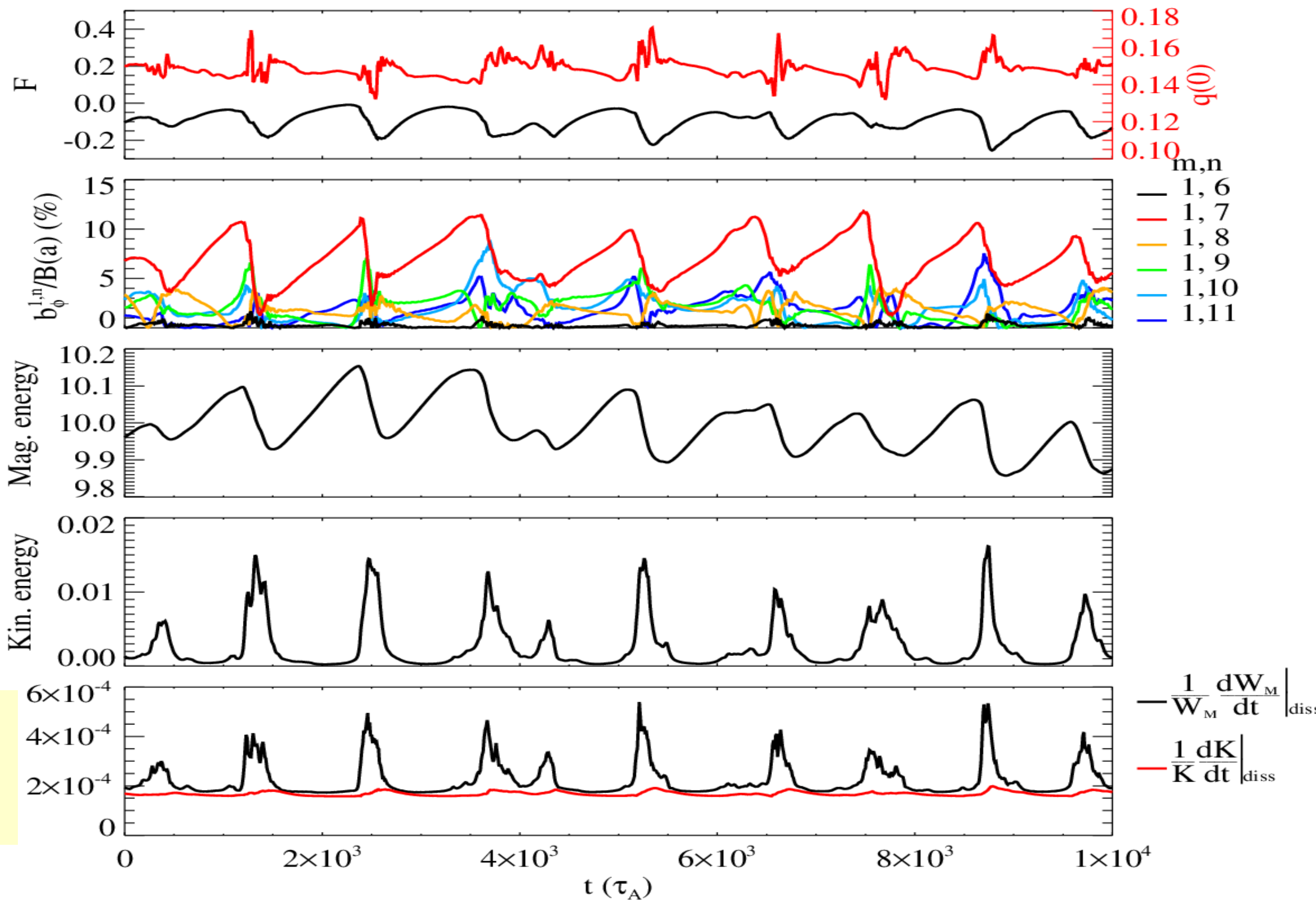

current sheets formation mode phase locking and excitation of Alfven waves

RFP $S=10^5$, $P=10$

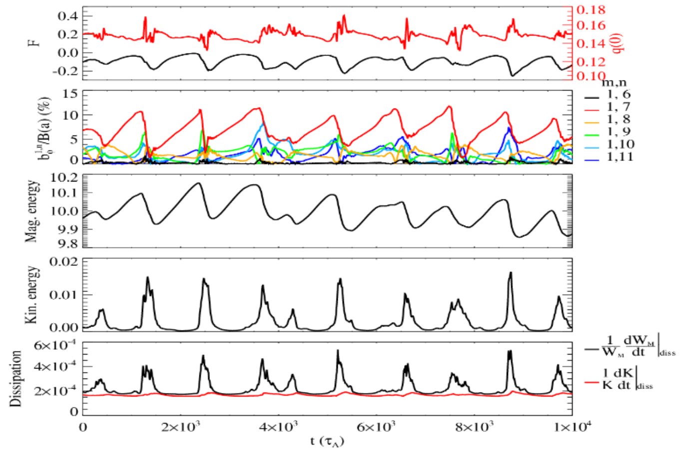

$J \cdot B$

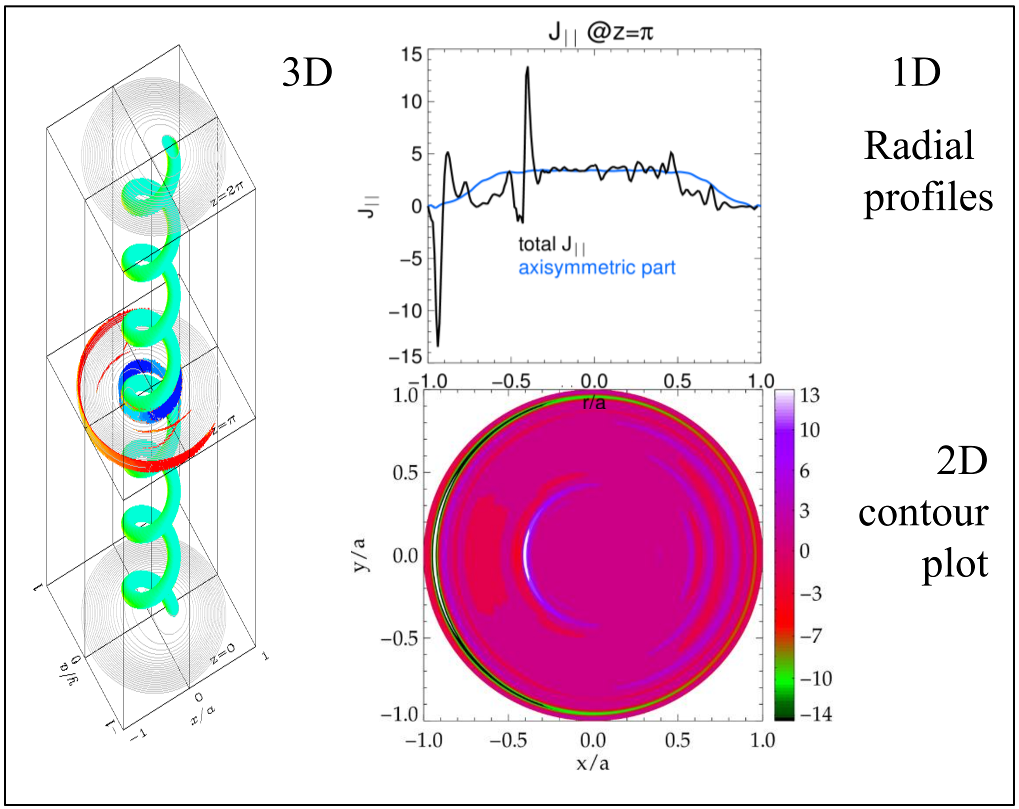

current sheets formation **mode phase locking** and excitation of Alfven waves

RFP $S=10^5$, P=10

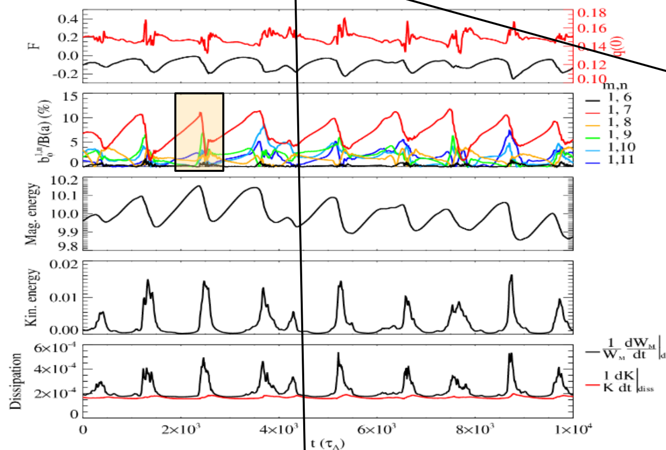

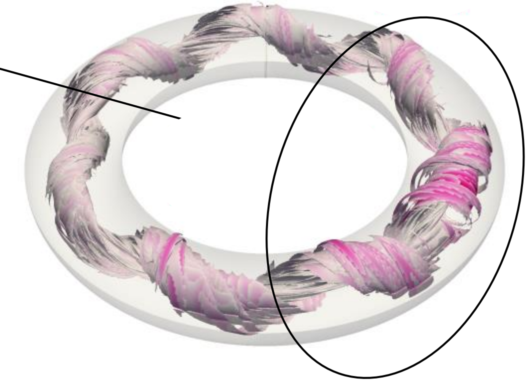

J// contours

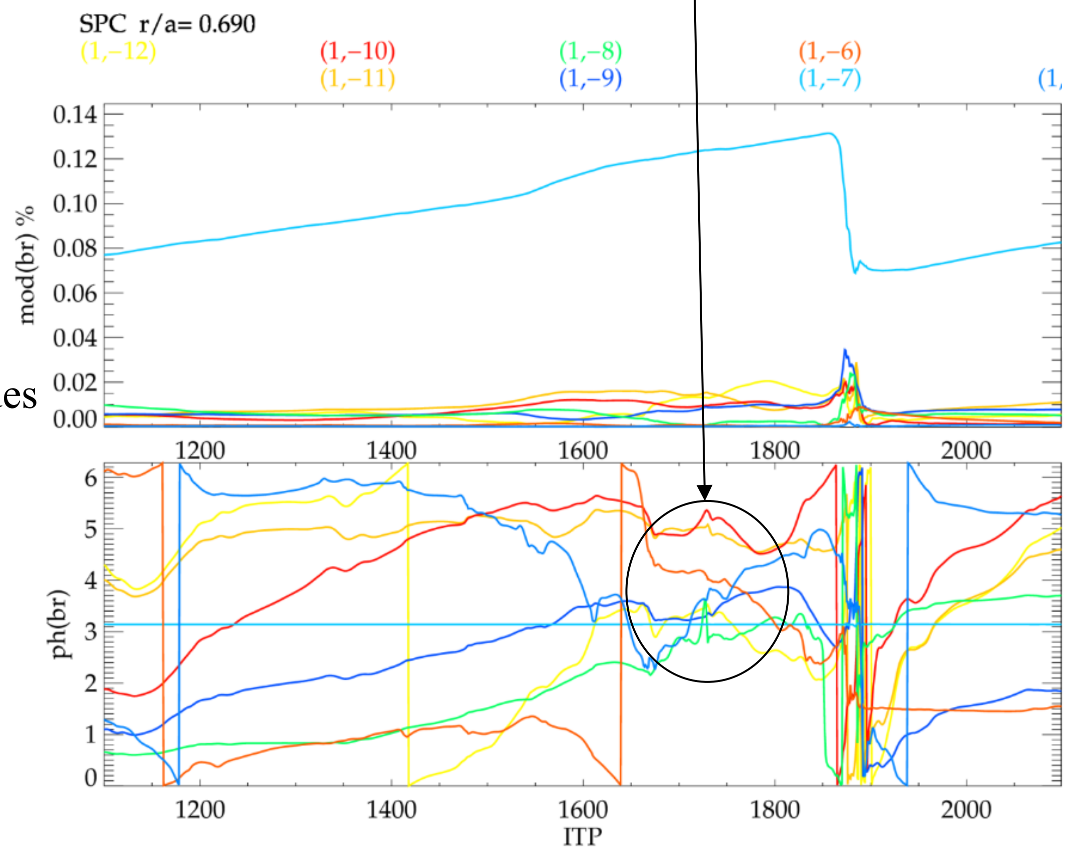

amplitudes

phases

current sheets formation mode phase locking and **excitation of Alfven waves**

RFP $S=10^5$, $P=10$

RFX-mod like density profile assigned

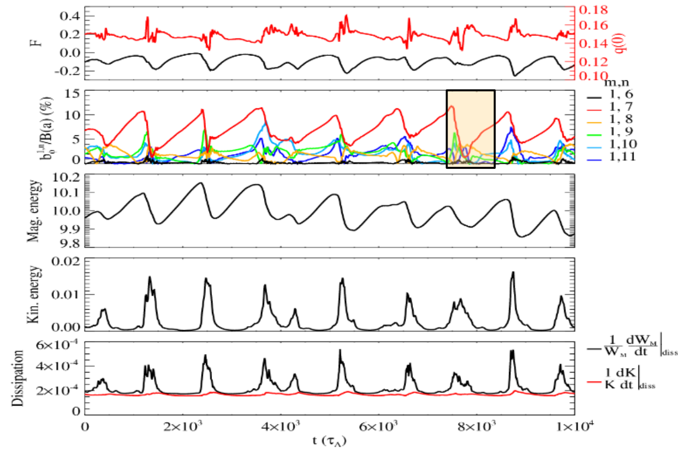

Alfvén Eigenmodes (in particular the GAE and the 1^{st} CAE) are excited by magnetic reconnection event.

Alfvén waves spectrum

(m=1, n=0) r= 0,6a

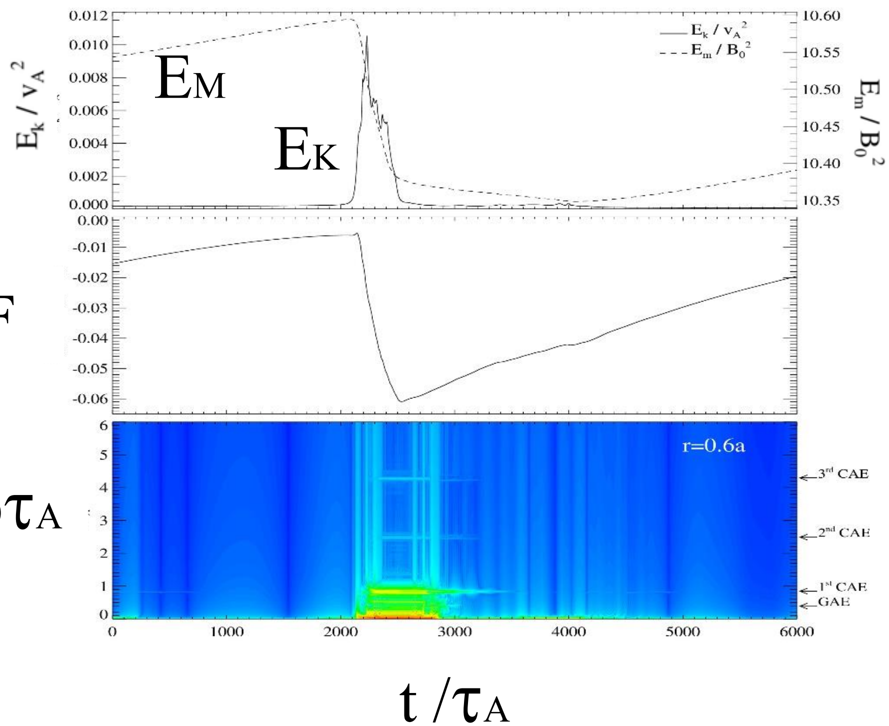

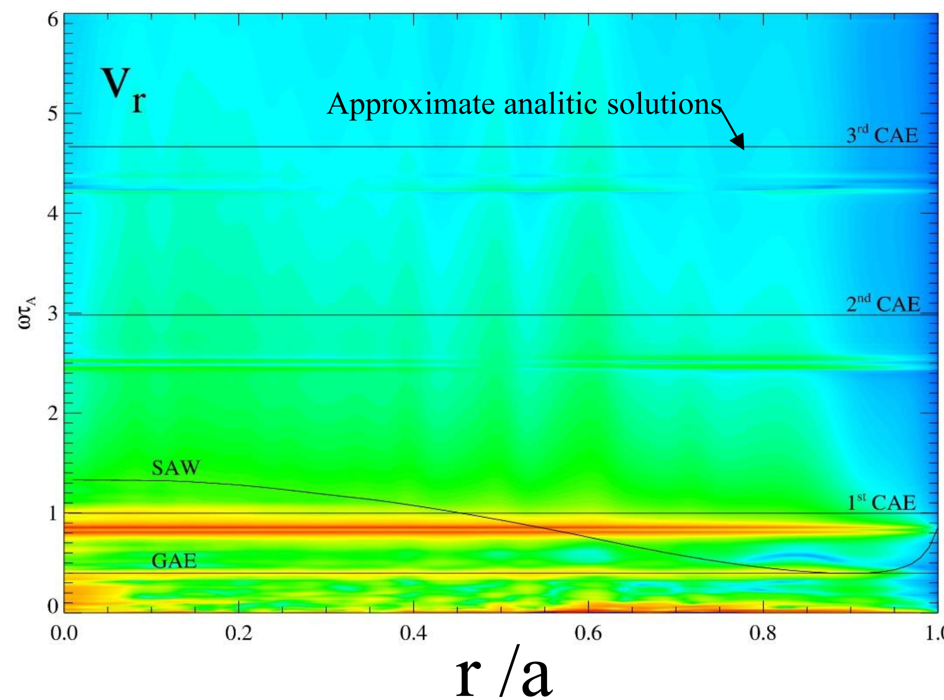

Artur Kryzhanovskyy - Master Thesis 2018 - PhD work

Experimentally observed in RFPs:

Spagnolo NF 2011 and therein refs, Koliner PRL 2012

Back to Chaos healing effect due to helical structure

… when we excite via suitable MP a Non-Resonant helical regime

More efficient chaos healing by stimulating n=6 (Non Resonant)

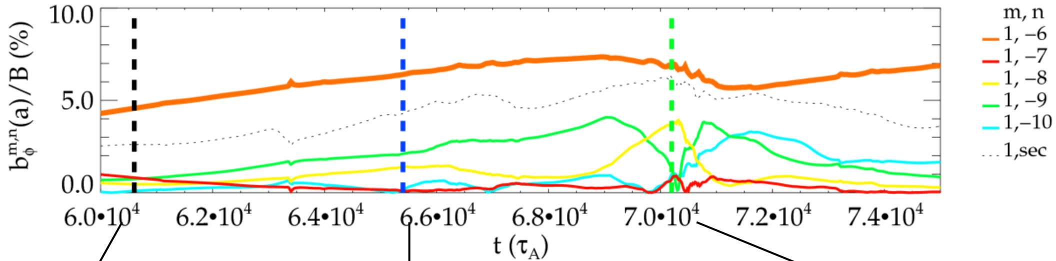

Conserved surfaces are never lost

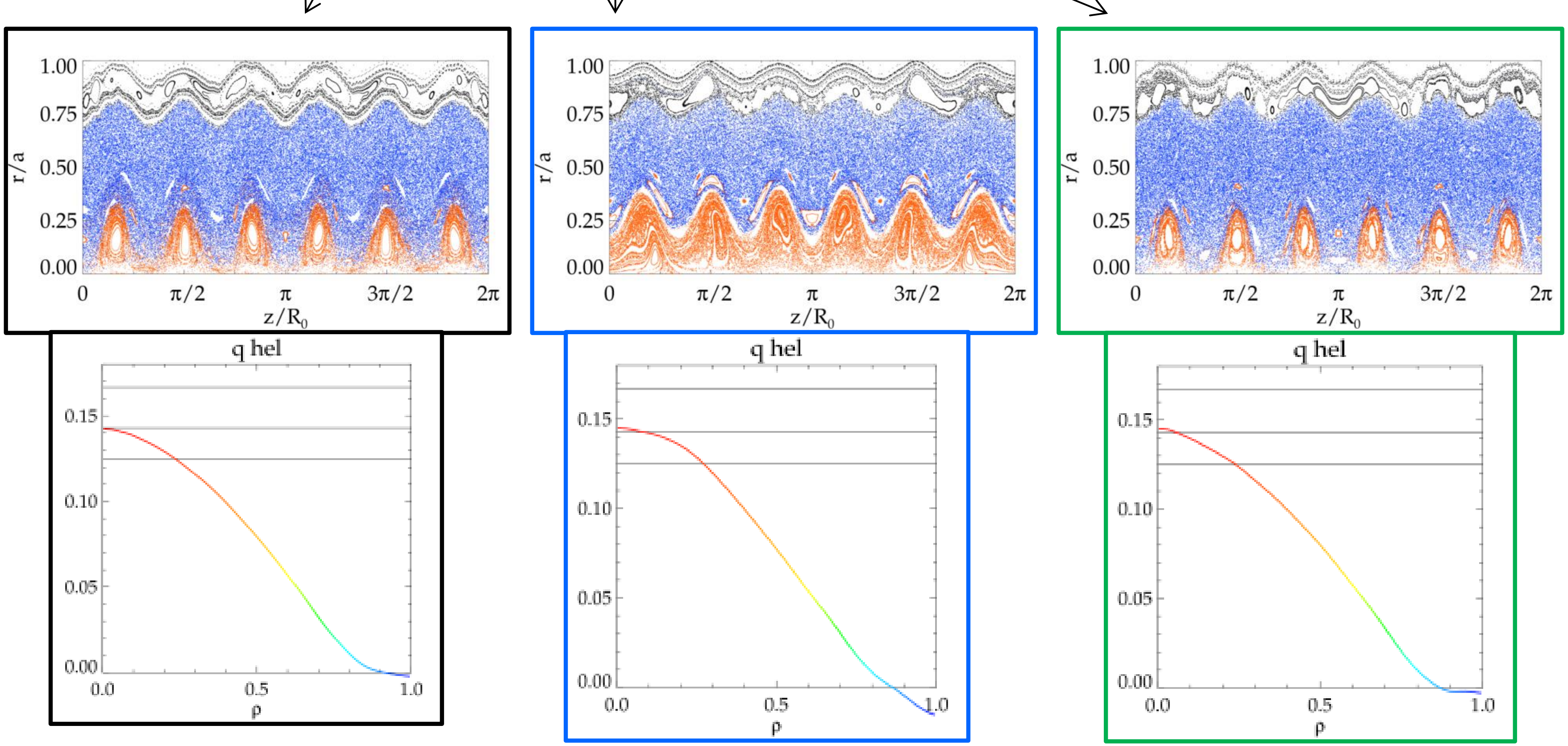

No shear reversal in such helical configurations built upon non resonant modes …

Poincare plots: secondary modes divided by 5 to match experimental amplitudes (as scaled to S= 10^7)

We started to develop:
numerical tools to detect Lagrangian Coherent Structures able to confine magnetic filed lines

Borrowed from ordinary fluid context

(spreading of “passive” entities: pollution, contaminants, pollen, …)

Collaboration with Grasso (CNR – ISC Torino, PoliTO), Pegoraro (Pisa Univesity), Borgogno (PoliTO Torino), Rubino (ENEA-Frascati)

Lagrangian Coherent Structures detection tool

Confining magnetic structures may exist hidden in the chaotic sea surrounding the conserved magnetic surfaces (KAM), “remnant” structures: small leakage Cantor sets.

Lagrangian Coherent Structures: coherent patterns that organize the transport of field lines, provide a signature of Cantor sets.

Two techniques have been developed and compared for our cases:

- FTLE “ridges” *[Shadden et al 2005 Physica D 212]*
- “most repelling structures” *[Haller, Yuan Physica D 2000 Haller Annu. Rev. Fluid Mech. 2015]*

[Di Giannatale et al, PoP2018 a,b
Di Giannatale et al, Varenna Lausanne Fusion Theory Conference, Journal of Physics: Conf. Series 2018
Pegoraro et al PPCF 2019
Soon: - Di Giannatale PhD Thesis 2019
- Di Giannatale AAPPS-DPP 2019 Poster Contribution]

First implementation of the technique to identify ridges

- simulation case (schematic one):

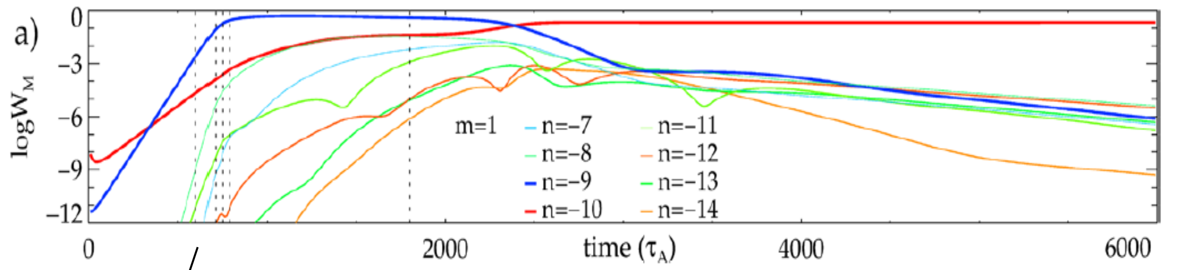

- Poincare' plot: developing chaos

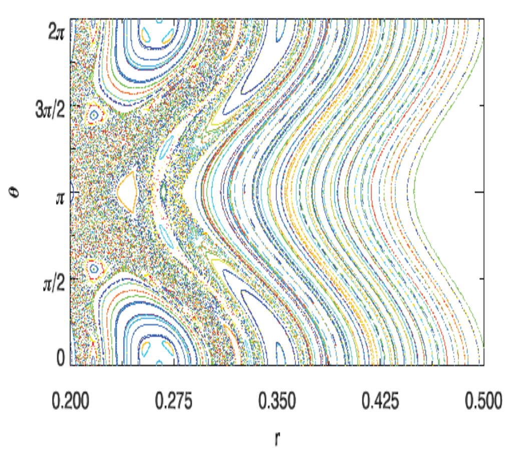

(integration length order of 1000 toroidal turns)

[Rubino, Borgogno, Veranda, Bonfiglio, Cappello, Grasso ***PPCF (2015)*** *]*

First implementation of the technique to identify ridges

- simulation case (schematic one):

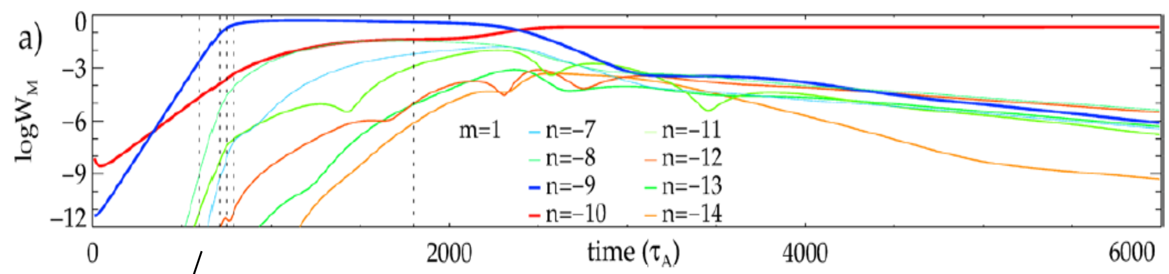

- Poincare' plot: developing chaos

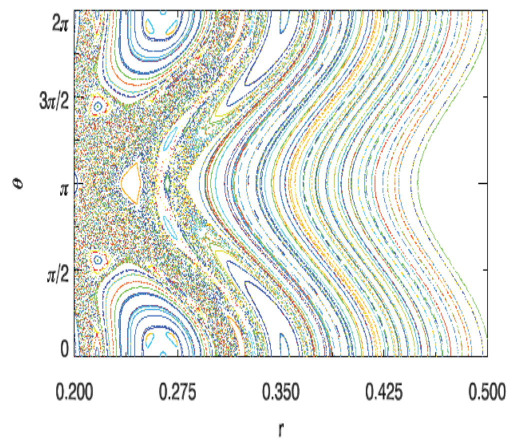

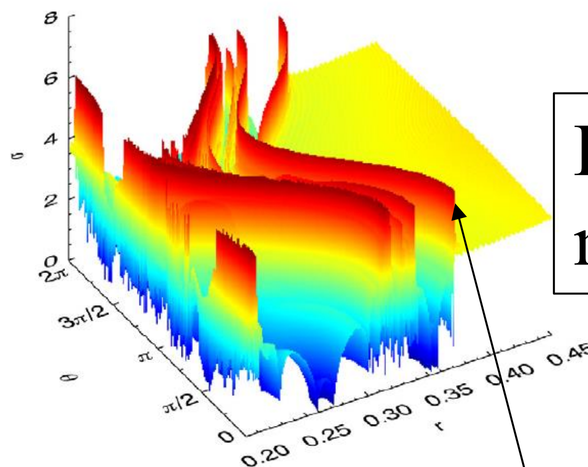

FTLE map

(integration length order of 1000 toroidal turns)

- Algorithm to extract extrema, which identify the ridges …

[Rubino, Borgogno, Veranda, Bonfiglio, Cappello, Grasso ***PPCF (2015)*** *]*

"Ridges": barriers to the transport of magnetic field lines

Black "curves": RIDGES

Color: magnetic field lines integrated for 100 toroidal turns

(>> FTLE computation time = 10 toroidal turns)

Ridges detect confining cantori structures

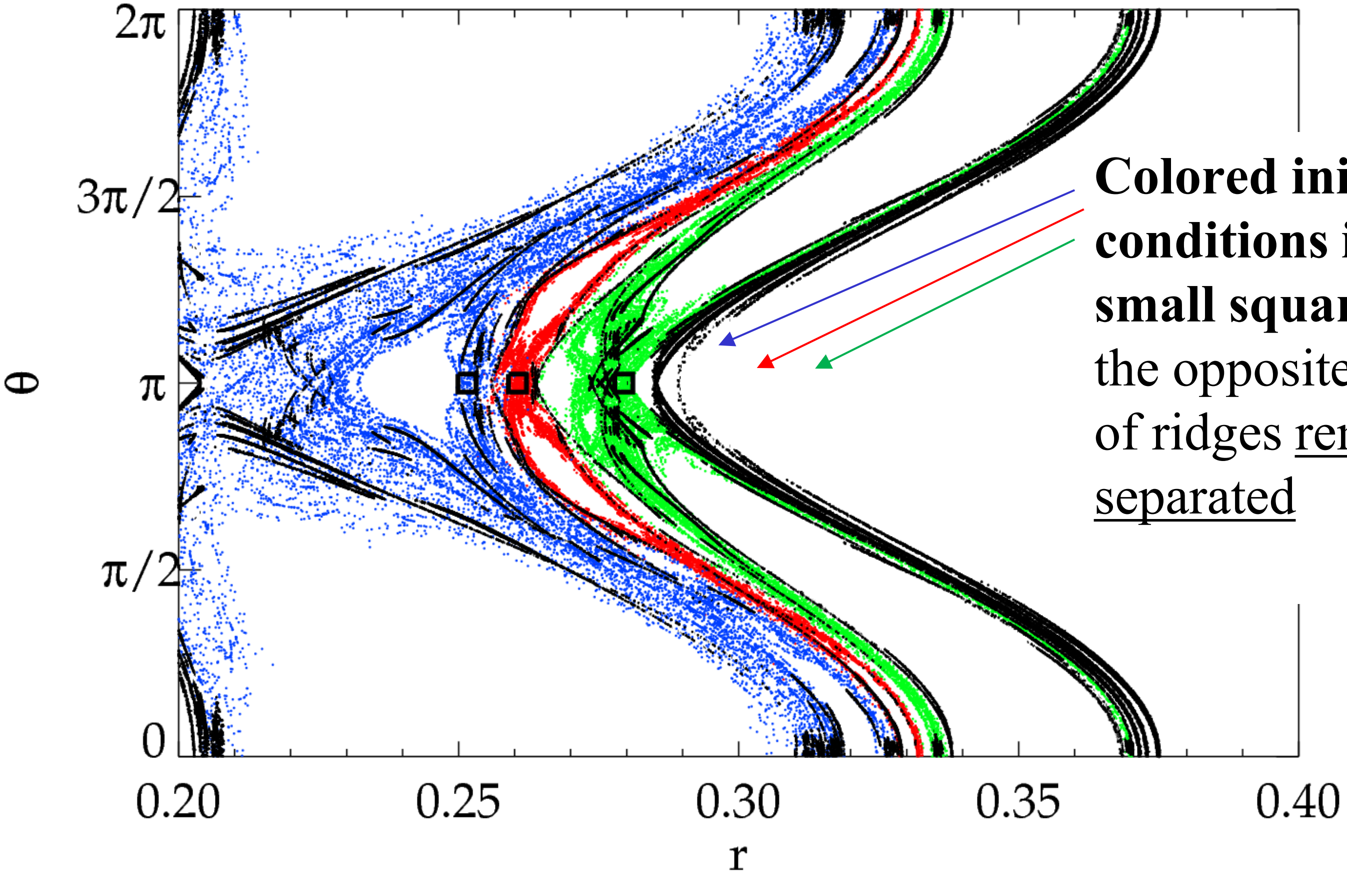

Colored initial conditions in the small squares at the opposite side of ridges <u>remain separated</u>

LCS (Haller) and "Ridges" (Shadden) techniques comparison:

No significant differences in our cases:

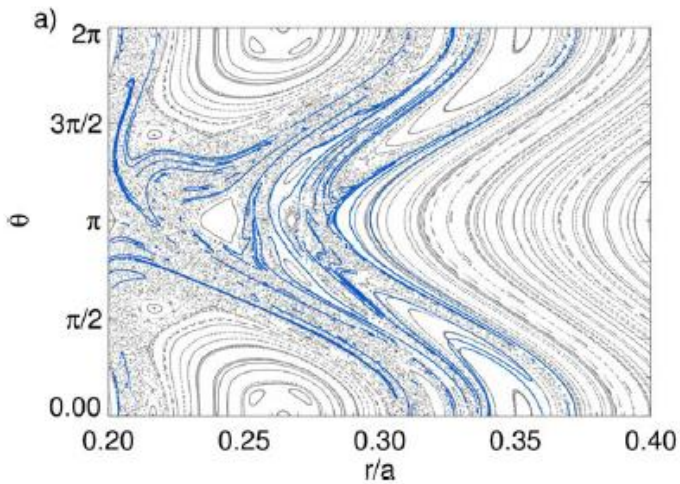

Figure 2. Poincaré map and Lagrangian coherent structures (LCS) of the magnetic configuration corresponding to the snapshot taken at $t = 600\ \tau_A$, i.e. before the formation of the quasi-helical state. LCS are overplotted in blue. In this picture we show only the relevant radial region around the $m = 1$, $n = 9$ helical core (at $r = 0.26a$, $\theta = 0$), where a weakly chaotic magnetic field is present.

Plasma Phys. Control. Fusion **61** (2019) 044003

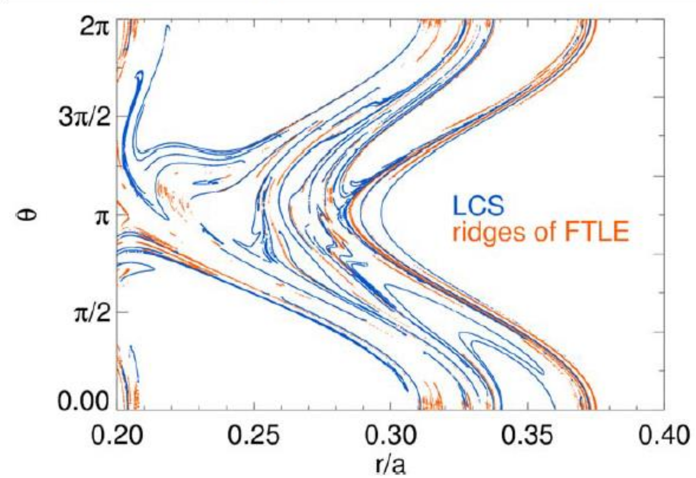

Figure 4. Comparison between the structure of repelling LCS in blue (the same as the ones in figure 3) and the ridges of the finite time Lyapunov exponents (FTLE) in orange (same as computed in figure 7 of [46]). They are qualitatively similar but LCS offer the deepest insight of the topological structure of coherent structures.

Pegoraro F., Bonfiglio, Cappello, Di Giannatale, Falessi, Grasso, Veranda, PPCF (2019)

Back to Chaos healing effect due to helical structure

… LCS detected in simulation cases

(soon application to RFX experimental data)

Lagrangian coherent structures **detected** nearby conserved surfaces

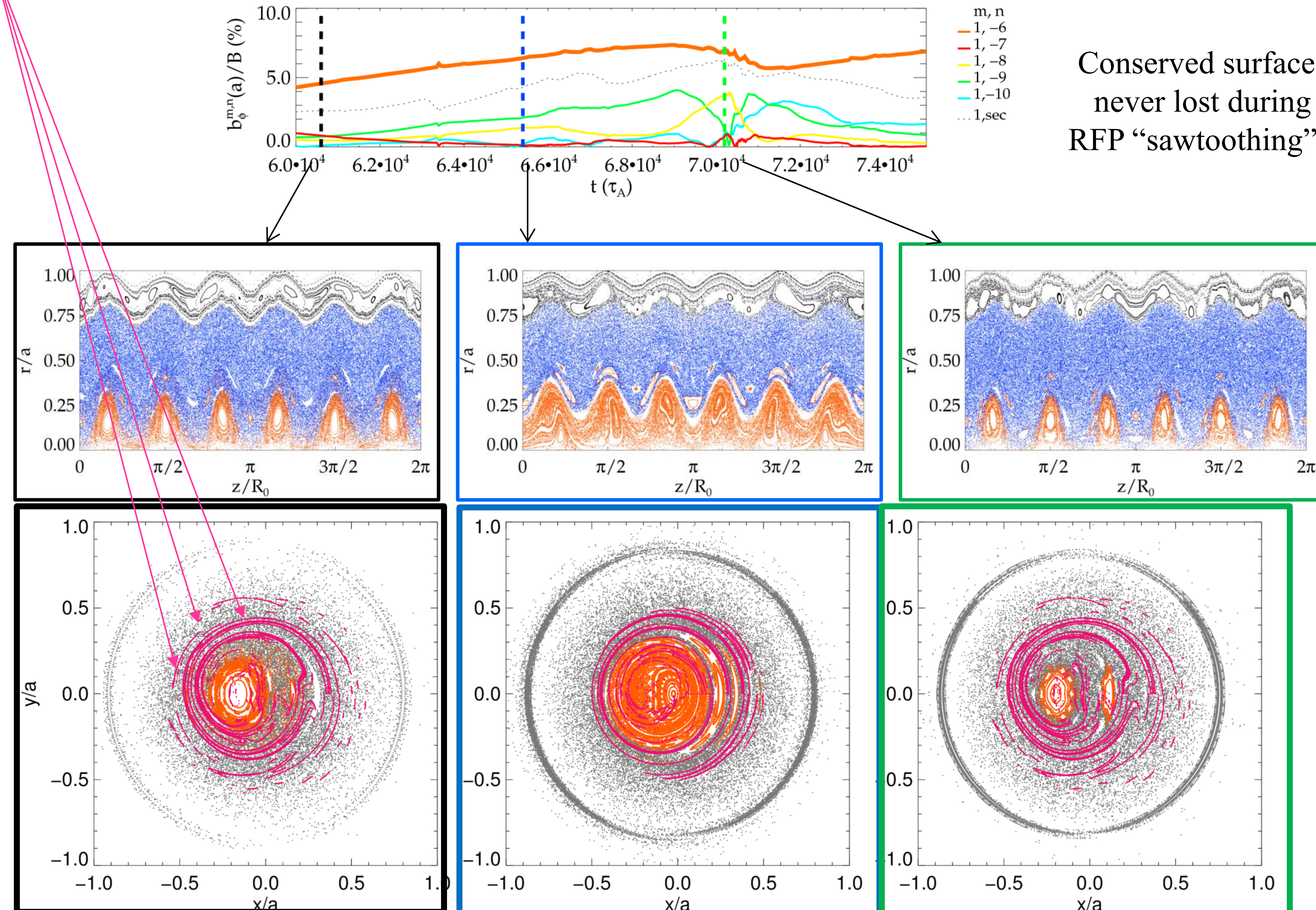

Conserved surfaces are never lost during the RFP "sawtoothing" cycle

The possibility to convey the experimental discharge toward a “new” chosen helical solution

In particular, low n non resonant helix, has been tested in RFX-mod ..

Dynamics successfully confirmed in RFX-mod experiment

<u>Small edge Magnetic Perturbations</u> (MP) **can drive new helical regimes**, with different pitch:

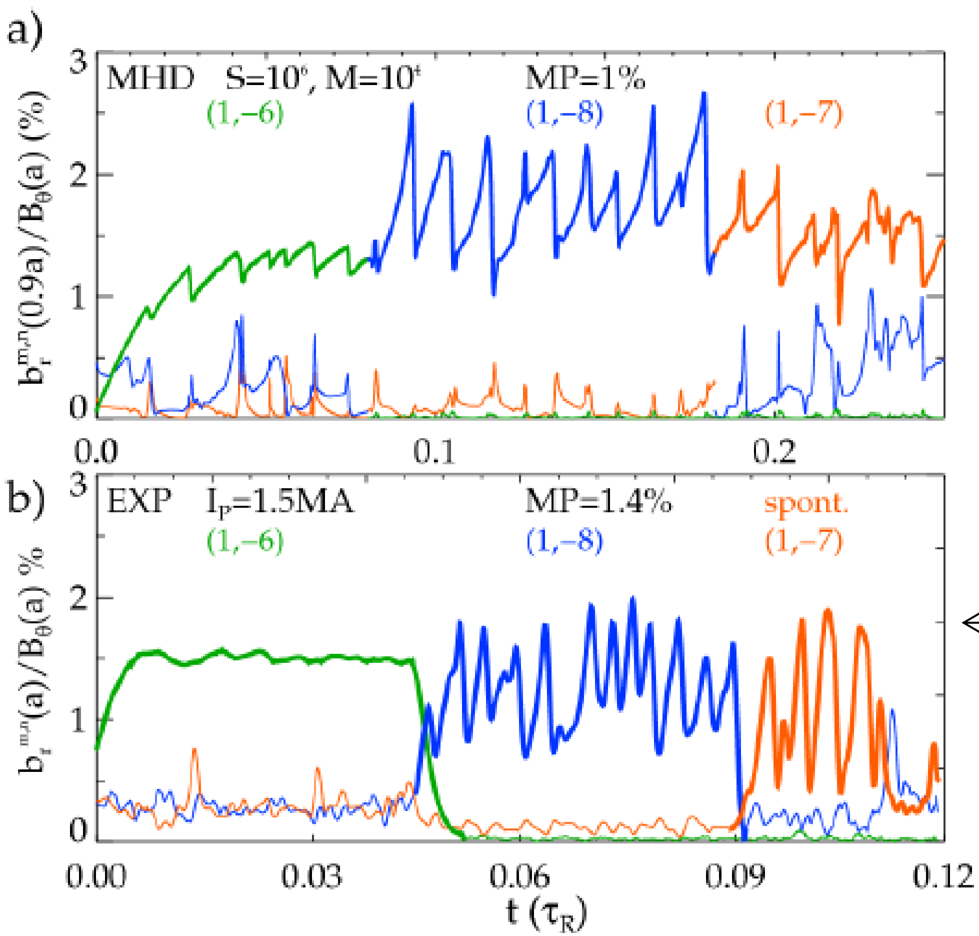

simulation

Successful RFX-mod experiments:
alternative *ns* stimulated by seed MP

Veranda, Bonfiglio, Cappello et al NF 2017

Summary

Helical self-organization characterizes the Reversed Field Pinch:

- Experiments show formation of thermal and impurity particle barriers,
- 3D MHD shows magnetic chaos healing and hidden coherent structures

(Lagrangian Coherent Structures LCS),

- New global helical regimes stimulated by seed Magnetic Pertubations,
  - ✓ Characterized by tunable amplitude and frequency of «sawtoothing»,
  - ✓ Suggested by MHD and obtained in RFX-mod,
  - ✓ 3DMHD Non resonant modes provide more efficient chaos healing

Await for further experiments in RFX-mod**2** from 2021

Where we expect lower secondary modes,
due to closer conductive shell and more effective feedback coils action.

RFX device evolution: plasma radius and magnetic front-end

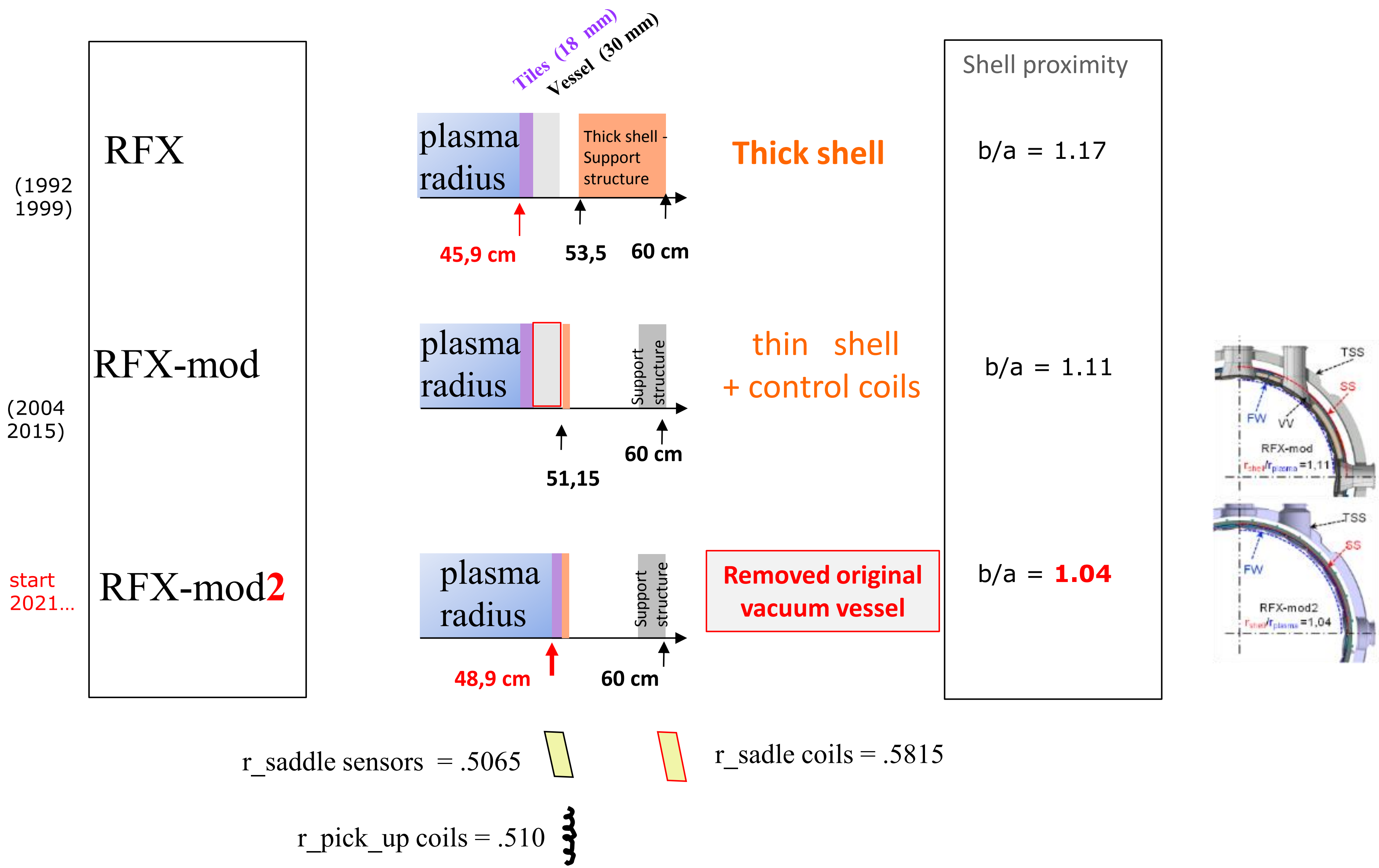

Bondary conditions SpeCyl, several options:

"typical" boundary conditions for mean fields B o,o:

- B'z =0 (**constant magnetic flux Φ**)
- Constant Ez (or **constant total toroidal current Iz**)
    - Ideal boundary
    - With MP on B r m,n (~ 2%, 4 %...)
    - Thin shell + vacuum layer
- velocity field: no slip.

For $b_{m,n}$

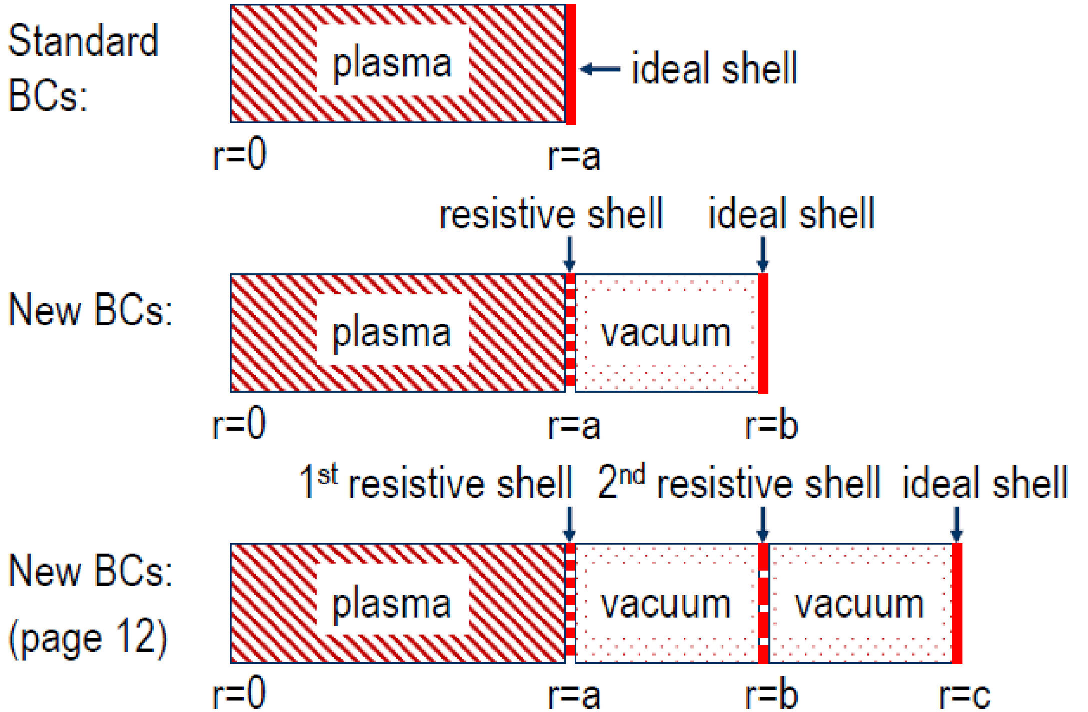

[1] S. Cappello and D.F. Escande, Phys. Rev. Lett **85**, 3838 (2000)
[2] R. Lorenzini, et al., Nature Physics **5**, 570 (2009); J.S. Sarff, et al., Nucl. Fusion **53**, 104017 (2013)
[3] D. Bonfiglio, M. Veranda, S. Cappello, et al., Phys. Rev. Lett **111**, 085002 (2013)
[4] M. Veranda, D. Bonfiglio, S. Cappello, et al., Nucl. Fusion **57**, 116029 (2017)
[5] L. Marrelli, R. Cavazzana, et al., Nucl. Fusion **59**, 076027 (2019)
[6] S. Cappello and D. Biskamp, Nucl. Fusion **36**, 571 (1996)
[7] D. Bonfiglio, L. Chacón, and S. Cappello, Phys. Plasmas **17**, 082501 (2010)
[8] T. C. Hender, C. G. Gimblett, and D. C. Robinson, Nucl. Fusion **29**, 1279 (1989)
[9] D. Schnack and S. Ortolani, Nucl. Fusion **30**, 277 (1990); R. Paccagnella et al., Nucl. Fusion **47**, 990 (2007)

When QSH dominant mode GROWS: separatrix expulsion occurs, and

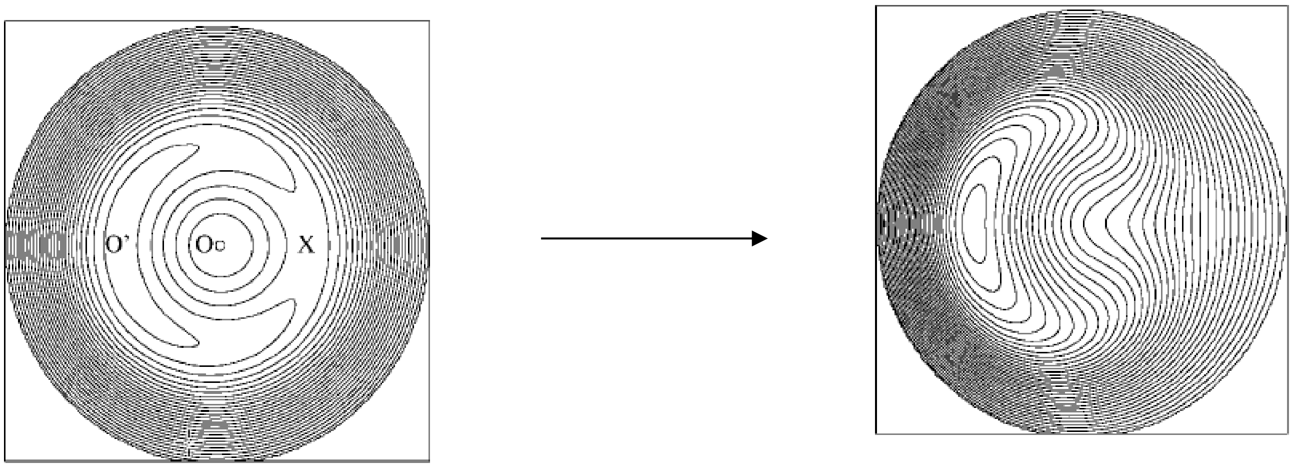

(a) (b)

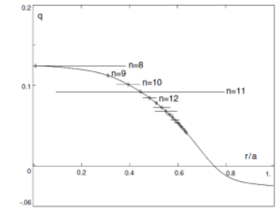

FIG. 2. q profile and magnetic islands width (shown by horizontal bars) of different $m = 1$ modes.

…clean helical topology emerges

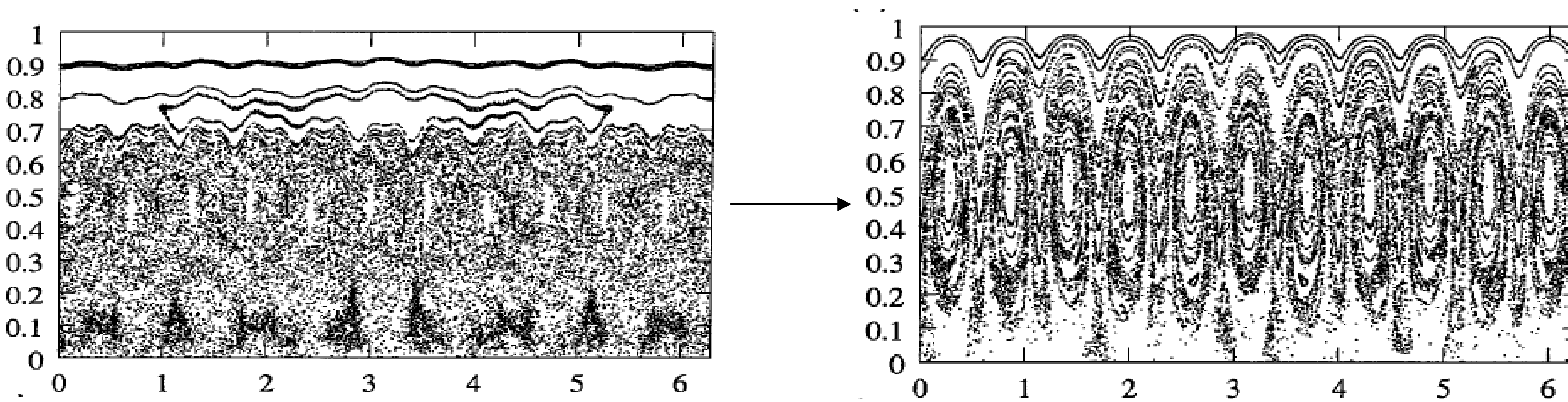

Escande, Paccagnella, Cappello et al PRL 2000

LCS (blue) and Connection length maps

LCS mark radii where large Lc gradients are seen

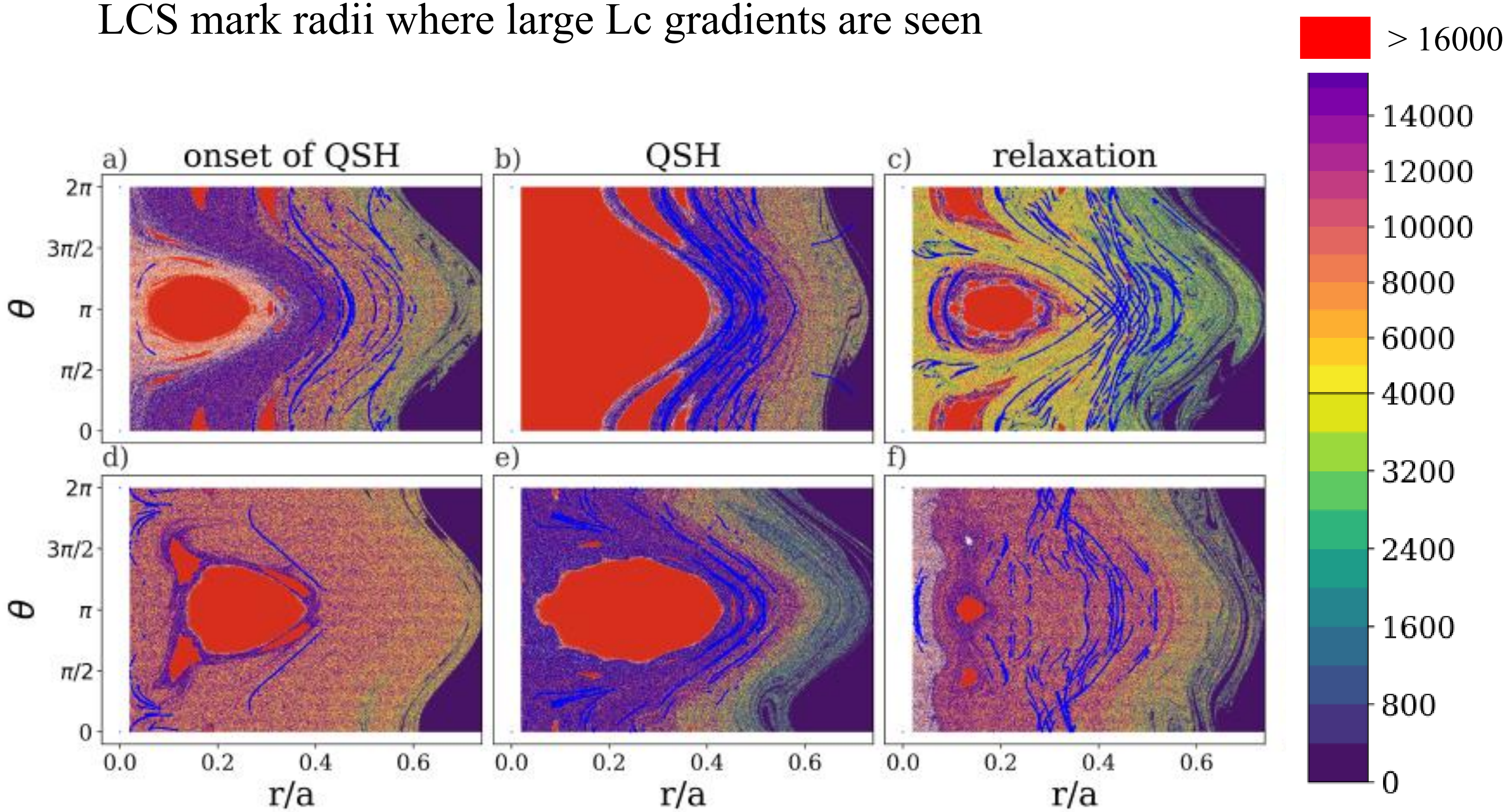

Figure 9. Bundles of Lagrangian Coherent Structures (LCS, blue lines) are a common feature of quasi-helical regimes. We plot the connection length to the edge confining structures of magnetic field lines. In red we color the regions where $L_c = L_{c,max} = 10^5$. The blue LCS divides regions with different connection length.

T_e, n_e get a helical shape - T_e steep gradients …

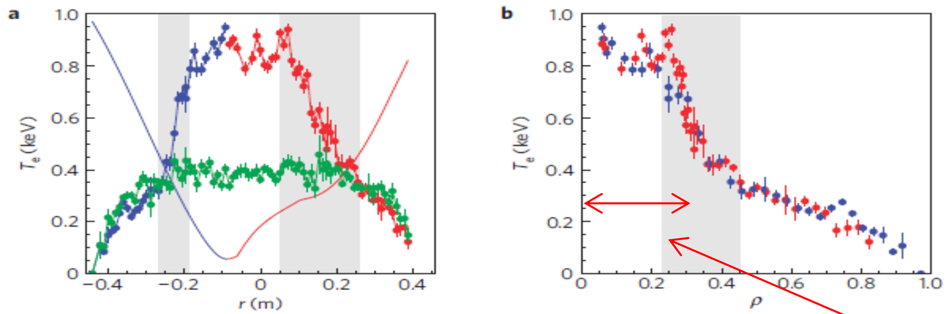

Lorenzini et al NatPhys 2009

... not stationary …
Temporal evolution of thermal structure under investigation

Grad (Te) vs time

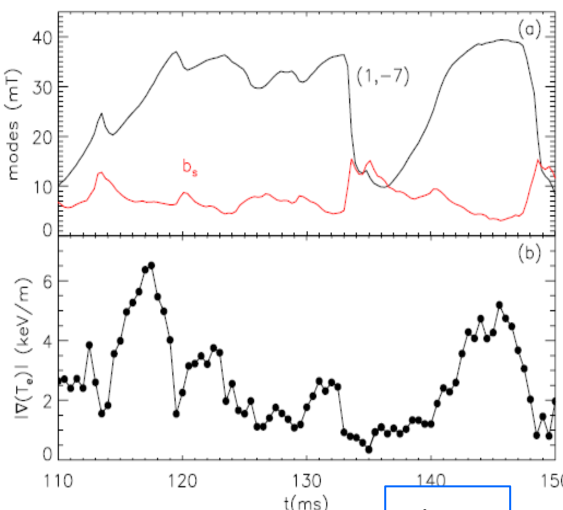

time

Franz et al NF 2013
Gobbin et al PPCF 2013

Thermal structure width: increases with helical amplitude

Secondary modes

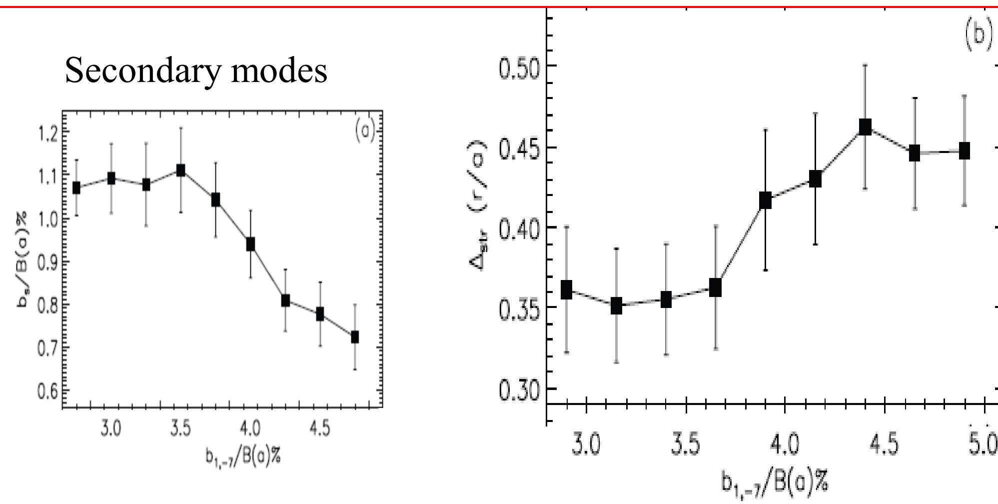

helical mode amplitude

helical mode amplitude

Gobbin et al PPCF 2015

Main NUMERICAL TOOLS involved on the modeling side

- **3D nonlinear MHD** – viscoresitive approximation:

  SpeCyl [a] - PIXIE3D [b] (benchmarked codes) [c]

- **Magnetic Field line integration**:

  NEMATO [d] (benchmarked vs ORBIT code [e])

- **Lagrangian Coherent Structures** detection [f, g]

[a] Cappello, Biskamp **NF** 1996
[b] Chacòn **CPC** 2004, Chacòn **PoP** 2008
[c] Bonfiglio, Chacon, Cappello **PoP** 2010
[d] Finn, Chacòn **PoP** 2005
[e] Ciaccio, Veranda, Bonfiglio, Cappello, Spizzo, White **PoP** (2013)
Recent collaboration with Borgogno (CNRS-Nice), Rubino and Grasso (CNR – ISC Torino, PoliTO) :
[f] Rubino, Borgogno, Veranda, Bonfiglio, Cappello, Grasso **PPCF** (2015)
[f] Di Giannatale, et al **POP** a,b (2019)
[f] Pegoraro, **PPCF** (2019)

Taylor's relaxation theory for the RFP.

Gained quickly an enormous success due to its ability to explain field reversal.

In fact, at the beginning, the solenoidal effect of the toy model appeared too small to provide a convincing explanation…

J. B. Taylor PRL 1974
J. B. Taylor Rev. Mod Phys. 1986

Taylor's relaxation theory for the RFP.

Taylor's conjecture involves
the **Magnetic Helicity** associated with a flux tube

$$K_V = \int_V \mathbf{A} \cdot \mathbf{B}\, d^3x$$

(**A:** vector potential)

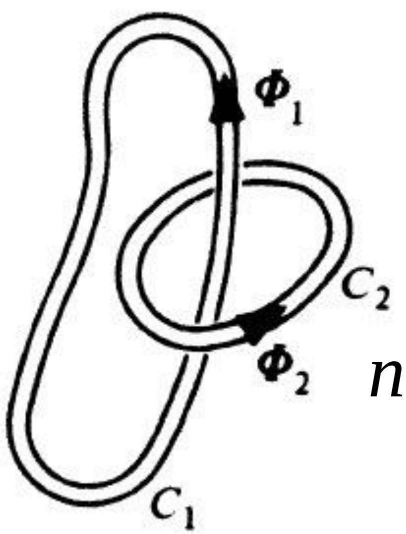

n=1

K is related to the topological complexity of B field, for example, for the two flux tubes knotted *n* times:

$$\boxed{K_V = (+/-)\ n\,\Phi_1\Phi_2}$$

Woltjer theorem (1958) showed that for an ideal plasma (must conserve Kv for any flux tube αi) the minimum energy solution requirement leads to the force free equation

$$\nabla \wedge \mathbf{B} = \alpha_i\, \mathbf{B}$$

Taylor's relaxation theory for the RFP.

Conjecture:

small resistivity allows for total magnetic helicity conservation in a flux conserving volume

<u>search for minimum energy states</u> with constraint on $\mathbf{K_0}$ and $\mathbf{\Phi}$

$$K_0 = \int_{Volume} \mathbf{A} \cdot \mathbf{B} \, d^3x$$

INVARIANT

$$\Phi = \int_S \mathbf{B} \cdot d\mathbf{s}$$

CONSERVED

$$W = \int_{Volume} \frac{\mathbf{B}^2}{2\mu_0} \cdot d^3x$$

(internal energy neglected)

Variational principle (related Euler-Lagrange equation), which ends up to coincide with force free condition:

$$\nabla \wedge \mathbf{B} = \mu \mathbf{B}$$

μ is the <u>Lagrange multiplier</u> determined by the invariants of the problem $\mathbf{K_o}$ and $\mathbf{\Phi}$, in particular :

$$\mu \leftrightarrow \frac{K_0}{\Phi^2}$$

being $\nabla \wedge \mathbf{B} = \mu_o \mathbf{J}$

the useful relation holds:

$$\mu = 2\Theta / a$$

Taylor 1986

Martin Taylor (Culham Rep) 1974

Axisymmetric solutions

Bessel Function Model (BFM)

For $\mu a \geq 2.4$ reversed field B_ϕ

$\Theta \geq 1.2$

compared with experimental measurements

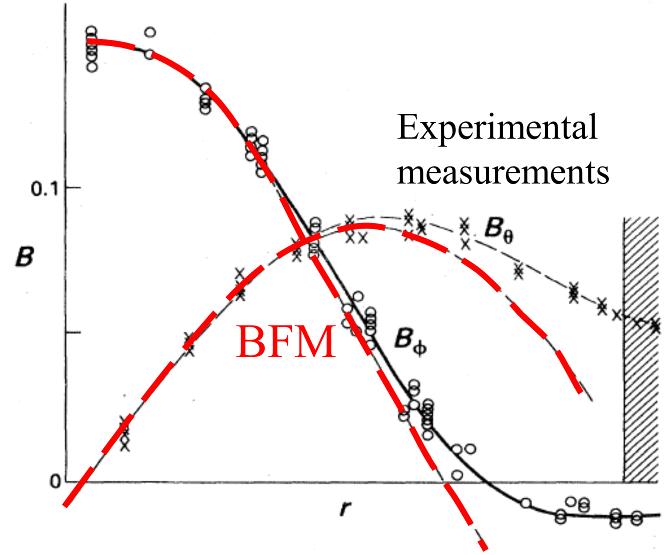

FIG. 2. Experimental and theoretical magnetic field profiles. HBTX-1A (from Bodin, 1984).

Rev. Mod. Phys., Vol. 58, No. 3, July 1986

Helical solutions for $\mu a \geq 3.12$

K_o / Φ^2 determine periodicity and amplitude

while $\mu a \geq 3.12$ remain fixed,

i.e. saturation of the pinch parameter at $\Theta = 1.56$

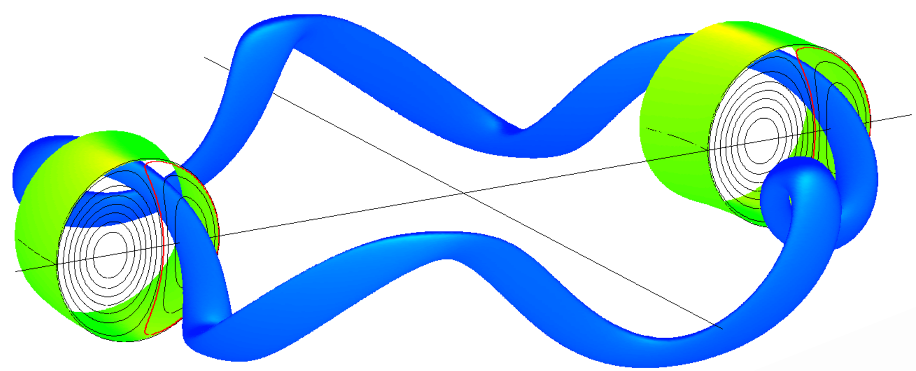

m=1, n=+5 (R/a=4)
(external helicity)

Lagrangian Coherent Structure (LCS)

- What:
  - ➢In a 2D configuration are material lines advected by the fluid which organize the flow transport processes by attracting or repelling the nearby elements

- use
  - ➢LCSs divide the phase space in regions that cannot exchange particles under the finite time considered ($t-t_0$)

Two different definitions:

1) LCSs as ridges of FTLE field. Ref Shadden et all 2005. Physica D 212 (3-4), 271{304

2) LCSs as " the most attracting or repelling material lines " Ref G. Haller, A variational theory of hyperbolic Lagrangian coherent structures, Phys. D 240 (7) (2011) 574-598

Implication of Haller's definition: in addition to other requirements, repelling LCS are found integrating the eigenvector field related to minimum eigenvalue of Cauchy-Green (CG) matrix. Such matrix gives indications about how strong and in which direction a blob of initial conditions, namely particles, evolve under the flow map F.

Cauchy-Green matrix $$C(x_0) = \left[\nabla F_{t_0}^t(x_0)\right]^T \nabla F_{t_0}^t(x_0)$$

A qualitative description

Qualitatively the difference between the two methods stays in the fact that only the second one (Haller's method) assures that the LCS are material lines, that is an invariant curve under the flow, and thus they cannot be crossed by other particles.

Moreover, the Haller's method is "*Lagrangian*": the barriers are found integrating the eigenvectors of the CG strain tensor.

On the opposite, the ridge method only focuses on an analysis point by point (*Eulerian*).

Mathematically speaking:

1) the Haller's method focuses on FTLE and eigenvector of CG matrix.

2) The ridge method only focuses on FTLE and to eigenvectors associated to FTLE Hessian matrix.

A graphical definition

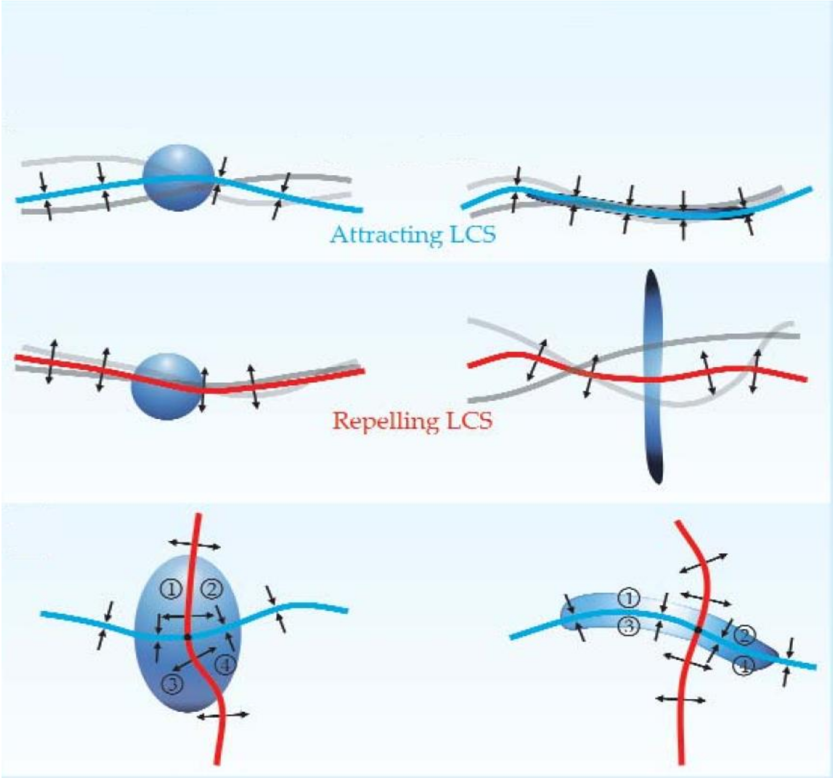

Next slides some features about the two regimes:

Saturated kink
Single Helicity - SH

Nearly periodic relaxations
Multiple Helicity - MH

SH regime: “ the simplest **RFP** ”

Magnetic flux surfaces - field lines

... and corresponding mean profile of B_T

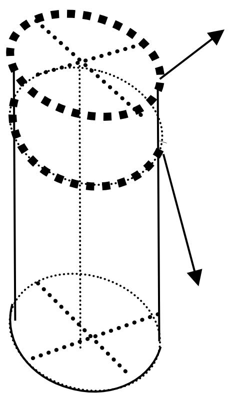

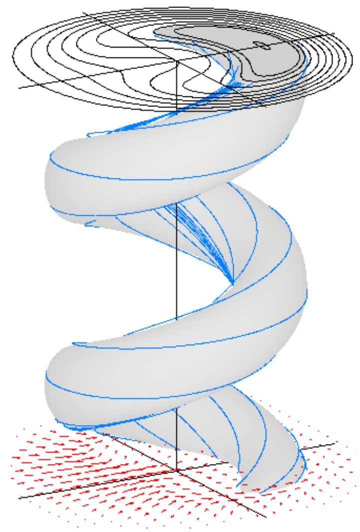

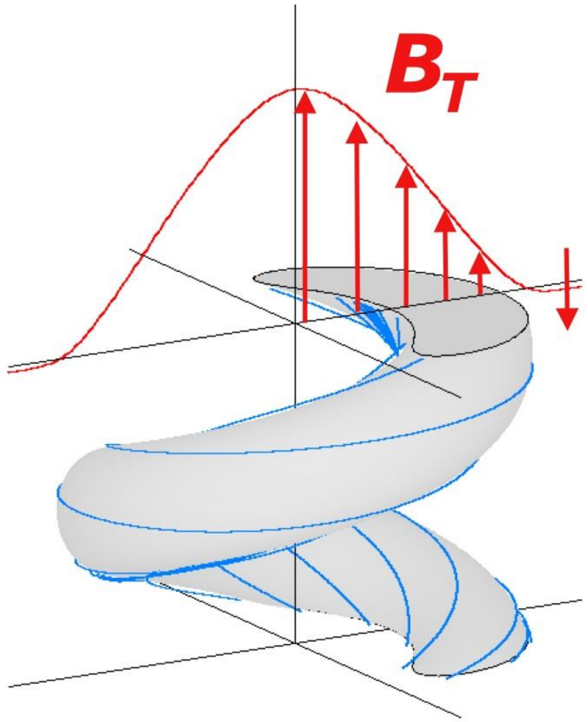

Helical Pinch Velocity

➔ drift velocity induced by the electrostatic potential …

Bonfiglio, et al PRL 2005

SH solutions resemble the toy model

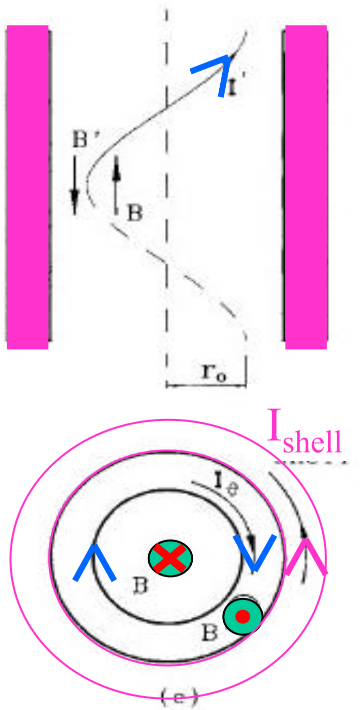

kinked wire

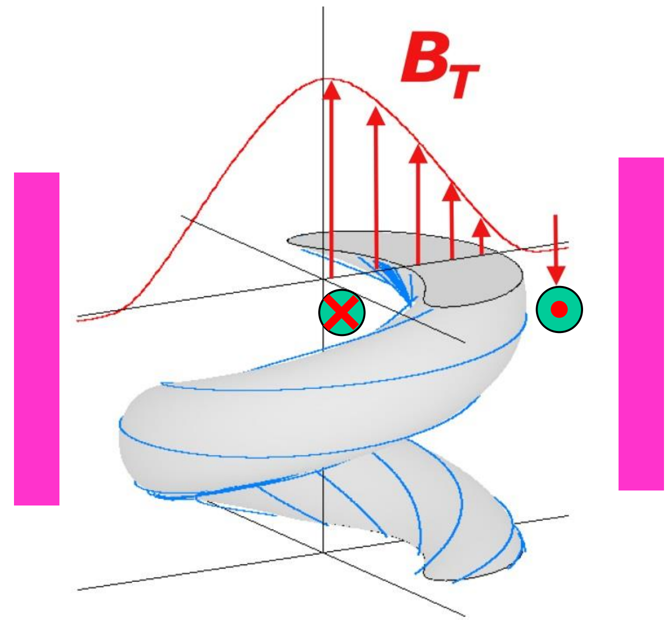

SH in viscoresistive modelling

SH solutions are different from Taylor's helical solutions

Helical RFP from 3D MHD

m=1, **n = – 10**

(R/a=4)

(internal helicity)

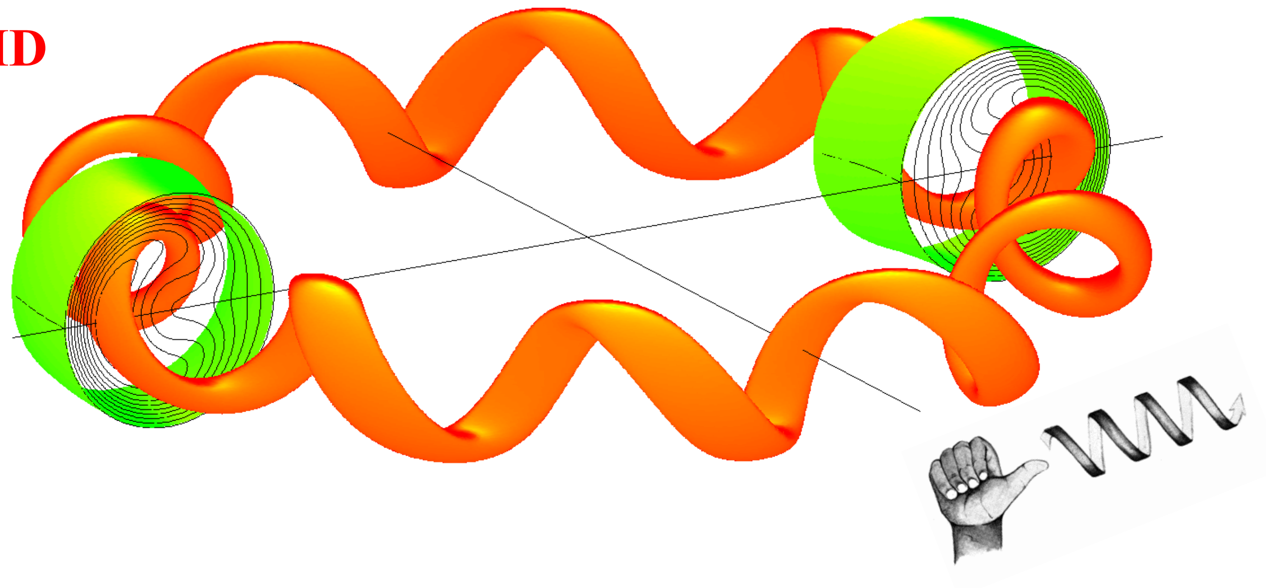

Taylor's helical state

m=1, **n = + 5**

(R/a=4)

(external helicity)

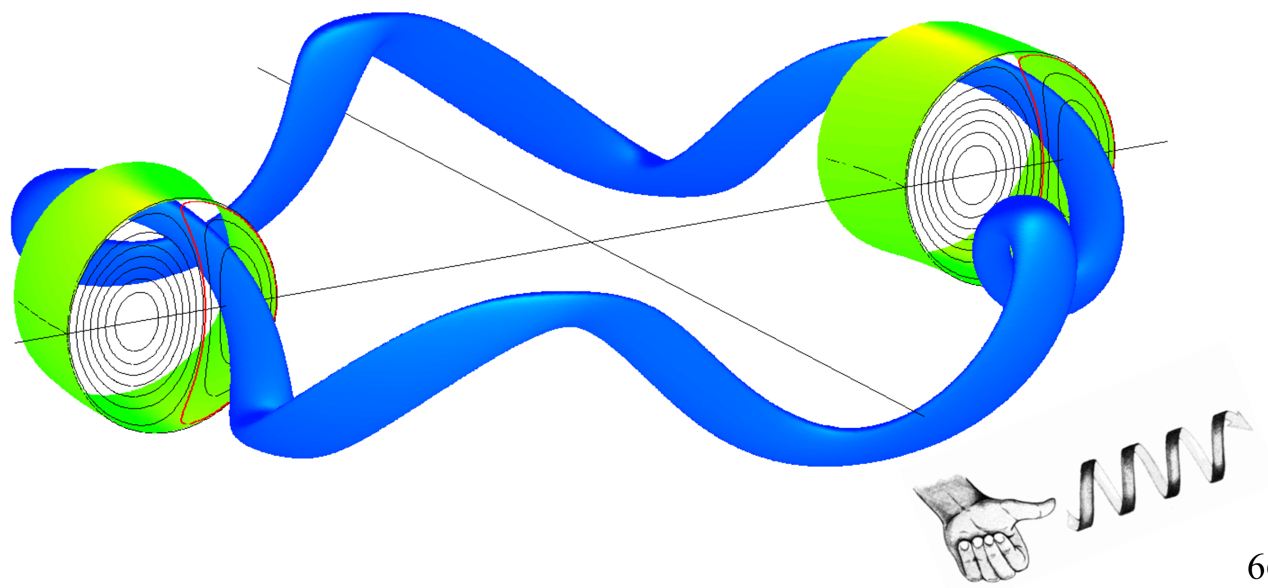

MH regime:

Nearly-periodic relaxation events

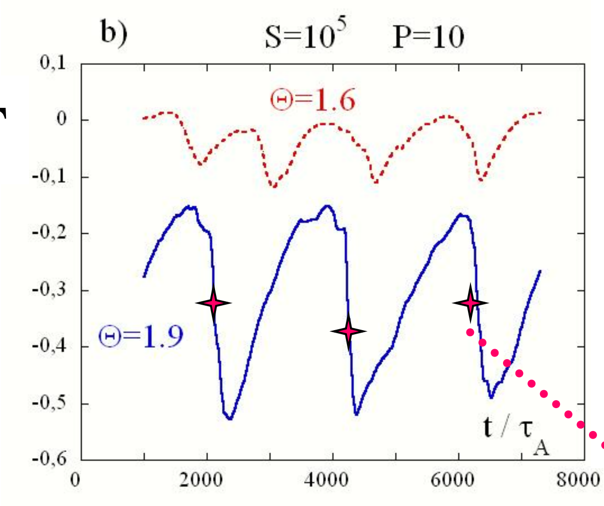

F

$t\,/\tau_A$

(similarly to low current experimental observations)

with formation of current sheets

$J \cdot B$

Current density contour plots (poloidal sections)

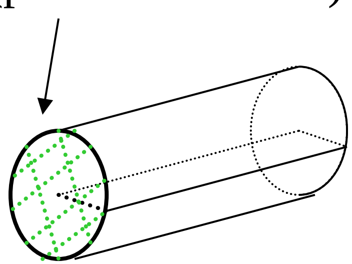

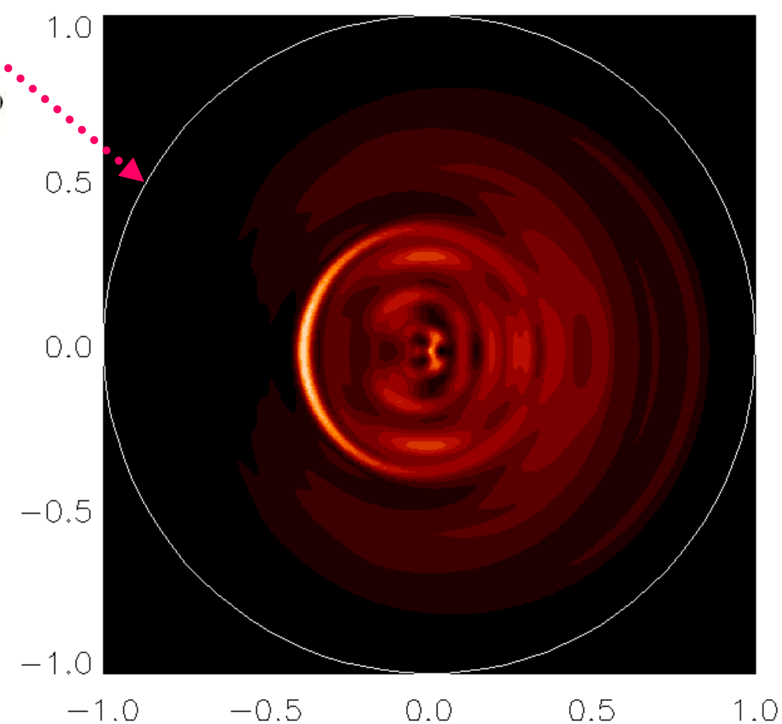

(3D: all of the modes contribute)

Bright colour => high current

Cappello & Biskamp Nucl Fus 1996

$J \cdot B$ contour plot and flow pattern

during RFP relaxation event

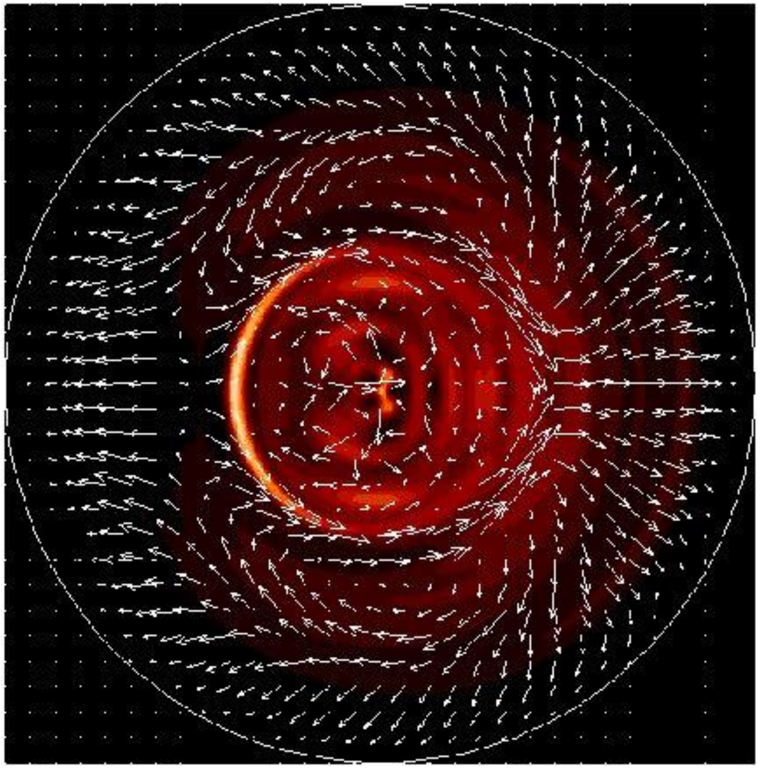

… in between relaxation events

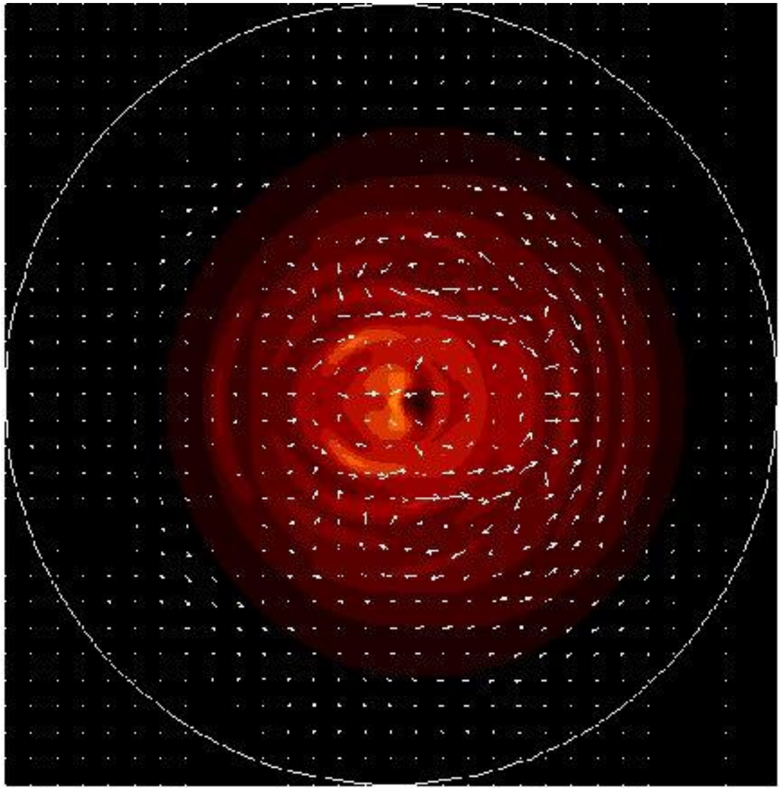

Bright colour => high current

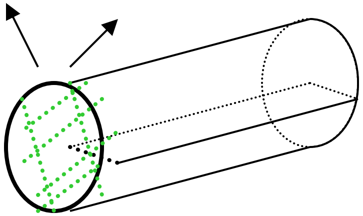

Larger MPs leads to steady helical saturation

(Similar to the ones obtained at high dissipation)

Veranda PPCF 2013
Bonfiglio PPCF 2015

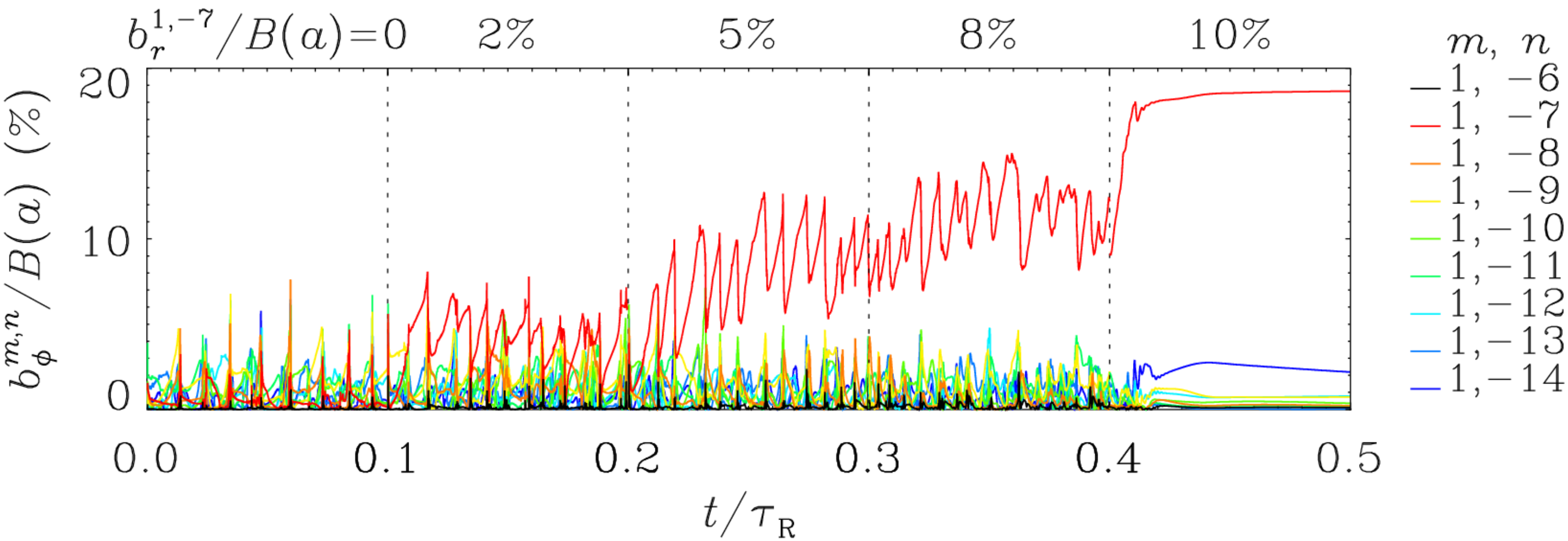

… to be explored in experiments

Possible to excite different *n*s

Dominant (1,-7) and sum of secondary modes

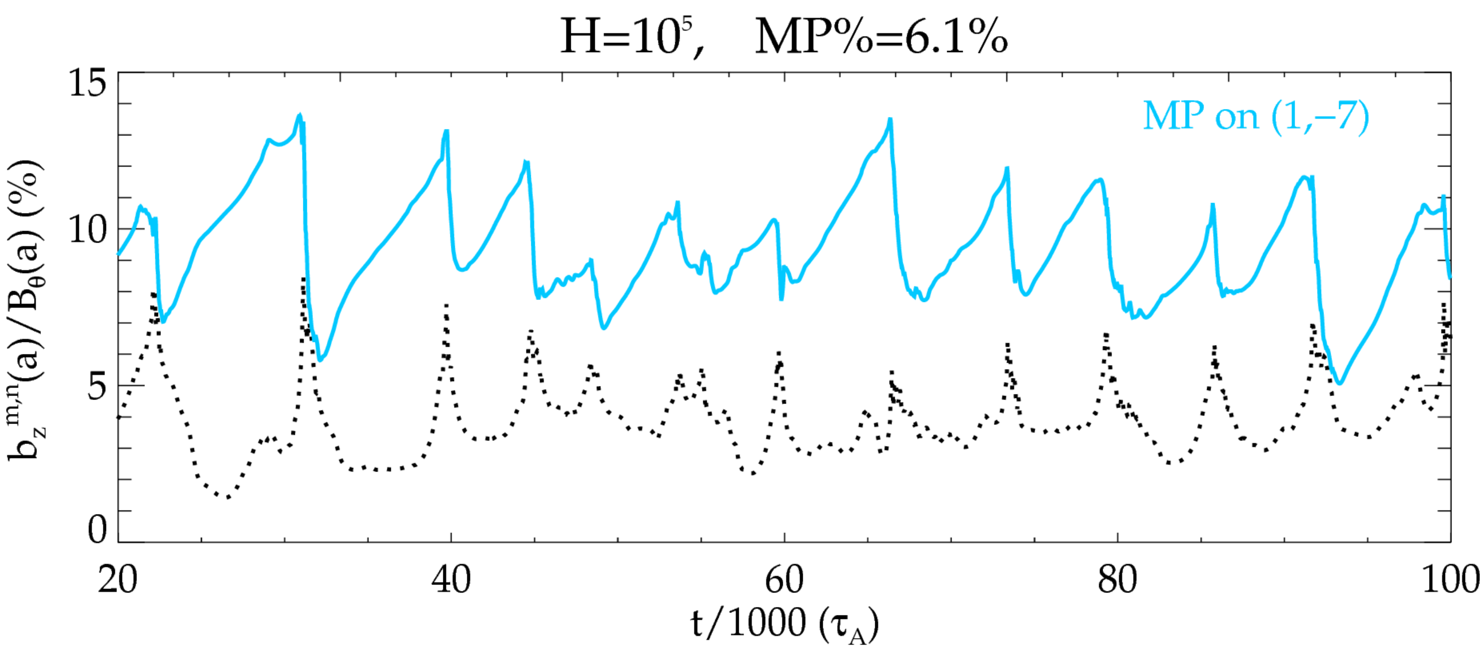

Response to different MPs : comparison

Dominant (1,-6) less reactive than -7

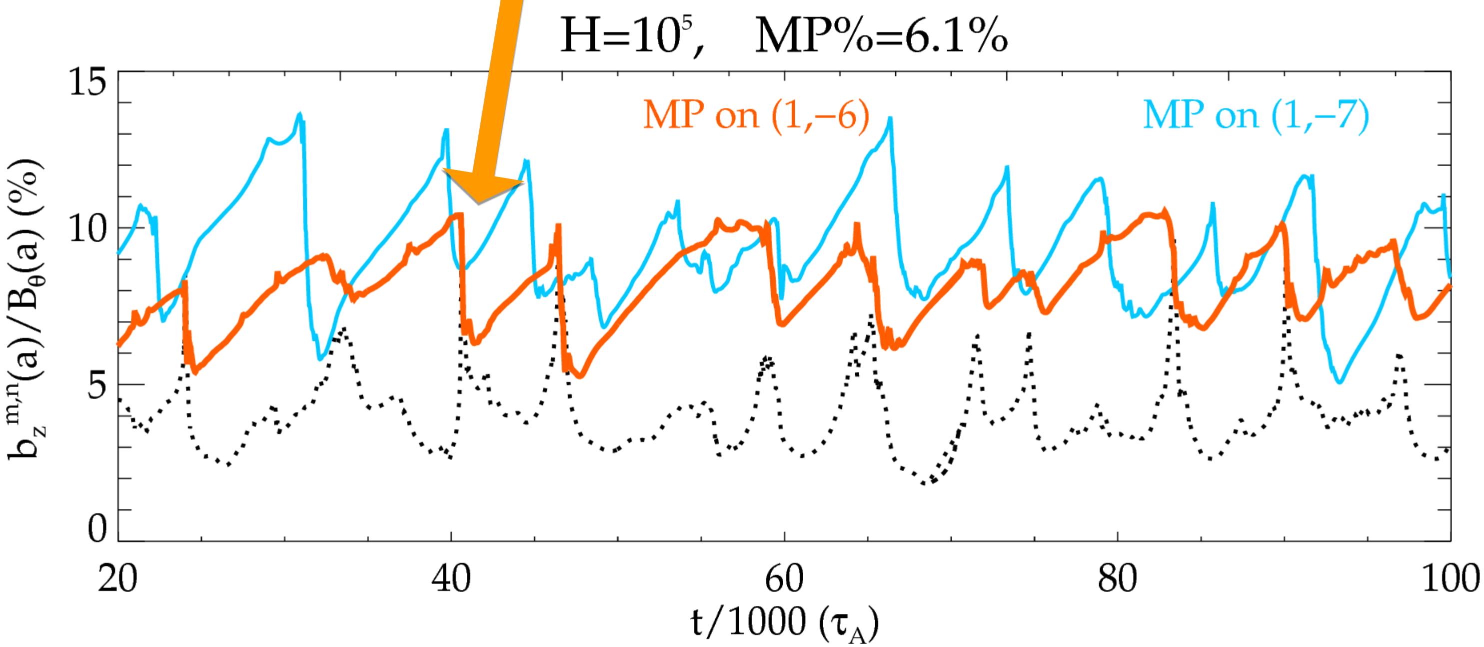

Response to different MPs : comparison

Dominant (1,-5) even less reactive

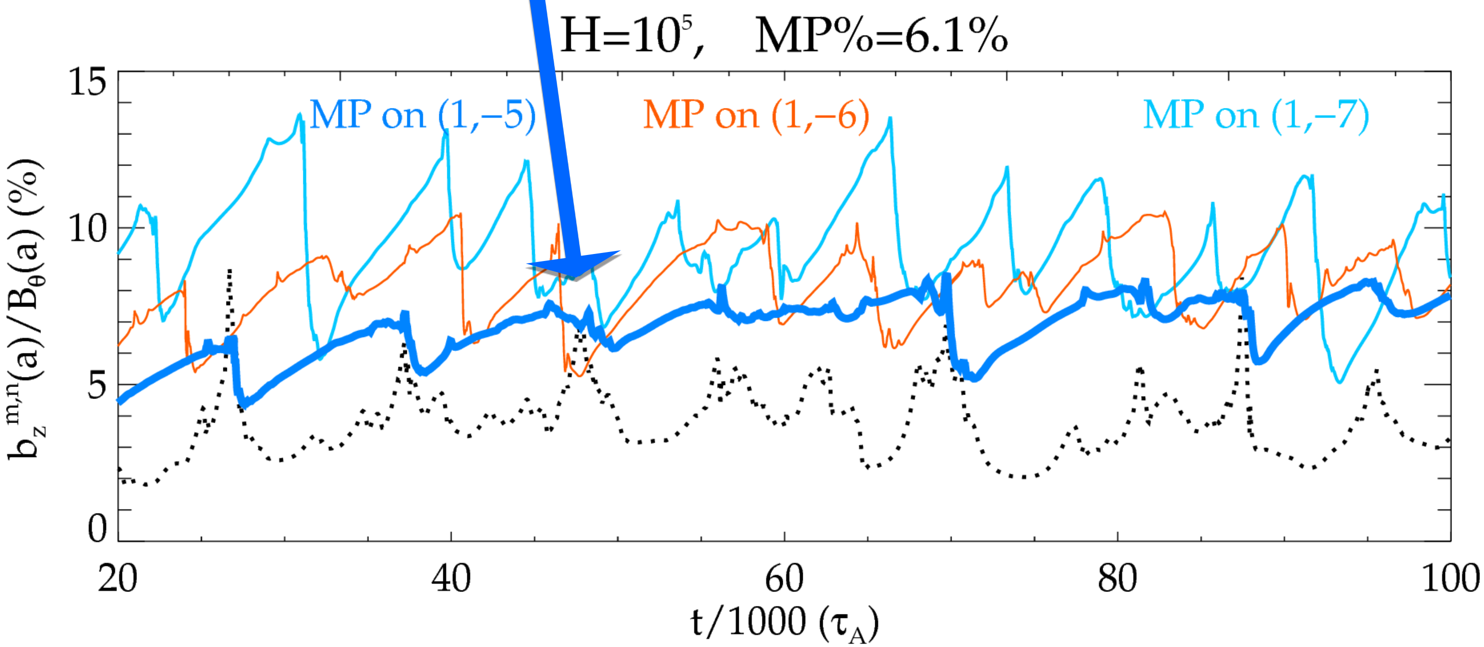

NOTE: the lower the n_{MP} -> the smaller the **Frequency&Amplitude** of cyclic oscillations

Comparison:

Numerical modelling – Experiments - Taylor's Theory

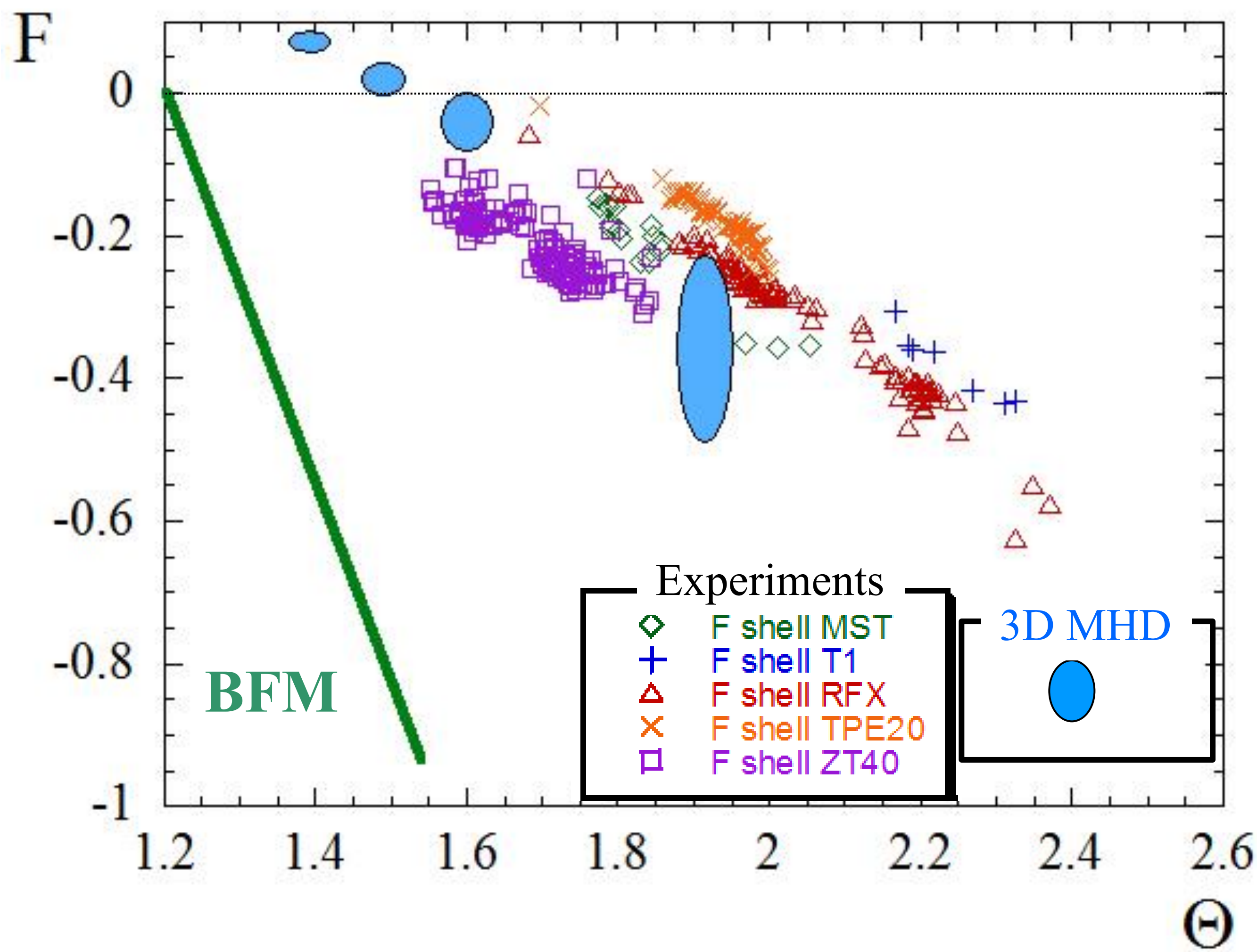

Moving around:

- Ultra-low-q and Low-q
- Circular Tokamak-like

2D (3D) visco-resistive MHD nonlinear simulations

circular cylindrical **(Ultra) low-q**

(SpeCyl – PIXIE3D)

(Ultra) low-q: Numerical modelling and Taylor's solutions

Bonfiglio NF 2008

Starting from RFP: Bz(a) is driven **upward** and **downward** again:

q(t)

Mode energies

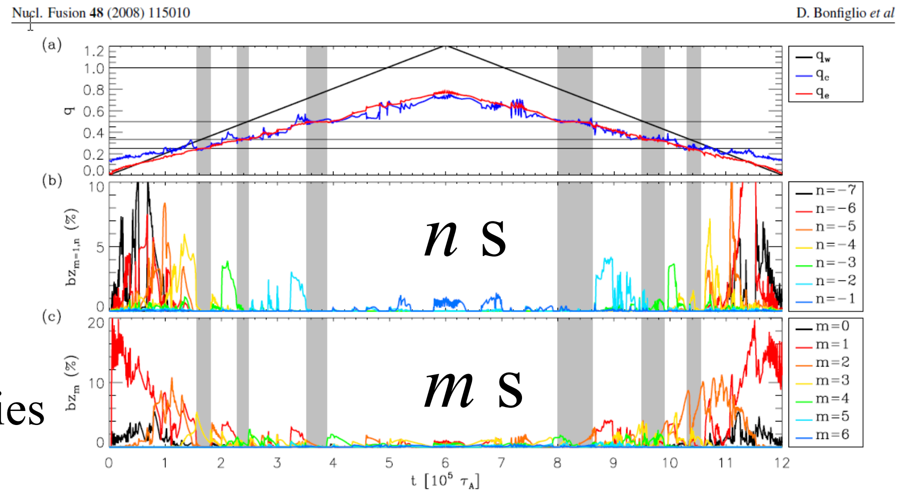

F(t)

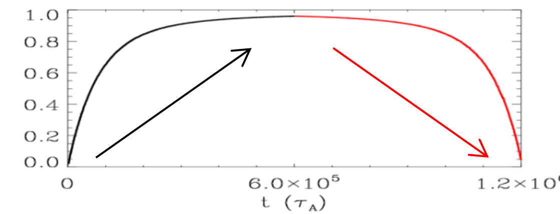

The initial phase (low-q) is closer to BFM than <u>Ultra-low-q</u> and <u>RFP</u>

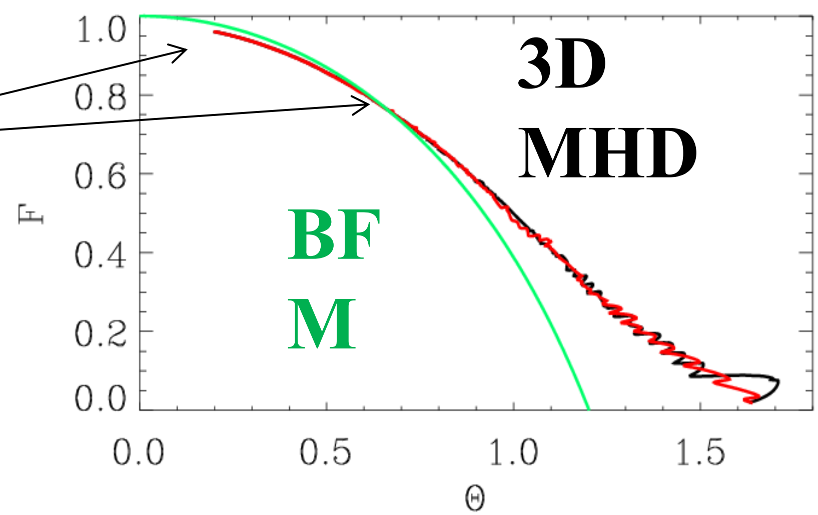

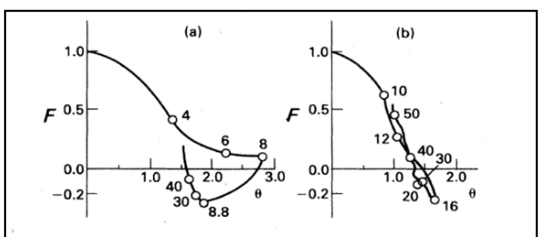

FIG. 5. Time-dependent F-θ curve for HBTX1. Times in μsec: (a) Fast mode; (b) slow mode (from Bodin and Newton, 1980).

2D (3D) visco-resistive MHD nonlinear simulations

circular cylindrical TOKAMAK

(SpeCyl – PIXIE3D)

Nonlinear verification benchmark **SpeCyl** – **PIXIE3D**

PIXIE3D is a massively parallel code in arbitrary curvilinear geometry conservative, solenoidal finite-volume discretization in space, fully implicit temporal advance.

Bonfiglio, Chacòn, Cappello POP 2010

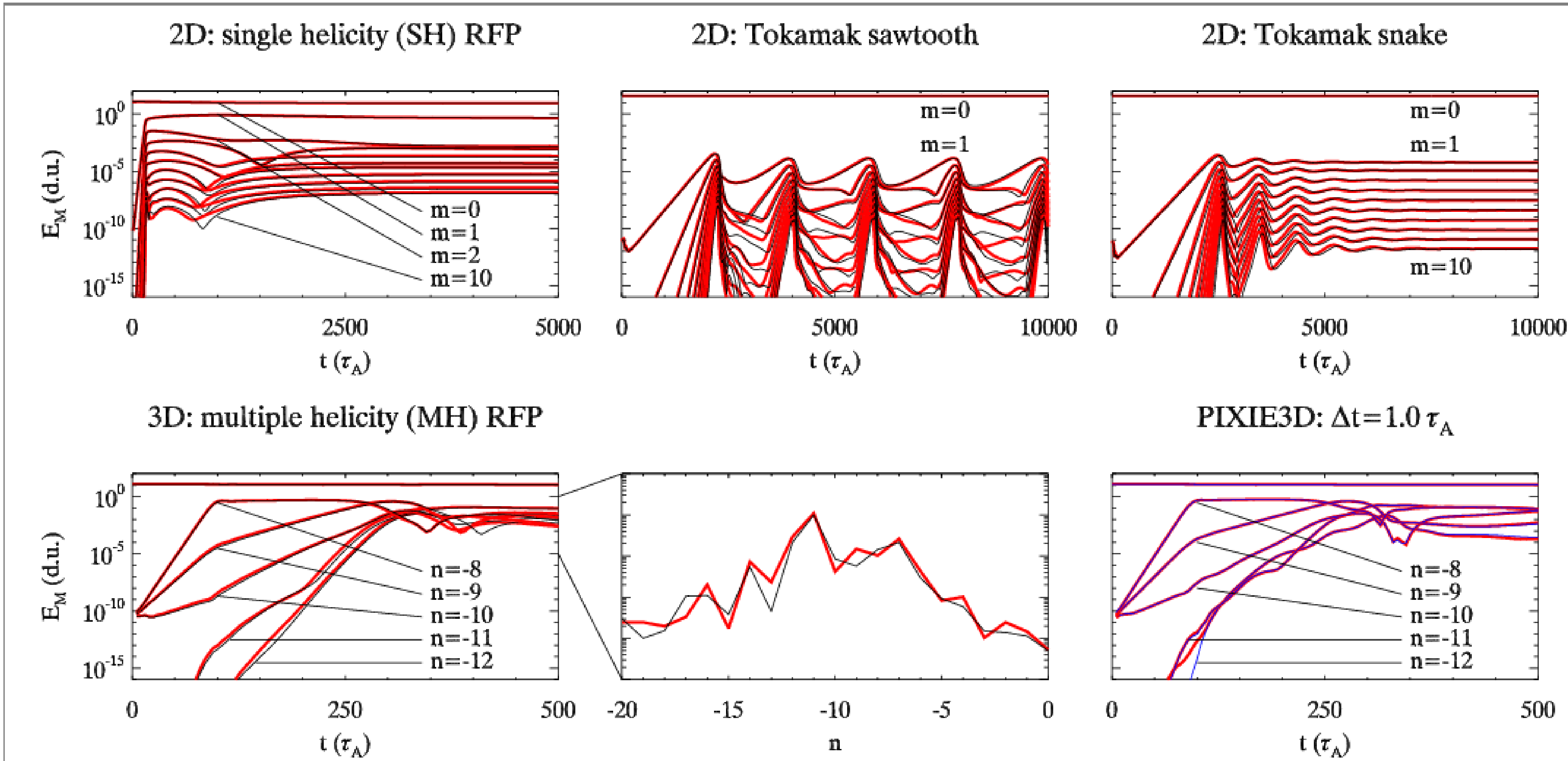

*Magnetic energy evolution from **SpeCyl** and PIXIE3D (black and red curves respectively).*
***Top panels 2D)** RFP and Tokamak.*
***Bottom 3D** left) RFP case. Bottom right) PIXIE3D with different time steps (red $\Delta t=5x10^{-3}$ blue $\Delta t=1\ \tau A$)*

Circular tokamak:
periodic sawtoothing (**low dissipation**)

snake (**high dissipation**)

Bonfiglio PoP 2010

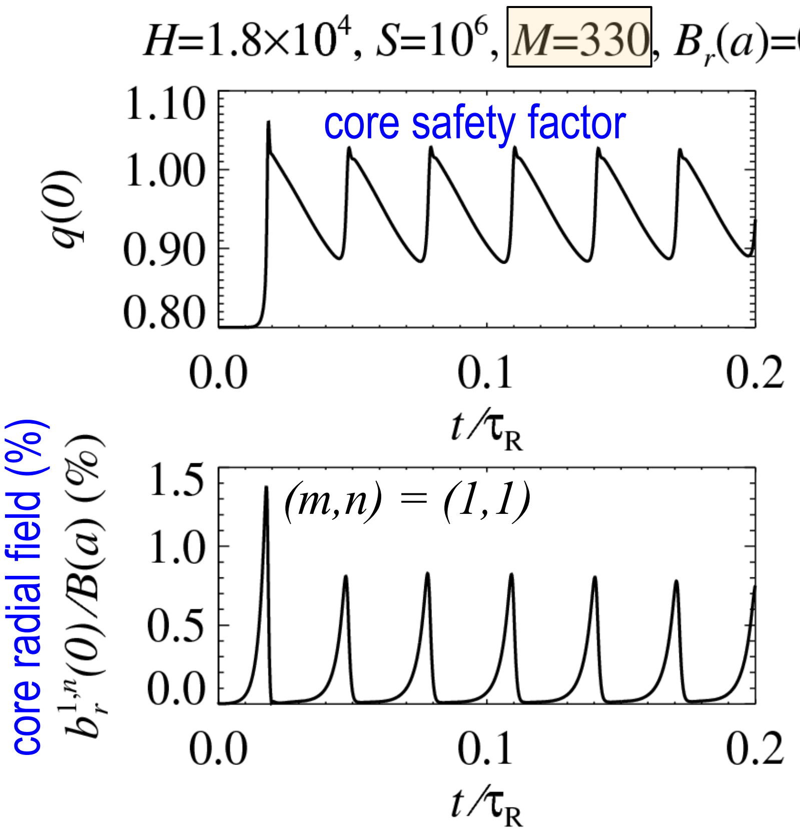

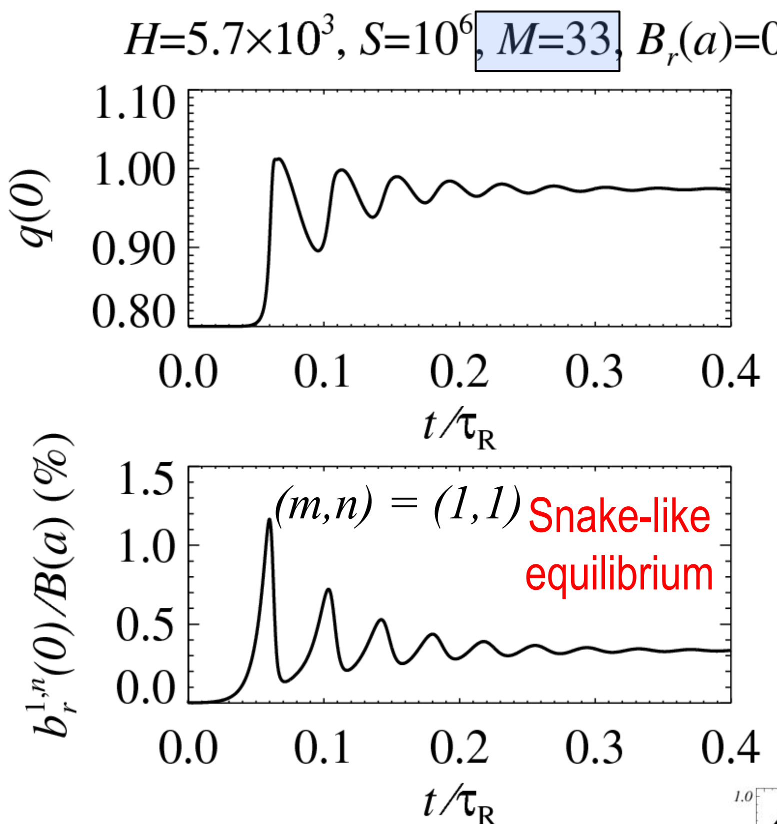

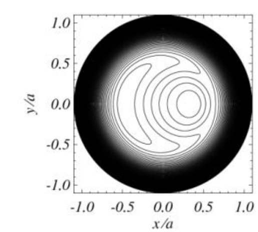

Circular tokamak:
periodic sawtoothing (**low dissipation**)

Magnetic energy relaxation and current sheet formation

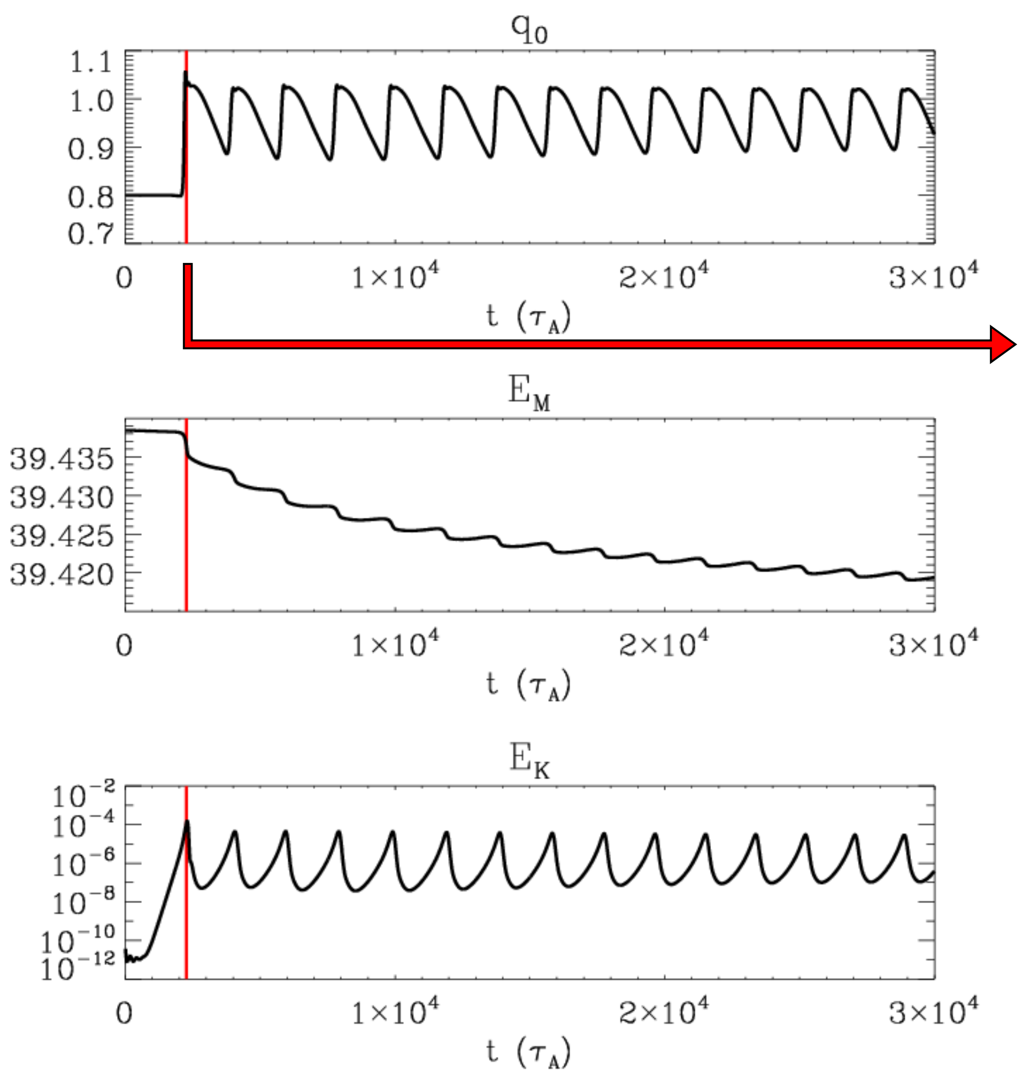

$\Delta E \sim 0.002$

B(0)=1

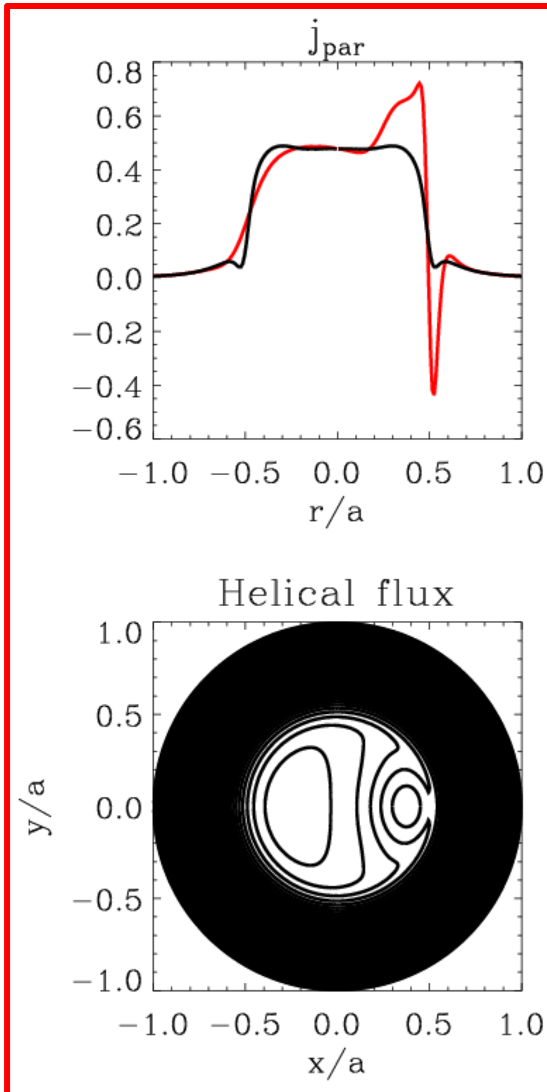

Circular tokamak … by using a seed edge perturbation (MP): sawtooth pacing and «mitigation» toward saturated kink.

Though not convenient for a Tokamak,
this dynamical effect is similar as in the RFP.

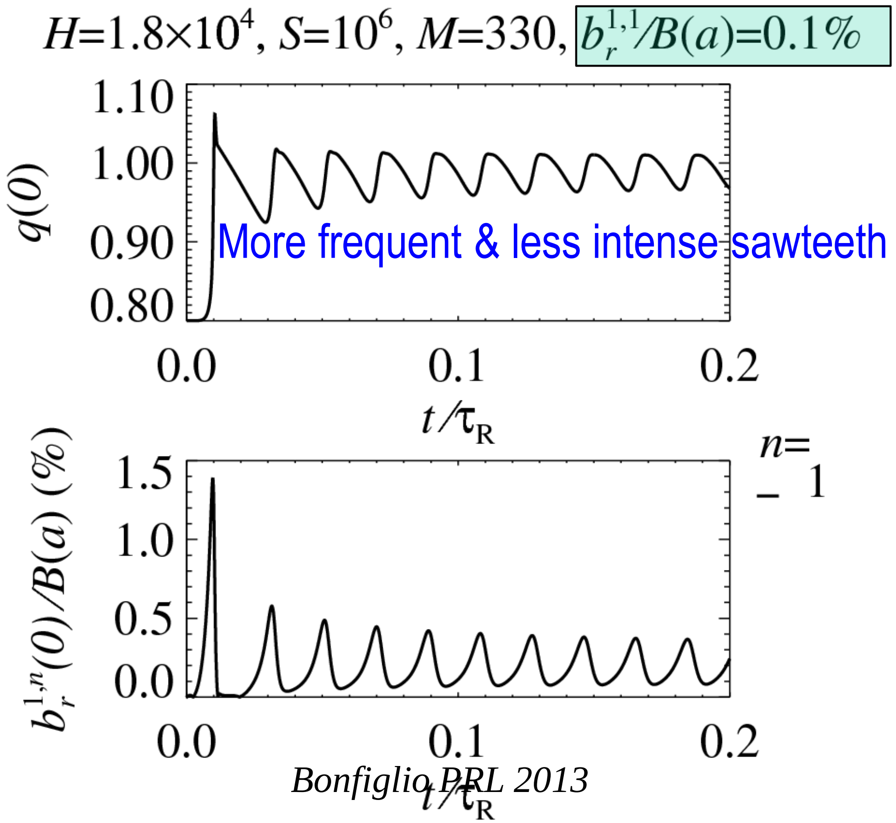

Bonfiglio PRL 2013

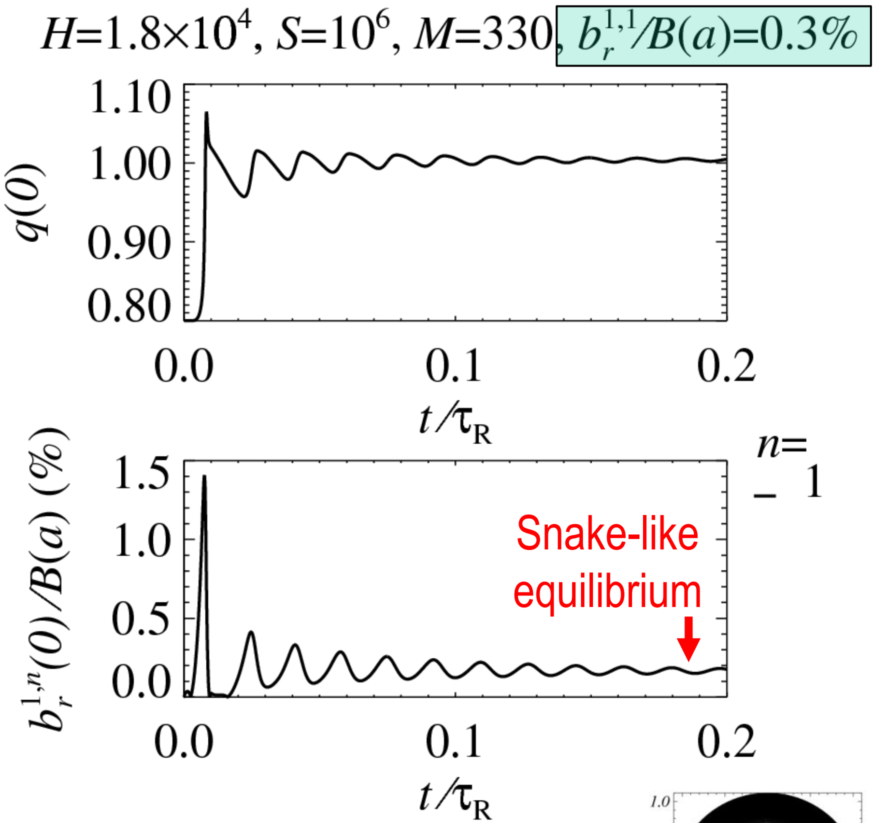

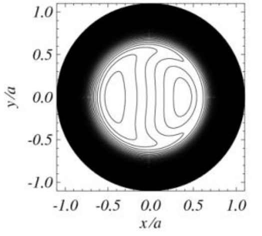

Bonfiglio, Escande , Zanca, Cappello NF 2011
Veranda, Bonfiglio Cappello et al EPS 2012
Bonfiglio, Veranda , Cappello et al PPCF 2015

SpeCyl & PIXIE3D model equations

PIXIE3D (supplementary terms in red)

Continuity equation:

$$\partial_t \rho + \nabla\cdot(\rho \mathbf{v} - D \nabla\rho) = 0 \text{ (SpeCyl: } \rho \equiv 1\text{)}$$

Momentum equation:

$$\partial_t (\rho \mathbf{v}) + \rho (\mathbf{v}\cdot\nabla) \mathbf{v} + \rho \mathbf{v} (\nabla\cdot\mathbf{v}) = \mathbf{J}\times\mathbf{B} - \nabla p + \nu\nabla^2\mathbf{v}$$

Energy equation:

$$\partial_t T + \mathbf{v}\cdot\nabla T + (\gamma-1) [T \nabla\cdot\mathbf{v} - (\chi\nabla^2 T+Q)/(2 n)]= 0$$

Faraday-Ohm equation:

$$\partial_t B = \nabla \times (\mathbf{v}\times\mathbf{B} - \eta\mathbf{J} - d_i/\rho (\mathbf{J}\times\mathbf{B} - \nabla p_e) + \nu_e\nabla^2\mathbf{J})$$

Gauss's law for magnetism: $\nabla\cdot B = 0$

RFX device evolution: plasma radius and magnetic front-end

Taylor's relaxation theory for the RFP

Taylor' conjecture (weak formulation of Woltjer's theory) is based on a minimum energy principle, (strictly meaningful for closed system),

The theory, with few ingredients, predicts minimum energy solutions with reversed Bz for high enough values of the pinch parameter Θ,
thus solutions toward which **the system should tend to**,
… **the RFP dynamo flows -essential for the RFP life- are neglected**.

There are several discrepancies :

- B(r) are smoother then Bessel … - μ *is not a constant*,
- a helical solution should be achieved … - *different from the ones observed* (*neither in exp nor in 3D nonlinear modelling*)
- after saturation of the pinch parameter - *not observed* (*neither in exp nor in 3Dmod*)

Such deficiencies should not surprise us,
the **RFP is not a closed system, it is a driven one** and we should not expect to obtain more then what promised by the Taylor's minimum energy solution itself !

RFP self-organization

ruled by Hartmann number

MHD Numerical simulations

Turbulent ⟷ **MH** : 3D non linear coupling resistive-kink tearing modes

RFP

Numerical simulations

(cylindrical approx.)

$\mathbf{H \sim (\nu\eta)^{-1/2}}$

Laminar ⟷ **SH** : 2D Stationary **helical symmetric** configurations

Model equations

3D MHD nonlinear code SpeCyl

Cappello & Biskamp
Nucl. Fus. 1996

$$\frac{\partial \boldsymbol{B}}{\partial t} = \nabla \wedge (\boldsymbol{v} \wedge \boldsymbol{B}) - \nabla \wedge (\boxed{\eta}\, \boldsymbol{J})$$

$$\frac{d\boldsymbol{v}}{dt} = \boldsymbol{J} \wedge \boldsymbol{B} + \boxed{\nu}\, \nabla^2 \boldsymbol{v}$$

$$\rho \equiv 1, p \equiv 0$$

$\eta = \tau_A / \tau_R$

(Lundquist: $S = 1 / \eta$)

$\nu = \tau_A / \tau_v$

simple visco - resistive approximation

(ideal boundary)

re-scaling :

$t \rightarrow \bar{t} = \sqrt{\frac{\eta}{\nu}}\, t$

$\mathrm{v} \rightarrow \bar{\mathrm{v}} = \sqrt{\frac{\nu}{\eta}}\, \mathrm{v}$

Model equations … transformed

… re-scaling : $t \to \bar{t} = \sqrt{\frac{\eta}{\nu}}\, t$ $\quad \mathrm{v} \to \bar{\mathrm{v}} = \sqrt{\frac{\nu}{\eta}}\, \mathrm{v}$

$(\eta, \nu) \Rightarrow (H, P)$

Hartmann: **$H = (\nu\eta)^{-1/2}$**

highlighted also in
D. Montgomery et al. PPCF 92-93
Tebaldi,Ottaviani JPP 99
(linear stab.)

magnetic Prandtl: **$P = \nu / \eta$**

$$\frac{\partial \bar{B}}{\partial \bar{t}} = \nabla \wedge (\bar{\mathrm{v}} \wedge \bar{B}) - \nabla \wedge (H^{-1}\, \bar{J})$$

$$\frac{1}{P}\frac{d\bar{\mathrm{v}}}{d\bar{t}} = \bar{J} \wedge \bar{B} + \nabla^2 (H^{-1}\, \bar{\mathrm{v}})$$

$$\rho \equiv 1, p \equiv 0$$

“H” is the important parameter when inertia is negligible

Cappello & Escande PRL 2000

Introduce m=0 mode energy as dynamical indicator

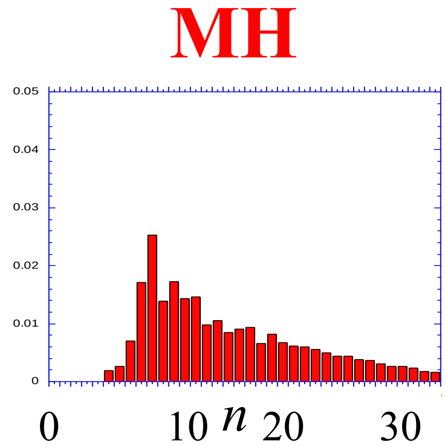

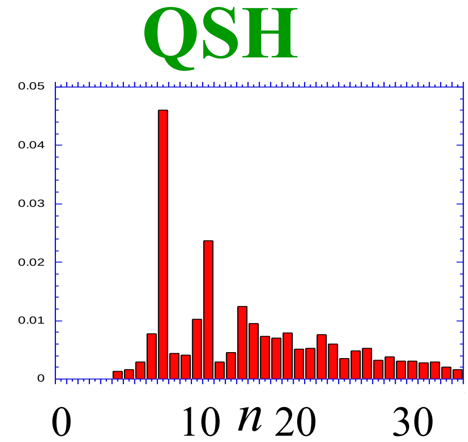

$\delta B_{m=1,n}$

m=1 modes
nonlinearly drive
m=0 modes

log $\delta E_{m=0}$

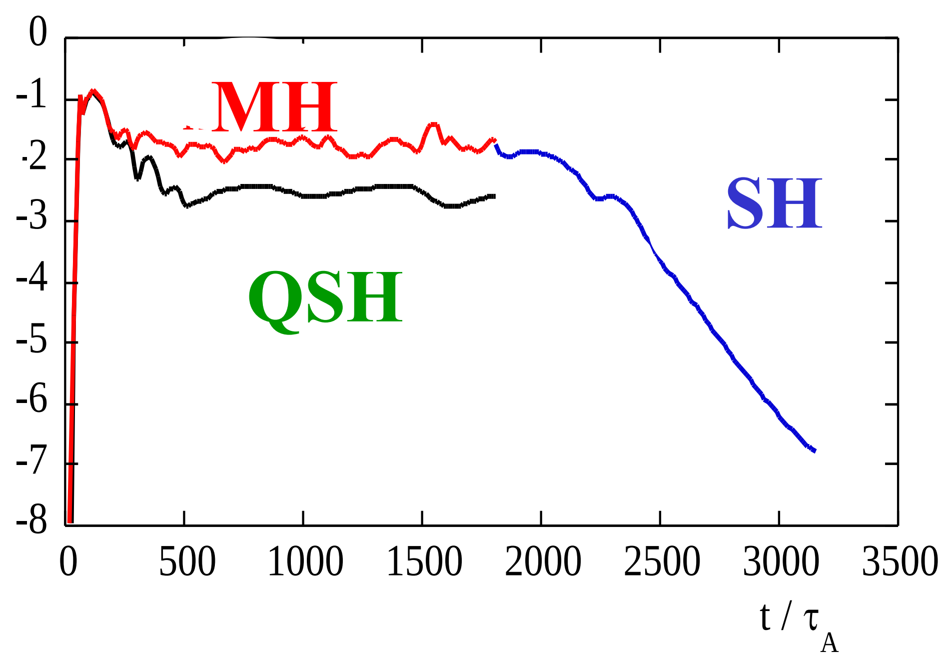

m = 0 modes are a <u>good indicator</u> of the dynamical regime

next slide : **RFP transition diagram**

m=0 mode energy

(Time averaged)

vs.

Hartmann number

Dynamical regimes in the numerical RFP : Transition diagram SH - QSH - MH

Numerical results

$\Theta = 1.9$

$E^{M}_{m=0}$

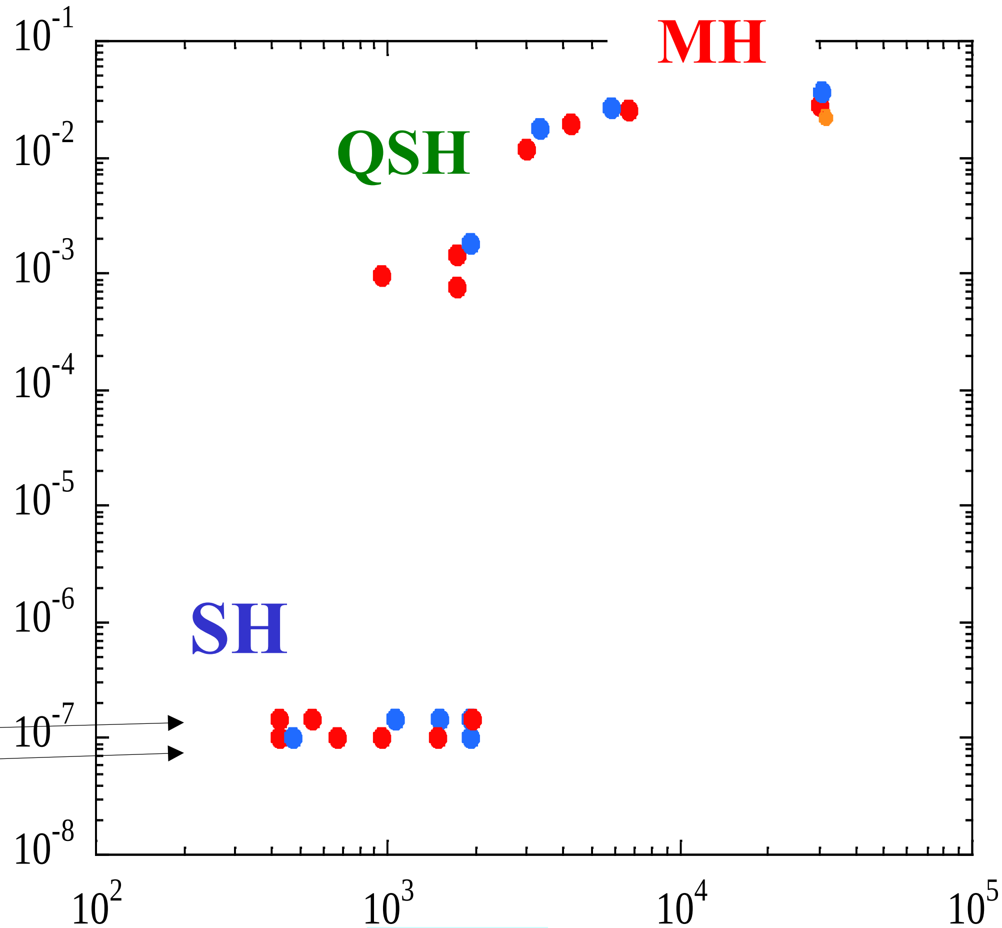

R/a =4

S=3.3x10^3 (P: 2/3-10)
S=3.0x10^4 (P: 1-5000)
S=10^5 (P = 10)

Two **S**ingle **H**elicity basins:

m/n **1/-12** **1/-11**

$H = 1/(\nu\eta)^{1/2}$

Cappello & Escande PRL 2000
Cappello PPCF 2004

- **transition to QSH – SH in viscoresistive MHD**

Most updated numerical transition diagrams (PPCF 2004)
minor dependence also on magnetic Prandtl and Θ

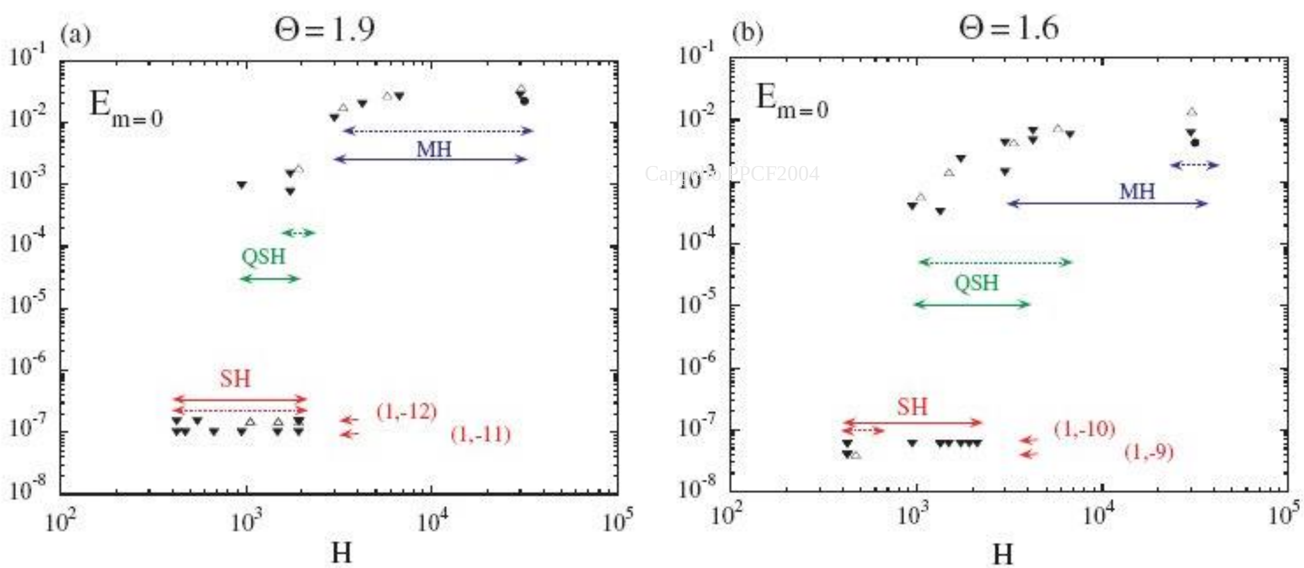

Figure 1. Transition diagrams at two values of the pinch parameter: (*a*) $\Theta = 1.9$, (*b*) $\Theta = 1.6$. The plots show the time-averaged magnetic energy of the $m = 0$ modes against the Hartmann number. Open triangles are used for $S = 3.3 \times 10^3$ with $P = [0.012, 50]$, black triangles for $S = 3.0 \times 10^4$ with $P = [1, 5000]$, the black circle is used for the case $S = 1.0 \times 10^5$ with $P = 10$. Note that for a convenient representation in the log-scale plot the vanishing SH $m = 0$ mode energy is represented as a finite conventional value with different offsets associated with the different preferred helicities developed by the system. The intervals associated with the different dynamical regimes, MH/QSH/SH, are highlighted by the horizontal bars (plain line $S = 3.0 \times 10^4$, dashed line $S = 3.3 \times 10^3$); at $S = 1.0 \times 10^5$ with $P = 10$ a MH regime is found.

Continuous transition ruled by ην (no MP)

High, intermediate, **low** dissipation

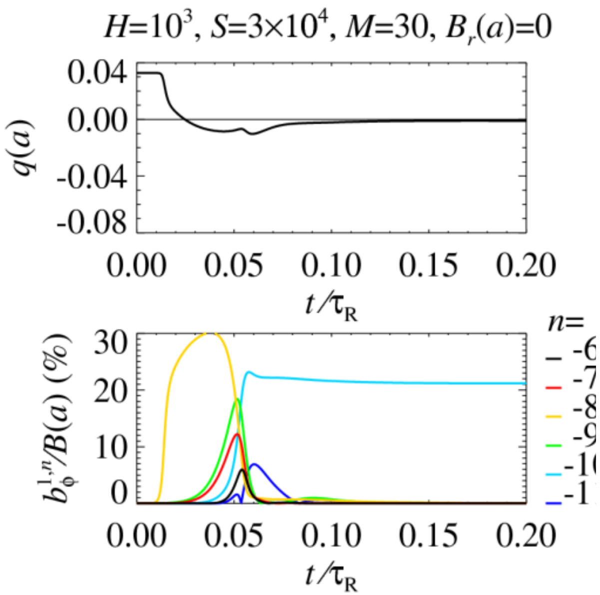

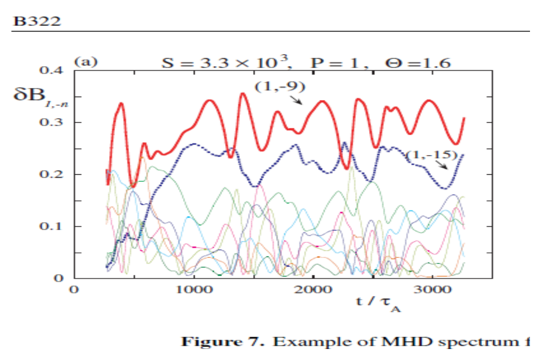

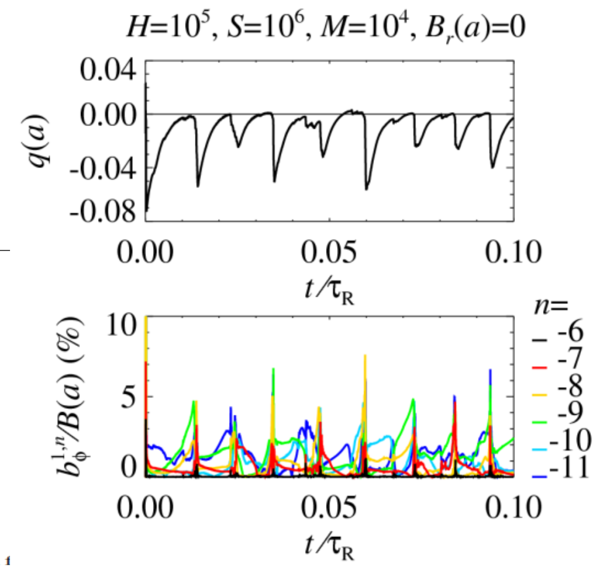

SH

MH

Cappello PPCF 2004

QSH regime:

Poincaré plot in **numerical** QSH regime

Topology reconstructions from **experimental** measures

conserved helical structure

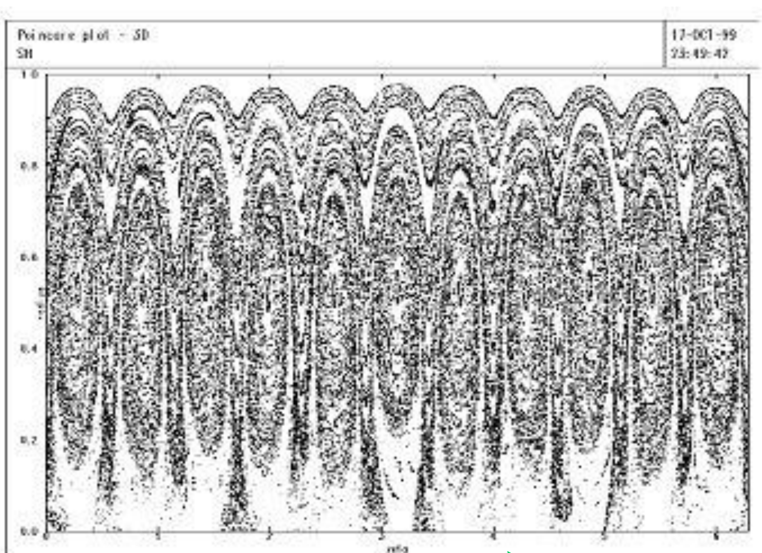

no separatrix

SXR emissivity

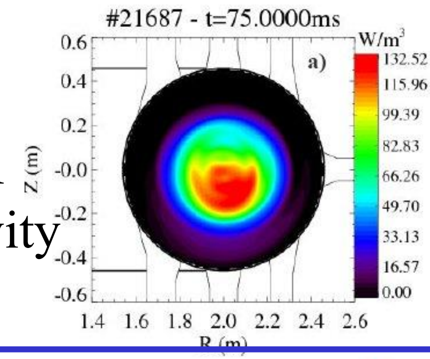

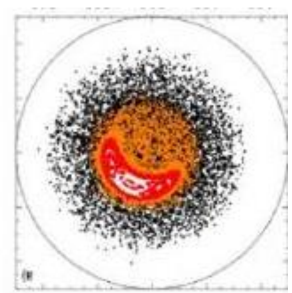

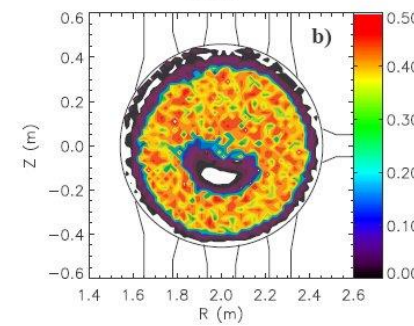

Gobbin et al. – Bonomo et al. - Innocente et al. EPS 2007

Escande et al. PRL 2000

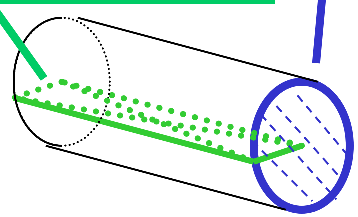

Lorenzini et al. PRL 2008

RFP plasma discharge set up

Historical observations ('*50ties* several toroidal pinches – ZETA –):

Quiescent regimes observed after B_T field reversal

RFP plasma discharge set up

Historical observations (‘*50ties* several toroidal pinches – ZETA –):

Quiescent regimes observed after B_T field reversal

Let us introduce two useful dimensionless parameters

Reversal parameter

$$F \equiv \frac{B_T(a)}{\langle B_T(r) \rangle}$$

Pinch parameter

$$\Theta \equiv \frac{B_P(a)}{\langle B_T(r) \rangle} \longrightarrow \propto \frac{I}{\Phi}$$

Historical observations

Quiescent regimes observed after B_T field reversal

… Faithfully replicated in modern experiments: RFX examples

F = **- 0.01**

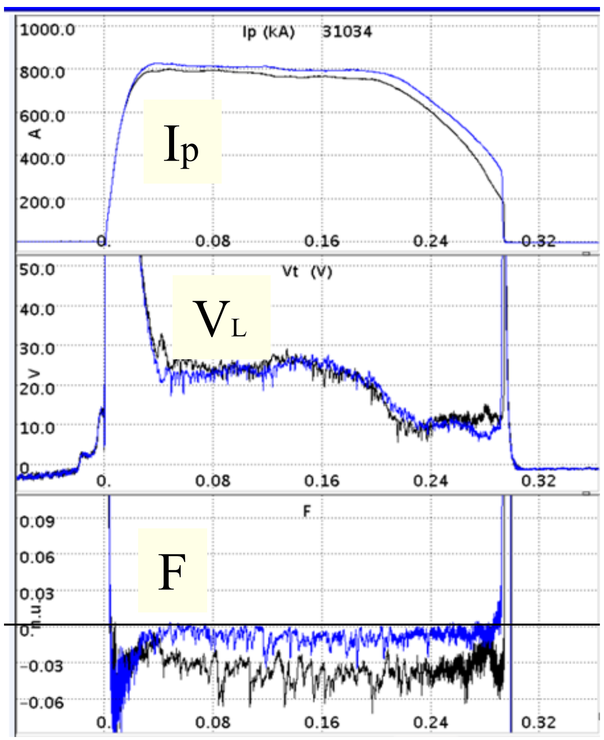

Time (s)

F > 0 disruptive instability

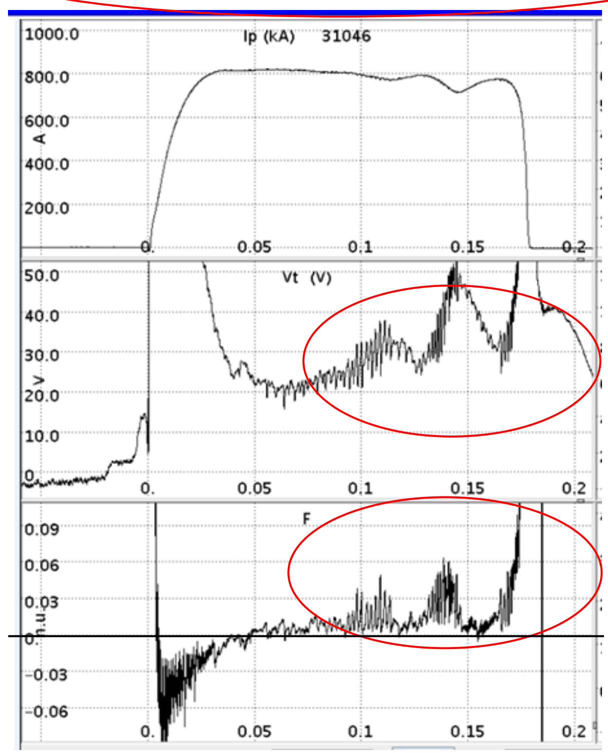

Time (s)

temporal trajectory
in the F – Θ plane

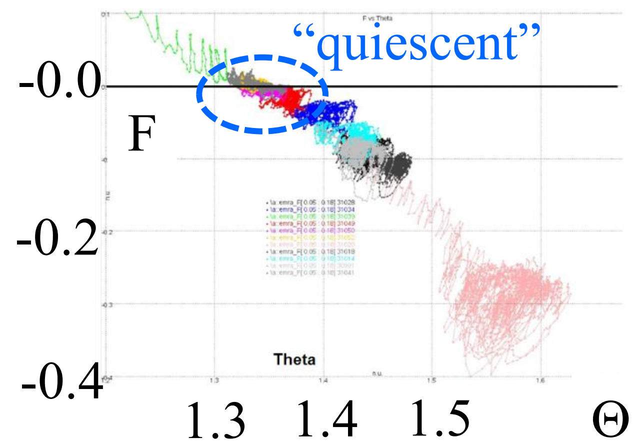

M. Zuin & RFX team
RFX internal presentation
2011.12.02

Example of QSH regime similar to experimental ones

Typical RFP sawtoothing

Mode amplitude

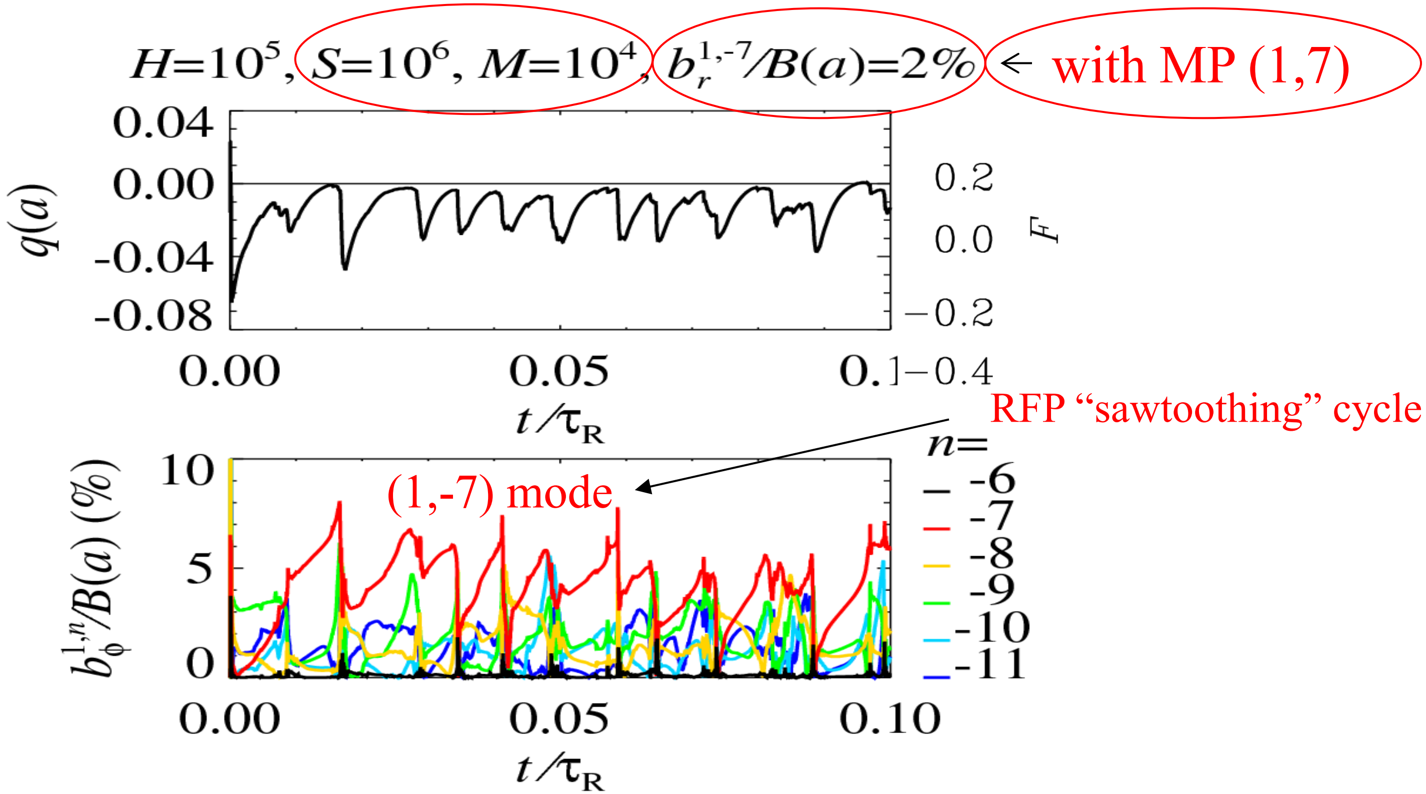

Bonfiglio NF 2011
Veranda PPCF 2013
Bonfiglio PRL 2013

The amplitude of secondary modes decreases with S,
The threshold MP% to excite a dominant mode decreases with S too.

RFX-mod:
I $\geq$ 1MA
S $\geq$ 5 10^6

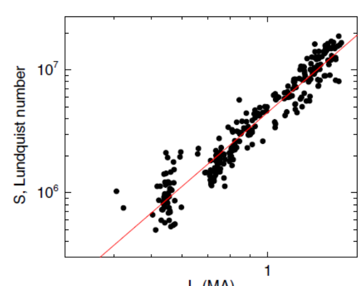

Piovesan, Zuin et al NF 2009

RFX-mod discharges

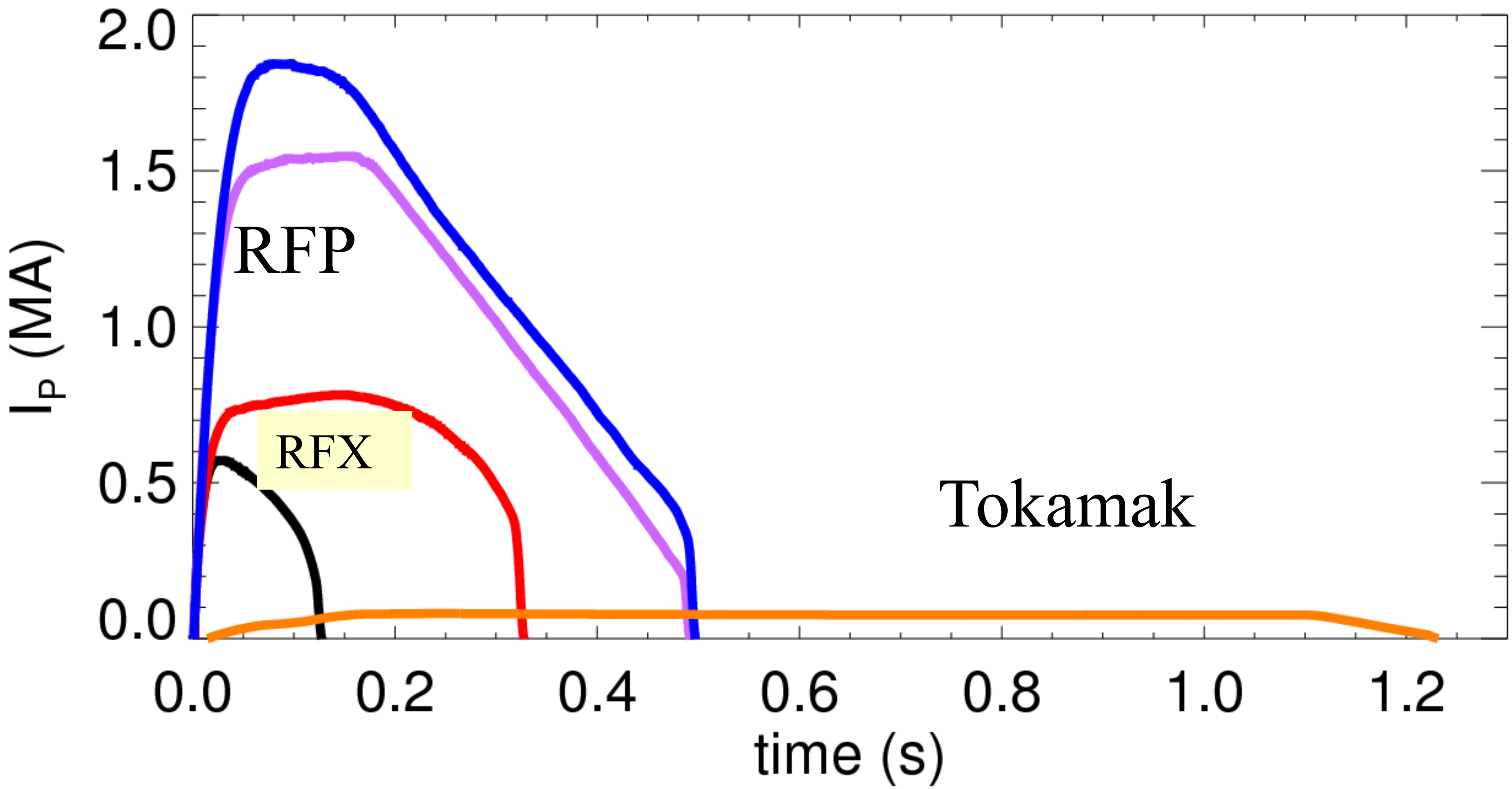

Shear Alfvén Wave and Compressional Alfvén Wave

SAW

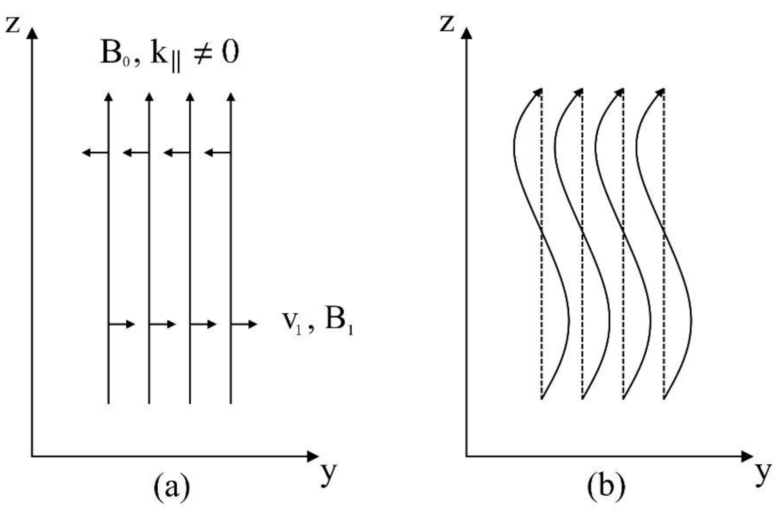

- The field lines are bent, giving the rise to a magnetic tension.
- There is no density or particle pressure perturbation for this mode.

CAW

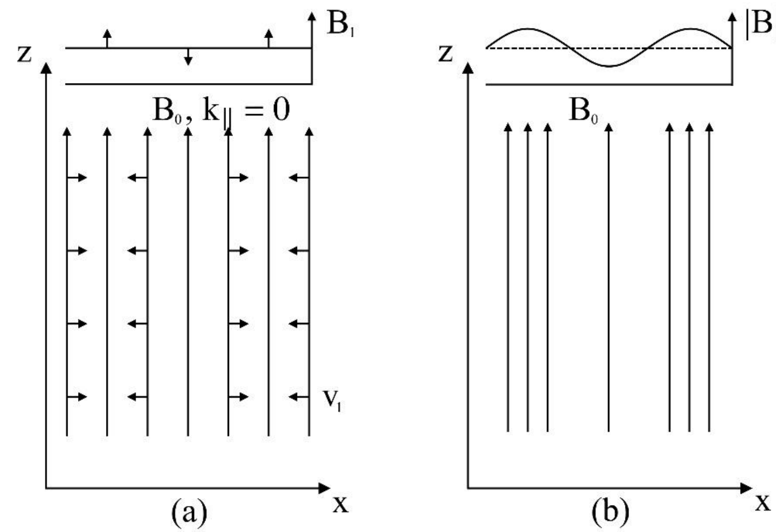

- These modes are compressive in nature, even if the sound speed is zero (cold plasma approximation).
- There are density perturbation in the wave, and perturbations of the magnetic field parallel to $\mathbf{B}_0$.

Experimental observations of AE in RFX-mod plasmas

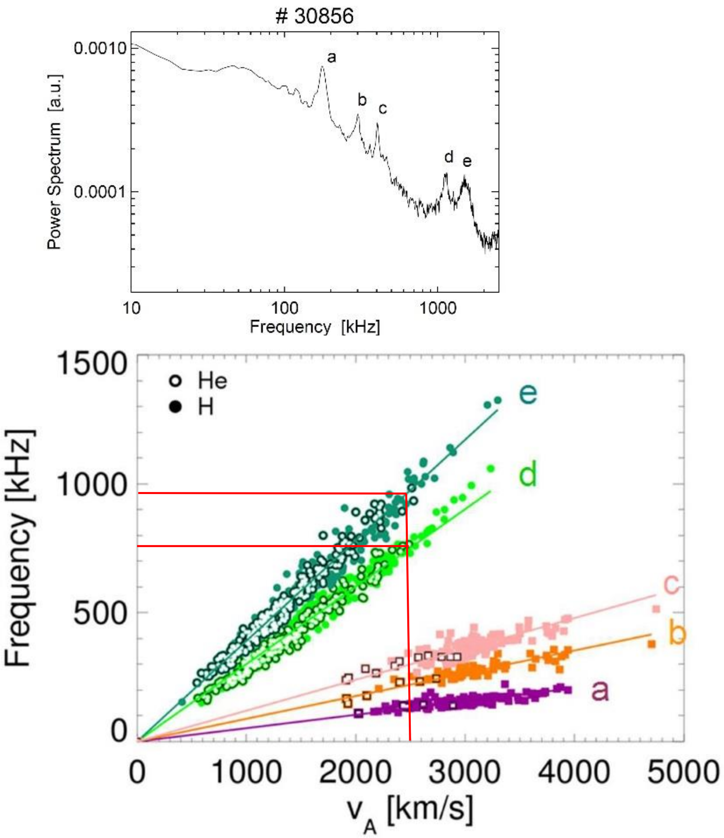

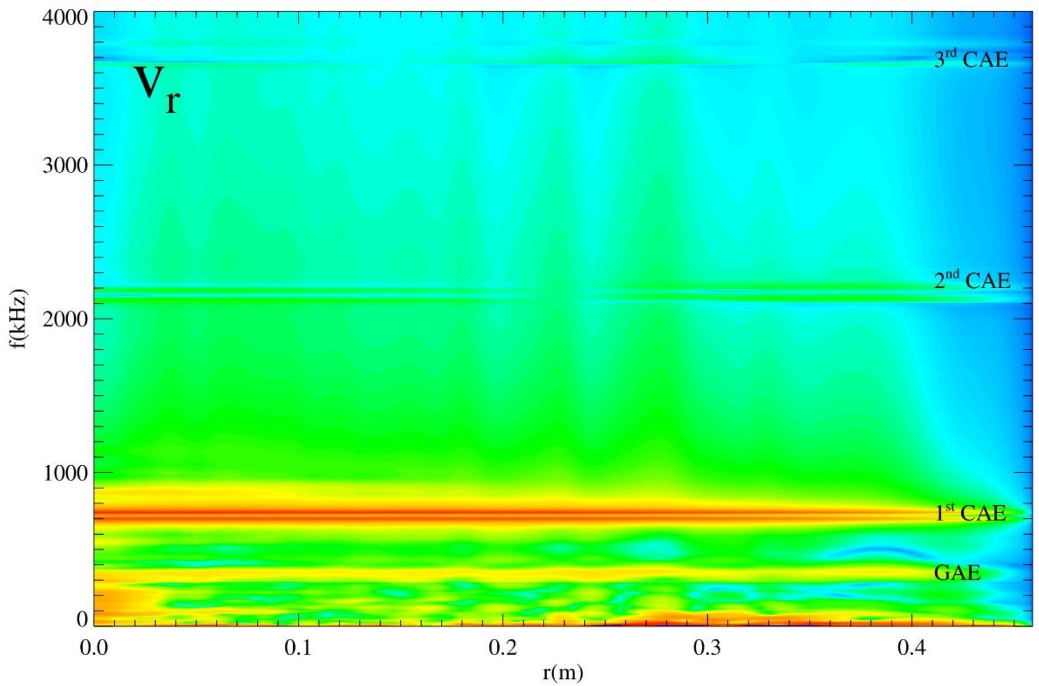

- Power spectrum of a $\dot{b}_p$ (r/a=1) signal evaluated during a SHAx state.
- d and e peaks are present during almost the full discharge duration.
- Physical units by taking $v_A = 2500$ km/s.

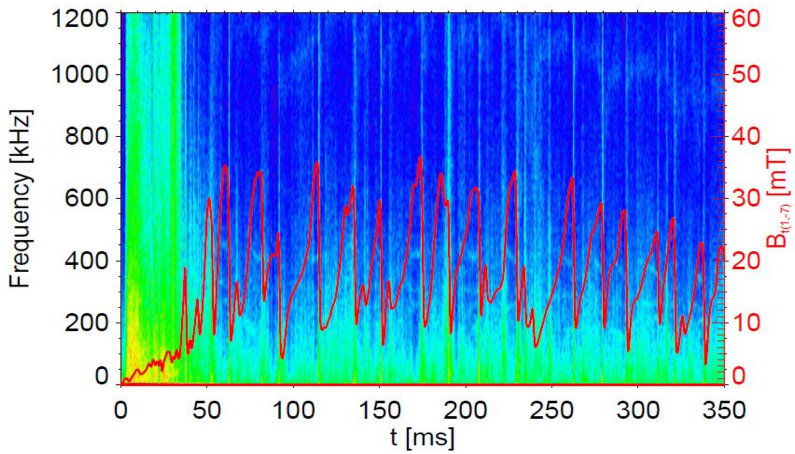

Figure 5.11: Spectrogram of U-probe $\dot{B}_\theta$ signal. The red line is the (m,n)=(1,-7) toroidal magnetic field component.

Spagnolo PhD Thesis 2012

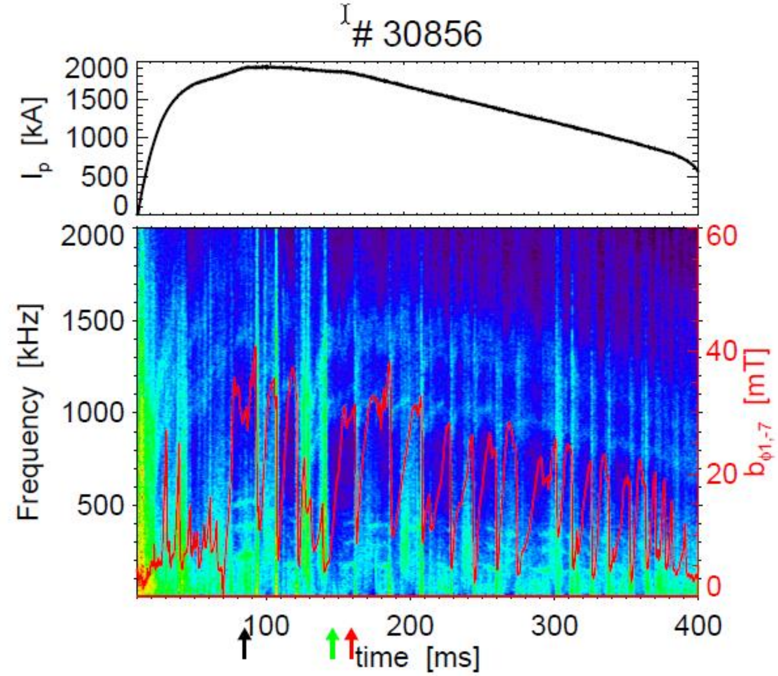

FIG. 1: Top: plasma current I_p time trace; bottom: spectrogram of a $\dot{b}_p$ signal and (red line) amplitude of the dominant $m/n = 1/-7$ mode (y-axis on the righthand side). The three arrows refer to the three time instants for the analysis in figure 3

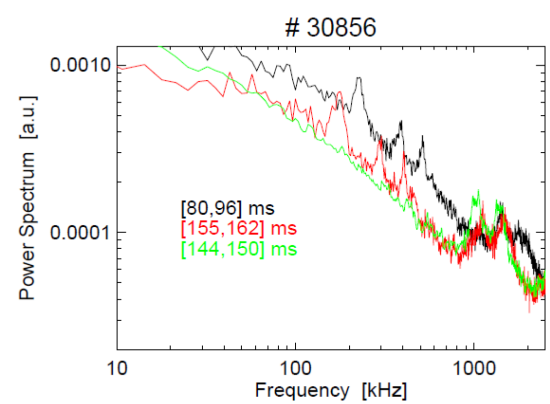

FIG. 3: Power spectrum of a $\dot{b}_p$ signal evaluated during the three time instants indicated by the arrows of figure 1: black and red lines refer to SHAx states, the green one to an axisymmetric state.